University of Alberta
Department of Civil &
Environmental Engineering

Structural Engineering Report No. 243

Behaviour of Slab-Colum Connections with Partially Debonded Reinforcement Under Cyclic Lateral Loading

By

Malika A. Ali

and

Scott D. B. Alexander

January 2002

Structural Engineering Report No. 243

BEHAVIOUR OF SLAB COLUMN CONNECTONSWITH PARTIALLY DEBONDED REINFOCEMENT UNDER CYCLIC LATERAL LOADING

by

Malika Abbas Ali

and

Scott D. B. Alexander

Department of Civil and Environmental Engineering
University of Alberta
Edmonton, Alberta
Canada

January 2002

Abstract

Flat plate slabs are one of the most widely used structural elements. In addition to carrying vertical load, a column supported flat plate must atleast accommodate the lateral drift resulting from wind or earthquake. The combination of vertical load and moment resulting from lateral drift places severe demands on the ductility of the slab-column structure and in particular, the connections. An efficient means of increasing the ductility of a slab-column structure is to partially debond the reinforcement.

Partial debonding of the flexural reinforcement could be an alternative to shear reinforcement in cases where the objective is increased drift capacity. It is feasible for new construction and perhaps for rehabilitation.

This report summarizes the results of tests conducted on two full-scale interior slab-column connections with and without partially debonded reinforcement subjected to cyclic loading. The test specimens were 4.2 m square in plan with a 355 mm square column in the middle. The slab thickness was 152 mm.

The test results showed that the specimen with partially debonded reinforcement exhibited more ductility than the fully bonded specimen. With partial debonding of the flexural reinforcement, cyclic load appeared to produce less damage to the connection in the vicinity of the slab-cloumn joint region.

Acknowledgements

This document is essentially a reproduction of the Masters thesis produced by the first author under the supervision of the second.

The authors wish to thank Larry Burden and Richard Helfrich for their technical assistance in conducting the tests at the I.F. Morrison Structural Laboratory of the University of Alberta.

Financial support was provided by the Natural Sciences and Engineering Research Council.

Table of Contents

	Page
1. Introduction	
1.1 General	1
1.2 Objective	2
2. Literature Survey	
2.1 Background of Previous Work	4
2.1.1 Hawkins, Mitchell and Hanna (1975)	5
2.1.2 Islam and Park (1976)	6
2.1.3 Robertson and Durrani (1992)	7
2.1.4 Megally and Ghali (2000)	8
2.1.5 Hwang and Moehle (2000)	10
2.2 Discussion of Previous Results	11
2.2.1 Discussion of Previous Test Methods	12
3. Test Specimen and Test Apparatus	
3.1 Experimental Program	18
3.2 Design of the Test Specimen	18
3.2.1 Prototype Structure	18
3.2.2 Geometry of the Specimen	18
3.2.3 Slab Design	19
3.2.4 Column Design	20

3.3 Materials 21

3.3.1 Concrete 21

3.3.2 Reinforcement 21

3.4 Fabrication Procedure 22

3.4.1 Form Work 22

3.4.2 Placing of Reinforcement 22

3.4.3 Partially Debonded Reinforcement 23

3.4.4 Placing of Concrete 23

3.5 Test Setup 24

3.5.1 Supports 24

3.5.2 Slab Boundary Restraining System 25

3.5.2.1 Edge Restraining System 26

3.5.2.2 Vertical Links 27

3.6 Loading Procedure 28

3.6.1 Gravity Loading 28

3.6.2 Lateral Loading 28

3.6.3 Column Loading 28

3.7 Instrumentation 29

3.7.1 Load and Reaction Measurements 29

3.7.2 Deflection Measurements 29

3.7.3 Rotation Measurements 30

3.7.4 Strain Measurements 31

3.7.5 Recording and Monitoring Data and Loads 31

3.8 Procedures 32

3.8.1 Setup Sequence 32

3.8.2 Sequence of Testing 33

4. Test Results and Discussions

4.1 Introduction 72

4.2 Lateral Load versus Lateral Drift Relationship 72

4.3 Lateral Load versus Slab-Column Rotation Relationship 74

4.4 Strain Distribution in Reinforcement at Peak Load Values 75

4.4.1 Bottom Reinforcement 75

4.4.2 Top Reinforcement 76

4.5 Bar Force Profile at Peak Load Values 77

4.6 Lateral Load Stiffness Relationship for Peak Drifts 77

4.7 Edge Expansion 79

4.8 Slab Deflection Profile 79

4.9 Crack Propagation 80

5. Conclusions and Recommendations

5.1 Summary and Conclusions 133

5.2 Recommendations 134

List of References 137

List of Tables

		Page
3.1	Concrete Properties	35
3.2	Properties of Reinforcing Bars	35
4.1	Peak Drift and Lateral Load Values at Different Load Cycles (SP-A)	82
4.2	Peak Drift and Lateral Load Values at Different Load Cycles (SP-B)	83
4.3	Strain Gauge Readings in Reinforcing Bars of SP-A	84
4.4	Strain Gauge Readings in Reinforcing Bars of SP-B	88

List of Figures

Figure		Page
2.1	Loading Arrangement of (Hawkins et al. (1975)) Test Specimen	14
2.2	Critical Punching Shear Peripheries	15
2.3	Plan of Islam and Park Test Specimen	16
2.4	Loading Arrangement of (Islam and Park (1976)) Test Specimen	16
2.5	Plan of (Megally and Ghali (2000)) Test Specimen	17
2.6	Loading Arrangement of Megally and Ghali Test Specimen	17
3.1	Prototype Flat Plate Structure	36
3.2	Typical Deflected Shape of Prototype Structure	37
3.3	Plan of Specimen	38
3.4	Side Elevation of Specimen	38
3.5	Layout of Negative Reinforcement in N-S Direction	39
3.6	Layout of Negative Reinforcement in E-W Direction	39
3.7	Detail of Reinforcement of Slab	40
3.8	Top Reinforcement Layout	41
3.9	Layout of Positive Reinforcement in N-S Direction	42
3.10	Layout of Positive Reinforcement in E-W Direction	42
3.11	Dimension and Reinforcement of Column	43
3.12	38 mm Thick Plate with Dowels	44
3.13	Stand Off for Post Tensioning	44
3.14	Stand Off for Post Tensioning Assembly	45
3.15	Typical Force-Strain Curve of Reinforcement of Specimen A	46

3.16	Typical Force-Strain Curve of Reinforcement of Specimen B	47
3.17	Form Work of Slab	48
3.18	Column Base Plate with 10M Dowels	48
3.19	Slab-Column Connection with Partially Debonded Rebars	49
3.20	Partially Debonded Reinforcement	50
3.21	Test Frame for Applying Lateral Load	51
3.22	Test Setup from S-W Corner Looking North East	52
3.23	Boundary Conditions of Column at Bottom	53
3.24	Horizontal Load Cell Pin Connected to Column	54
3.25	Horizontal Jack Attached to Steel Reaction Frame	54
3.26	Ideal Deflected Shape and Moment Diagram of Structure Under Gravity Load	55
3.27	Deflected Shape under Gravity Load	55
3.28	Top Edge Restraining System	56
3.29	Edge Restraining System	57
3.30	Deflected Shape under Combined Gravity and Lateral Load	58
3.31	Bottom Edge Restraining System	59
3.32	Vertical Link	60
3.33	Bottom Edge Restraining System	61
3.34	Detail of Vertical Link	62
3.35	Concrete Block Hanged to Simulate Additional Gravity Load	63
3.36	Hookup of Horizontal Jacks to Two-way Pump	64
3.37	Position of Vertical LVDTs	65
3.38	Position of Horizontal LVDTs and Cable Transducer	66

3.39	Position of RVDTs	67
3.40	Layout of Strain Gauges of Positive Reinforcement in E-W Direction	68
3.41	Layout of Strain Gauges of Positive Reinforcement in N-S Direction	69
3.42	Layout of Strain Gauges of Negative Reinforcement in E-W Direction	70
3.43	Layout of Strain Gauges of Negative Reinforcement in N-S Direction	71
4.1	Lateral Load vs Column Drift Hysteresis of SP-A (Partially Debonded Reinforcement)	93
4.2	Lateral Load vs Column Drift Hysteresis of SP-B (Fully Debonded Reinforcement)	94
4.3	Slab-Column Rotation of SP-A at Peak Drift Values – Loading North	95
4.4	Slab-Column Rotation of SP-A at Peak Drift Values – Loading South	96
4.5	Slab-Column Rotation of SP-B at Peak Drift Values – Loading North	97
4.6	Slab-Column Rotation of SP-B at Peak Drift Values – Loading South	98
4.7	Strain profile of N-S bottom bars of SP-A at north face of column-Loading North	99
4.8	Strain profile of N-S bottom bars of SP-A at south face of column-Loading North	100
4.9	Strain profile of N-S bottom bars of SP-A at north face of column-Loading South	101
4.10	Strain profile of N-S bottom bars of SP-A at south face of column-Loading South	102
4.11	Strain profile of N-S bottom bars of SP-B at north face of column-Loading North	103
4.12	Strain profile of N-S bottom bars of SP-B at south face of column-Loading North	104
4.13	Strain profile of N-S bottom bars of SP-B at north face of column-Loading South	105
4.14	Strain profile of N-S bottom bars of SP-B at south face of column-	

Loading South 106

4.15 Strain profile of N-S top bars of SP-A at north face of column-Loading North 107

4.16 Strain profile of N-S top bars of SP-A at south face of column-Loading North 108

4.17 Strain profile of N-S top bars of SP-A at north face of column-Loading South 109

4.18 Strain profile of N-S top bars of SP-A at south face of column-Loading South 110

4.19 Strain Profile of N-S top bars of SP-B at north face of column-Loading North 111

4.20 Strain profile of N-S top bars of SP-B at south face of column-Loading North 112

4.21 Strain profile of N-S top bars of SP-B at north face of column-Loading South 113

4.22 Strain profile of N-S top bars of SP-B at south face of column-Loading South 114

4.23 Top N-S bar force profile of SP-A at north face of column-Loading North 115

4.24 Top N-S bar force profile of SP-A at south face of column-Loading North 116

4.25 Top N-S bar force profile of SP-A at north face of column-Loading South 117

4.26 Top N-S bar force profile of SP-A at south face of column-Loading South 118

4.27 Top N-S bar force profile of SP-B at north face of column-Loading North 119

4.28 Top N-S bar force profile of SP-B at south face of column-Loading North 120

4.29 Top N-S bar force profile of SP-B at north face of column-

	Loading South	121
4.30	Top N-S bar force profile of SP-B at south face of column- Loading South	122
4.31	Stiffness Parameter (K)	123
4.32	Lateral Drift Vs Stiffness	124
4.33	Column Deflection vs Overall Expansion at Mid-Height of Slab of SP-A- Loading North	125
4.34	Column Deflection vs Overall Expansion at Mid-Height of Slab of SP-A- Loading South	126
4.35	Column Deflection vs Overall Expansion at Mid-Height of Slab of SP-B- Loading North	127
4.36	Column Deflection vs Overall Expansion at Mid-Height of Slab of SP-B- Loading South	128
4.37	Slab Deflection Profile of SP-B at Peak Drift Values – Loading North	129
4.38	Slab Deflection Profile of SP-B at Peak Drift Values – Loading South	130
4.39	Photographs of SP-A after Failure	131
4.40	Photographs of SP-B after Failure	132

Notations

b	Width of beam strip.
D	Dead load.
d	Flexural depth of the slab.
$\mathbf{E_c}$	Modulus of Elasticity of concrete.
$\mathbf{E_s}$	Modulus of Elasticity of steel.
f'c	Compressive strength of concrete in MPa.
$\mathbf{f_y}$	Yield strength of flexural reinforcement.
h	Story height.
$\mathbf{I_c}$	Moment of Inertia of Column.
$\mathbf{I_s}$	Moment of Inertia of Slab.
l	Clear span of slab.
K	Stiffness of Connection.
L	Live load.
M	Total unbalanced moment.
$\mathbf{M_u}$	Total ultimate unbalanced moment transferred.
t	Total thickness of slab.
V	Total shear force around critical section.
v_c	Factored shear stress resistance provided by the concrete.
$\mathbf{V_f}$	Factored shear force.
v_f	Factored shear stress.
$\mathbf{V_o}$	Ultimate shear capacity without moment transfer.

V_u Ultimate shear force.

γ Importance factor.

Δ Inter-story drift.

1. Introduction

1.1 General

Reinforced concrete slabs are one of the most widely used structural elements. In addition to providing a versatile and economical method of supporting the vertical loads, the slabs in many structures form an integral portion of the structural frame to resist lateral loads. A common structural form is a column-supported flat plate. A flat plate is a two-way slab without projecting beams, drop panels or capitals. Flat plates are an economical form of high-rise construction because the absence of projections simplifies formwork and reduces field labor. In addition, the flat plate provides flexibility on the layout of columns and requires the least storey height.

The design of a flat plate is often controlled by the shear strength of the slab around the column. The non-linear behavior of concrete makes analysis of slab-column connections extremely difficult. Despite the considerable research no usable design method has been developed for slab-column joints that is based on a theoretically sound model of behavior.

The nature of the shear strength of the slab around the column becomes more critical due to lateral loads caused by wind or earthquake. Lateral loads produce moment transfer at the slab-column connections, and may cause brittle fracture of the connection. The brittle failure of a connection during an earthquake may cause significant damage to the whole building structure.

In order to increase the ductility and avoid brittle failure of flat plate, a general trend is the provision of carefully detailed shear reinforcement in the slabs.

Earlier research has proved that load carrying capacity and ductility of flat plate structure increased considerably by using different kind of shear reinforcement in the form of stirrups, shear heads or inclined cranked bars.

1.2 Objective

The purpose of this experimental program is to investigate the viability of partially debonding the flexural reinforcement of the slab in the vicinity of the connection as a means of increasing drift capacity. The debonding of reinforcement can reduce the strain concentration around the joint region, thus reducing the accumulated damage at the slab-column junction due to cyclic loading.

The debonding of reinforcement requires minimal preparation compared to conventional shear reinforcement. It can be used in new construction as well as for rehabilitation purposes.

The main objectives of this experimental study are:

a) To model a full scale specimen with accurate boundary conditions, to investigate and understand the true behavior of the slab-column connection subjected to cyclic loading.

b) To determine the structural behavior of a partially debonded slab-column connection subjected to cyclic loading and compare it to the behavior of a conventional, fully bonded slab-column connection.

c) To assess the effect of cyclic loading on the deterioration of load capacity and stiffness of the slab-column connection.

2. Literature Survey

2.1 Background of Previous Work

Many tests have been performed to investigate the strength of concentrically loaded flat-plate column connections transferring shear only between the slab and the column. These tests have led to several semi-empirical design procedures.

For eccentrically loaded flat-plate column connections transferring both moment and shear there is an apparent decrease in shear capacity with increasing moment transferred. The problem of shear and moment transfer becomes particularly important when lateral loads due to earthquake or wind cause a substantial unbalanced moment to be transferred between the slab and the column. Cyclic lateral loading causes the stiffness of slab-column connections to deteriorate gradually with increasing drift.

Previous investigations by (Hawkins, Mitchell et al. (1975), Islam and Park (1976), Megally and Ghali (2000)) have shown that stiffness and drift and shear capacity of the connection can be increased markedly by using shear reinforcement in the form of stirrups and shear studs.

A review of previous research for transferring unbalanced moment in slab-column connection subjected to cyclic loading with or without shear reinforcement is discussed below

2.1.1 Hawkins, Mitchell and Hanna (1975)

Hawkins, Mitchell and Hanna report tests on five full-scale slab column specimens containing integral beam stirrups. The specimens were tested under constant gravity load coupled with reversed cyclic lateral loads. A typical plan view of test specimen and test setup is shown in Figure 2.1.

All slabs measured 3960 x 2130 x 152 mm with 304 mm square column extended 1220 mm above and below the slab. The main variables were the amount and distribution and the extent of shear reinforcement.

Concentrating the slab reinforcement in the vicinity of the column did not markedly improve either the strength or the ductility. Extending the shear reinforcement zone markedly improved the ductility. The additional reinforcement length also prevented bond failure and permitted development of all the flexural reinforcement across the full width of the slab.

The authors conclude that the provision of shear reinforcement in the form of stirrups can increase the ductility, energy dissipation and strength characteristics of slab-column connection. But in order for shear reinforcement to be fully effective they suggest that :

(a) Stirrups should be closed hoops, anchored by 135° standard bends around one or more longitudinal bars.

(b) The shear reinforced zone should extend far enough out from the column face into each column strip so that the wide beam shear force V_u on the punching shear periphery outside the stirrups, shown in Figure 2.2, satisfies the relation $\frac{V_u}{bd} \leq 0.17\sqrt{f'c}$.

Where f'c is the concrete strength in MPa, b is the width of beam strip and d is the flexural depth of the slab.

(c) The perimeter of the shear reinforced zone should not approach closer than 1.5h to the column perimeter.

2.1.2 Islam and Park (1976)

Islam and Park report eight tests conducted on interior flat plate column connection subjected to combined gravity and seismic loading. All slabs were 3048 x 2286 x 89 mm. The main variable was the kind of shear reinforcement. Three specimens had no shear reinforcement, three had closed ties, one had cranked bars and one had a shearhead.

A typical plan view of test specimen and test setup is shown in Figures 2.3 and 2.4.

The authors conclude from their test results that slab-column connections with no shear reinforcement have little ductility. Failure occurs suddenly by diagonal tension cracking and splitting of the concrete along the bars in the top of the slab on the more critically loaded side of the column.

Cranked bars resulted in an increase in the shear strength of the connection but did not cause an increase in the ductility of the connection.

Closed stirrups produced more ductile behavior at large deflections than did the shearhead reinforcement. The authors attribute the success of closed stirrups not only to the torsion and shear resistance provided by the stirrups but also to their ability to hold the top and bottom slab reinforcement together in the vicinity of the column. This holding action prevents the slab bars at the tension face of the slab from splitting off the cover concrete, and thus prevents the column from punching through the slab on critical side.

2.1.3 Robertson and Durrani (1992)

Robertson and Durrani tested three half-scale models of a single story two-bay prototype frame. The test specimens measured 2900 x 2000 with a 114 mm thick slab.

All specimens had the same amount of flexural reinforcement. Stirrups were provided in the two exterior connections across the whole width of the specimen.

The main variable was the level of gravity load. The top of the columns were connected to a distribution beam by means of load cells that measured shear in each column. The lateral load was applied to the distribution beam.

Specimen A with lightest gravity load sustained the highest lateral load. Specimen A reached a peak lateral load of 88 kN at 3.5 % drift. Specimen B with medium gravity load, reached a peak lateral load of 58.2 kN at 1.5% drift and specimen C with the highest gravity load reached a peak lateral load of 42.7 kN at 1 % drift.

Punching failure occurred at exterior connection of specimen A whereas the other two specimens with higher levels of gravity load failed at the interior connection. For all three specimens, the interior connection stiffness decreased rapidly with increasing amount of drift. The post-punching stiffness of the two specimens B and C was 20 % of the value prior to punching.

From their test results the authors conclude that increasing gravity load at the interior connection considerably reduces the stiffness and capacity of the connection to transfer unbalanced moment. For the two specimens where the applied shear exceeded 30 % of the nominal concentric punching capacity, the ACI building code design approach for transferring shear and unbalanced moment at an interior connection was unconservative.

2.1.4 Megally and Ghali (2000)

Megally and Ghali report five tests to examine the seismic behavior of edge-column connections. All test specimens were 1900 x 1351 mm with 152 mm thick slab. Four slabs were provided with shear reinforcement in the form of shear studs. The fifth specimen contained no shear reinforcement. The main variables in their test were the provision of shear studs, spacing between shear studs and value of shearing force V_u transferred between the column and the slab.

The loading was applied in three stages. In stage I shearing force V and unbalanced moment M are applied simultaneously to simulate gravity loads. In stage II cyclic lateral

displacements were applied on the column ends with their amplitude increased in increments. Each increment represents an approximate increase in the drift ratio equal to 0.3 percent. In stage III shearing force V and unbalanced moment M are applied simultaneously in load control mode to examine the residual strength of the slab-column connections. The test specimen and loading arrangement is shown in Figures 2.5 and 2.6.

All specimens failed by punching shear of the slab in the column vicinity. Specimens with shear stud reinforcement had higher ductility, lateral drift capacity, stiffness and strength than specimens without shear reinforcement.

The authors conclude that slab-column connections with no shear reinforcement subjected to cyclic loading fail in brittle punching shear mode at relatively low drift ratios particularly if applied shear V_u is high.

Using shear studs not only increases the ductility and punching strength of the slab-column connection but significantly reduces the rate of stiffness deterioration under cyclic lateral loading. Also with shear studs no limit on applied shear V_u is necessary to achieve ductile behavior. Based on their experiments on edge-column connections they propose that the value of v_c given in ACI 421.1 R-92 (revised 1999) for the design of shear reinforcement as

$$v_c = 3\sqrt{f'c} \text{ psi} \qquad [2.1]$$

should be replaced by

$$v_c = 1.5\sqrt{f'c} \text{ psi} \qquad [2.2]$$

where v_c is a limiting shear stress to be carried by concrete.

2.1.5 Hwang and Moehle (2000)

Hwang and Moehle tested a 0.4 scale 9-panel flat-plate structure subjected to gravity and reversed cyclic loading. The test specimen measured 8230 x 5490 mm with 81 mm thick slab. The floor slab was symmetrical about the centerline in the longer direction. The design philosophy for the selection of the reinforcement was different for the two halves of the floor on either side of the longitudinal centerline. The specimen was designed according to ACI 318-83. In one half of the specimen, redistribution of slab moments from negative to positive was assumed. No redistribution was assumed in the other half. This resulted in a different arrangement of reinforcement in two halves of the specimen.

Nineteen different variations of loading were applied to the specimen. Lateral load was applied in both N-S and E-W directions. The gravity load was varied during each test sequence. The gravity load was applied using dead weights on the slab.

The authors conclude that the part of the specimen designed without redistribution responded within acceptable limits of cracking and deflection under service loads. The half of the structure designed with moment redistribution had lower connection stiffness and higher reinforcement strains.

The effect of different arrangement of reinforcement detail at the edge of the slab was not apparent at service or ultimate load levels.

The measured stiffness was compared with values calculated using the effective beam width and equivalent frame models. The effective beam width and equivalent frame

models overestimate the slab stiffness at an inter-story drift ratio of 1/400. Even if the beam stiffness of either model is reduced by 1/3 to account for cracking, the system stiffness is still overestimated.

2.2 Discussion of Previous Results

In previous research, failure of a slab-column connection under lateral cyclic loading has been defined as loss of moment transfer capacity. It is generally accepted that a slab-column system should be able to undergo a drift of between 1.5 % and 2 % without failure.

It has been found that the drift capacity of a connection decreases with increasing gravity load. For connections with $V_u < 0.3\ V_o$, achieving 1.5 % to 2 % drift is generally not a problem. Values of drift as high as 4 % are possible with shear reinforcement, even with gravity loads in excess of $0.3\ V_o$. Failure for connections with no shear reinforcement is marked by a sudden and nearly complete loss of moment capacity, in the order of 80 %. Connections with shear reinforcement show a gradual softening response after peak moment.

Previous research shows that the equivalent frame method adopted in CSA 23.3-94 and ACI (318-95) for calculating the stiffness of the connection is appropriate for gravity load analysis where lateral load deflections are not an issue. For lateral load analysis, cracking under applied load considerably reduces the stiffness of the system at larger drifts.

Modifications are required in calculating the stiffness of the system by using equivalent frame model to accurately represent the lateral load behavior of connections at higher drifts.

2.2.1 Discussion of Previous Test Methods

Previous tests can be categorized as either :

1) Multicolumn, multipanel tests such as those by Hwang and Moehle or Robertson and Durrani ; or
2) Single column tests such as those by Hawkins, Mitchell and Hanna, Islam and Park or Megally and Ghali.

The two types of test each have advantages and disadvantages as outlined below.

Multicolumn, multipanel specimens generally have the most accurate boundary conditions. As a result, they provide the best information regarding the stiffness and deflections of slab-column systems. Because multicolumn tests are to some degree indeterminate, it may be difficult to measure internal stress resultants. The specimens are large and expensive to test and produce. In addition, they may have to be scaled down to fit laboratory facilities.

Single column tests are relatively inexpensive and easy to produce and test. Most laboratories can accommodate full-scale specimens. As the specimens are or at least can be made statically determinate, internal forces can be calculated from measured loads.

Rotational boundary conditions are particularly difficult to achieve, with the result that internal force distributions may not accurately model a prototype. For example, the tests by Islam & Park resulted in unequal vertical boundary loads to achieve the desired deflected shape. With poor boundary conditions, the deflections of single column tests do not accurately represent true behavior. As a result, measurements and stiffness and deflections are unreliable.

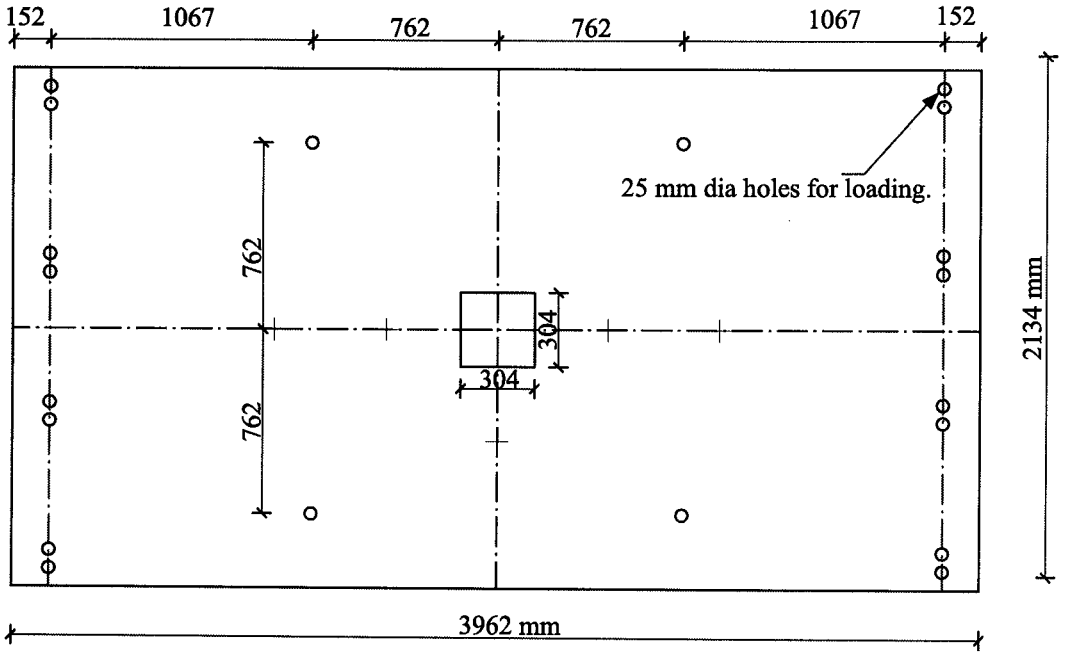

Plan View

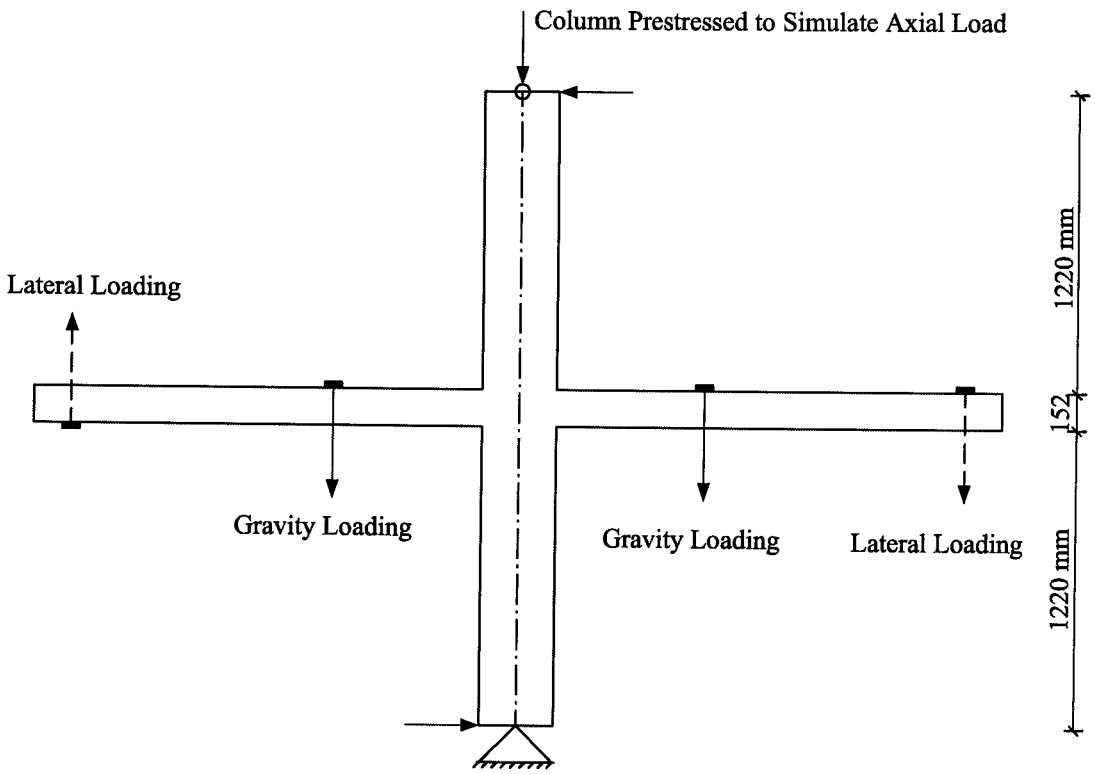

Elevation

Figure 2.1 Loading Arrangement for (Hawkins et al. (1975)) Test Specimen

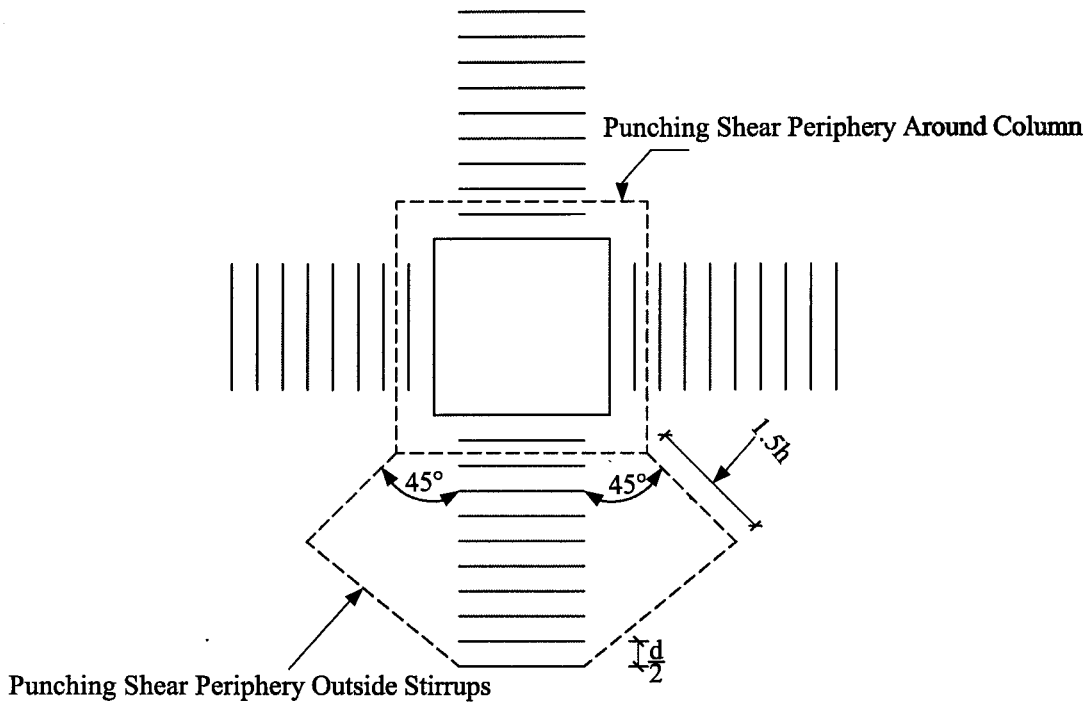

Figure 2.2 Critical Punching Shear Peripheries

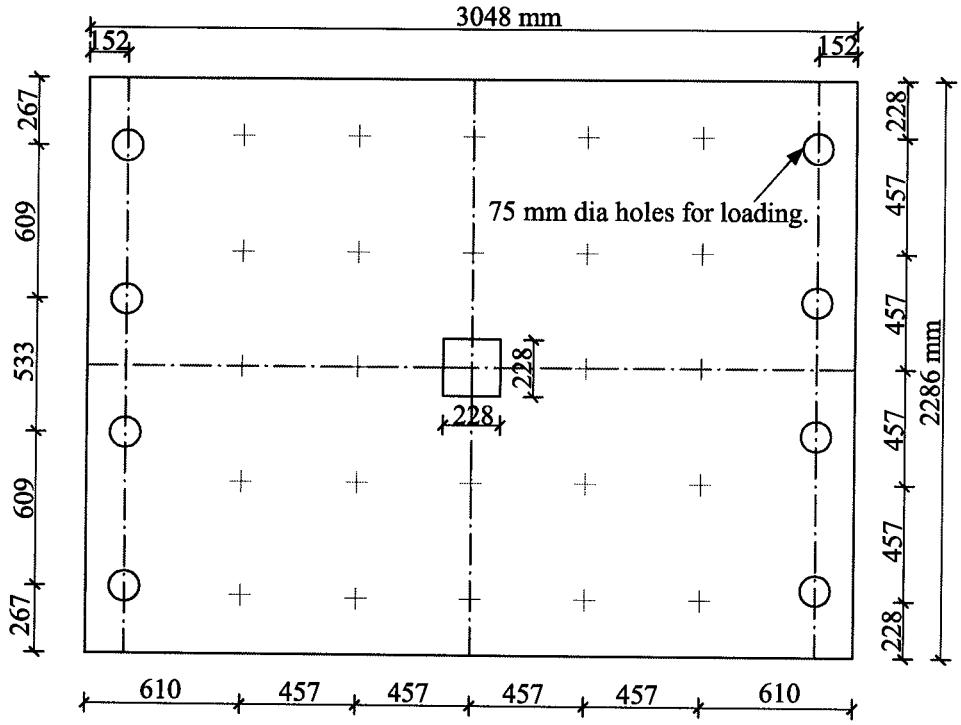

Figure 2.3 Plan of (Islam and Park (1976)) Test Specimen

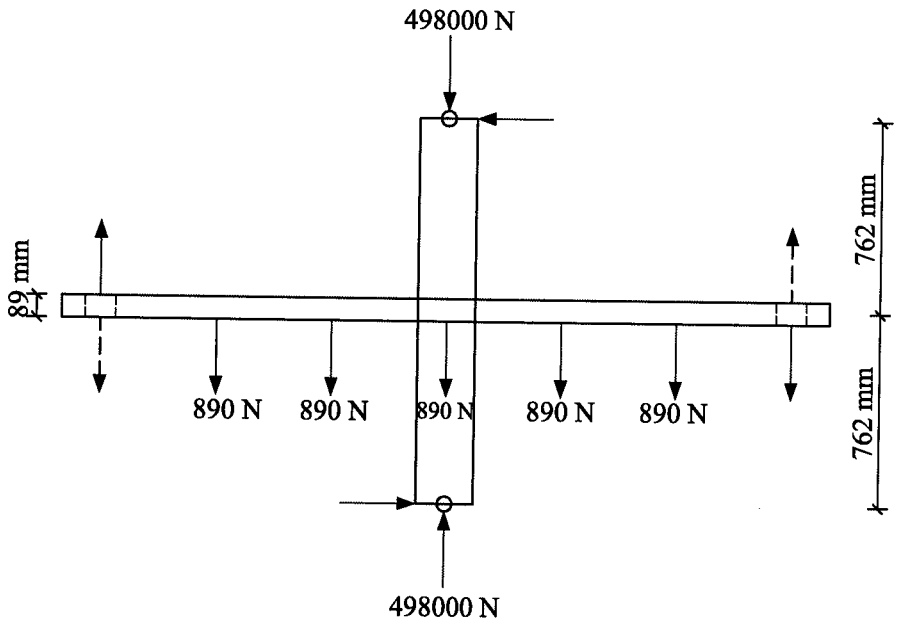

Figure 2.4 Loading Arrangement of (Islam and Park (1976)) Test Specimen

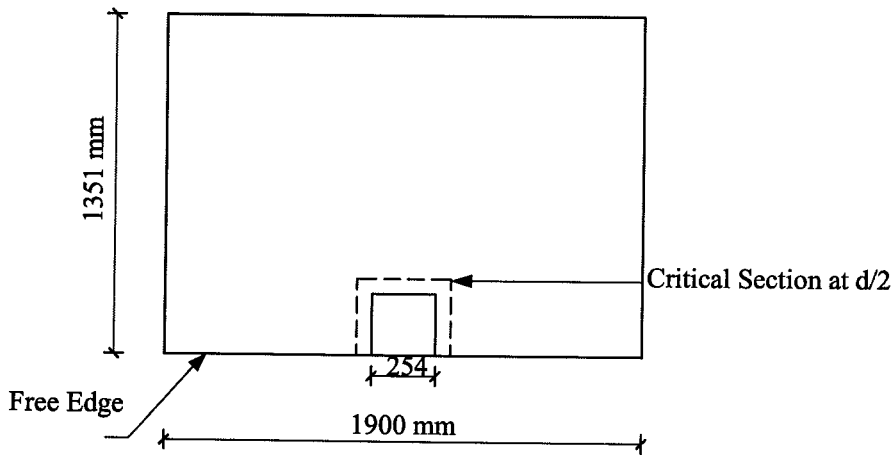

Figure 2.5 Plan of (Megally and Ghali (2000)) Test Specimen

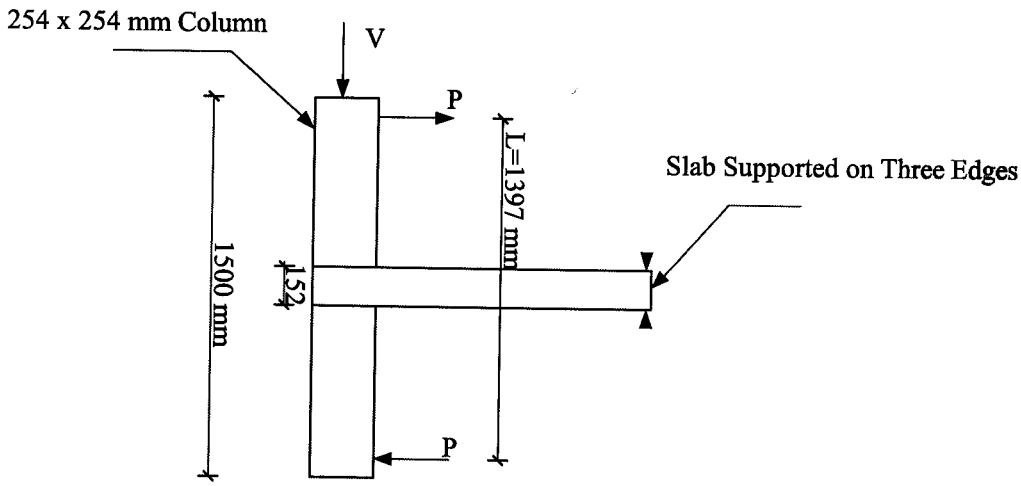

Figure 2.6 Loading Arrangement of (Megally and Ghali (2000)) Test Specimen

3. Test Specimen and Test Apparatus

3.1 EXPERIMENTAL PROGRAM

Two full-scale specimens designated SP-A and SP-B were built to model reinforced concrete flat plate-column connections of a multi-story building. The only difference between the two was that SP-A contained partially debonded reinforcement whereas SP-B contained fully bonded reinforcement.

3.2 DESIGN OF THE TEST SPECIMEN

3.2.1 Prototype Structure

A plan and elevation of the prototype structure on which test specimens were based are shown in Figures 3.1 and 3.2. The prototype is a flat plate structure typical of multi-story apartment buildings. The slab was designed in accordance with CSA-A33.3-94 for a service live load of 1.9 kN/m^2 as prescribed by NBC for apartment buildings and a total service dead load of 4.35 kN/m^2. The dead load included the self weight of slab as well as partitions and finishes.

3.2.2 Geometry of the Specimen

A plan and elevation of the test specimen is shown in Figure 3.3 and Figure 3.4.
The test specimen consisted of a 4.2 m square slab with a 355mm (14") square column protruding 1.5 m above and below the slab. The slab thickness was 152mm (6"). The dimensions of the test specimen were selected similar to those of a prototype connection.

However the flexibility of the edge restraining system necessitated reducing the size of the specimen from 4.5 m square to 4.2 m square, as discussed in section 3.5.2.1.

The lateral load was applied in the N-S direction.

3.2.3 Slab Design

Slab was designed for both gravity and lateral loading. The governing factored load combination for design, consistent with A23.3-94 Cl 8.3.2, is

$1.0D + \gamma\,(0.5\,L + 1.0\,E)$

where D is the dead load, L is the live load and E is the effect of earthquake, γ importance factor, in this case unity. A yield strength of 400 MPa for the flexural reinforcement and a compressive strength of 30 MPa were assumed in the design.The direct design method was used to calculate gravity load moments. The total unbalanced moment resulting from lateral load was calculated based on a 2% inter story drift and was estimated to be 82 kN-m. The following relationship was used for calculating the lateral load moment

$$V = \frac{\Delta}{\frac{h^3}{12\,E_c\,I_c} + \frac{l\,h^2}{12\,E_s\,I_s}} \qquad [3.1]$$

where V is the column shear, h is the story height and $E_c\,I_c$ ans $E_s\,I_s$ are the product of the modulus of elasticity and the moment of inertia for the column and slab respectively.

A23.3-94 requires that a fraction of the unbalanced moment be transferred by flexure within a width extending 1.5 times the slab thickness past the sides of column. The top flexural reinforcement of the specimen consist of six 15M bars placed within this defined

width and remaining eight 15M bars @ 250 mm were centered outside this region. The top mat reinforcement layout is shown in Figure 3.5 to Figure 3.8.

Minimum reinforcement governed for the bottom mat, shown in Figure 3.9 and 3.10. Bottom bars through the column were increased to 15M to satisfy integrity steel requirement of A23.3-94.

3.2.4 Column Design

The column reinforcement is shown in Figure 3.11 and Figure 3.12. The column was designed to carry an axial load of 760 kN. This load was intended to represent gravity loading equivalent to approximately of 10 stories. The load was imposed on the column by means of post-tensioning. The post tensioning assembly is shown in Figure 3.13 and Figure 3.14. The column was extended to mid-story height of 1424 mm above and below the slab.

The column was reinforced with eight 20M longitudinal bars and 10M ties and had a flexural capacity greater than that of the slab. The specified yield strength of the bonded reinforcement was 400 MPa. The column was concentrically post-tensioned with an unbonded M35 Dywidag prestressing bar in a 44 mm diameter duct.

3.3 MATERIALS

3.3.1 Concrete

Concrete for the column was mixed in the lab and had a nominal 28 days compressive strength of 35 MPa. Type 10 Portland cement, coarse washed sand and local coarse aggregate composed primarily of high quartzite sandstone, quartzite and hard stone with a 14 mm maximum size were used for the casting of column. Three concrete cylinders (150 x 300) were taken to measure the compressive strength of the mix.

For the slab, normal density concrete with a specified slump of 75mm and a specified design strength f'c of 30 MPa was obtained from a local ready mix supplier. Ten concrete cylinders (150 x 300) were cast for determining the compressive and tensile properties of the mix. The cylinder tests were carried out immediately after the testing of corresponding slab. Results of the compression and split cylinder tested at different ages of the concrete are shown in Table 3.1.

3.3.2 Reinforcement

For each specimen bars of the same size came from the same heat. Tension coupon tests were performed on two samples from each heat. Each sample measured 254 mm in length. The test results are shown in Table 3.2. Force-strain curves are shown in Figure 3.15 and Figure 3.16.

3.4 Fabrication Procedure

3.4.1 Form Work

The slab form work, shown in Figure 3.17, was constructed from 20mm thick plywood. The plywood was suitably stiffened by wooden I-beams.

It was necessary to provide forty-eight holes in the slab. Sixteen holes were required to hang the dead weights and thirty-two holes were required for the edge restraining system. To provide the holes in the slab, the form work included forty-eight 25 mm dia round steel rods supported on the plywood vertically by means of screws. These steel rods were greased and covered with plastic tubes to ease removing them later on.

Strain gauge wires passed through the side walls of the form.

After assembly, the slab form work was set on a scaffold consisting of steel frames with adjustable legs and aluminum beams. Prior to casting of each slab, the form work was coated with a light form oil.

The column form work was made from 20 mm thick plywood in such a way that column could be casted separately.

3.4.2 Placing of Reinforcement

The column reinforcement was assembled separately and was placed into the wooden forms. For post-tensioning of column, a 35 mm diameter Diwydag bar, 4000 mm in length was placed inside a 44 mm diameter duct. To hold the duct in position, the top end

was wired to the column cage. The column cage was placed on a 355 x 355 x 38 mm plate with four 75 mm long studs welded to the plate at the positions shown in Figure 3.18.

The bars for the bottom mat in N-S direction were welded with 75x75x6 mm thick plate at each end so that bars would not pull out during the application of lateral load. The bars for the bottom mat in E-W direction were anchored with standard 180° hooks at each end.

3.4.3 Partially Debonded Reinforcement

Specimen A contained partially debonded reinforcement. The central four top bars in both the N-S and E-W direction were partially debonded. In total eight 15M bars were debonded for a length of 795 mm as shown in Figure 3.19 and Figure 3.20. The debonded region was greased and enclosed in a plastic tube. The plastic tube was then wrapped with plastic tape.

3.4.4 Placing of Concrete

Each specimen was cast in three stages. The column steel cage was placed and aligned in the lower wooden forms. Concrete was mixed and placed up to the level of the slab soffit. Due to the mixture size, two batches were required for the casting. Three control cylinders were taken from the second batch to determine f 'c of the mixture. After two days, the lower column form was stripped and column was placed under the slab formwork on a temporary support.

The slab was cast four weeks later. A local ready-mix company provided concrete for the slab. Three concrete control cylinders were taken at the beginning of pouring of the slab and seven more cylinders were taken when half of the slab was poured. Concrete was placed by hand and compacted with an internal vibrator. The top surface of slab was leveled using timber screeds and later trowelled smooth. About 6 hours after concrete was placed , the test specimen and control cylinders were covered with polythene sheets. Moist curing continued for seven days. From then until the time of testing the specimen were exposed in the laboratory which has a fairly constant temperature of 20°C. Side formwork was stripped off after three days.

The upper portion of the column was cast two days after the slab.

3.5 TEST SETUP

The test set-up of specimen is shown in Figures 3.21 and 3.22. The main features of test-setup are column supports, edge restraining system, vertical links and steel reaction frame.

3.5.1 Supports

The lower end of the column representing mid-height of the story was designed to act as pin. The supports consisted of a ball and socket joint with load cell and rollers as shown

in Figure 3.23. The roller was needed so that the horizontal load cell would measure the full horizontal reaction at the bottom of column.

The top of the column on both the north and south side was connected to horizontal jacks by means of a 25mm dia threaded rod. One end of the threaded rod was attached to the jack by a coupler and the other end was connected to a horizontal load cell. The horizontal load cell measuring the load in the threaded rod was fitted in to the slots mounted on the side of the column as shown in Figure 3.24, creating a pin connection. Each jack was connected to a steel bracket fixed to the steel reaction frame as shown in Figure 3.25.

To restrain sideway, the steel reaction frame was braced on top by means of beams attached to the frame. The bottom of the frame was bolted to the strong floor.

3.5.2 Slab Boundary Restraining System

The slab boundary restraining system was designed to accurately reflect the boundary conditions of the prototype structure under both gravity and lateral load. The boundary restraining system allowed horizontal translation in the N-S direction at all edges. Rotations at all edges were constrained and vertical deflections at the N-S edges were prevented. The boundary restraining system consisted of an edge restraining system and vertical links.

3.5.2.1 Edge Restraining System (ERS)

Ideally the edge restraining system under gravity load should produce the moment diagram and deflected shape shown in Figure 3.26 (i.e. zero rotation and maximum moment at edge) representing the midspan of the prototype. Since the ERS was not infinitely stiff, it could not produce a non-zero moment with zero rotation. The combination of moment and rotation at 2.1 m from the column centerline was found to be consistent with the stiffness of the ERS. Hence, the specimen dimensions were set at 4.2 m square. The deflected shape of specimen under gravity load with ERS is shown in Figure 3.27.

The edge restraining system was mounted on the top of the slab. It consisted of eight independent frame-type assemblies, evenly spaced in the N-S and E-W directions. Each assembly consisted of two rectangular HSS and a 25mm dia threaded tie rod. The tie rod was made with two pieces linked with a coupler. Each HSS measured 160 x 160 x 10 mm with a base plate 300 x 235 x 35 mm tied down to the slab by means of two 350mm long 25mm dia threaded rods. The height of rectangular HSS in N-S direction was more than the HSS in E-W direction to avoid conflict between the crossing tie rods measure the force in the rods. Each tie rod was equipped with a 30 kN load cell. This measurement was used to determine the positive moment along the free edges. The gravity ERS system is shown in Figure 3.28 and Figure 3.29.

3.5.2.2 Vertical Links

Ideally under lateral load the edges of the specimen perpendicular to the direction of lateral load should be restrained against vertical deflection but left free to rotate and to translate horizontally. The deflected shape of the specimen under lateral load should be as shown in Figure 3.2. To achieve the desired deflected shape, eight vertical links attached to the bottom of slab near the N-S edges (i-e the direction of lateral load). The vertical links acted as horizontal rollers, allowing the slab to move horizontally but restraining its movement in the vertical direction.

The deflected shape of specimen under both gravity and lateral load with vertical links and ERS is shown in Figure 3.30.

Each vertical link consisted of a 25 mm dia threaded rod. Vertical links were capable of resisting both a compressive and tensile force. To prevent the buckling of threaded rod under compression, bracing was provided consisting of four 75 x 50 x 6 mm plates attached to the threaded rod and bearing on the surrounding rectangular HSS 76 x 51 x 5.8 mm section. The detail of vertical links is shown in Figure 3.31 to Figure 3.34.

3.6 LOADING PROCEDURE

3.6.1 Gravity Loading

To simulate the prototype superimposed dead load plus live load, sixteen concrete blocks each weighing 1.9 kN was suspended from the slab in a symmetrical manner. The size of each block was 400 x 400 x 525 mm. The applied load approximated a superimposed dead load of 0.75 kN/m^2 and a live load of 0.95 kN/m^2 (i-e ½ of the service load of 1.9 kN/m^2 which was considered to be present during the earthquake). A 1500mm long chain and a coupler were used to hang the blocks as shown in Figure 3.35.

3.6.2 Lateral Loading

The lateral load system consisted of two reversible jacks setup to act in tension only. The jacks were hooked to a two-way pump as shown in Figure 3.36. The compression side of the two jacks linked together while the tension side was connected to the two-way pump. The jacks displaced the top of the column in N-S direction.

3.6.3 Column Loading

An axial load of 760 kN was maintained in the column throughout the test by means of a hydraulic jack. This load represents the column load in the lower storey of a 10 storey apartment building. The oil pressure was applied and regulated throughout the test by a hand pump.

3.7 INSTRUMENTATION

3.7.1 Load and Reaction Measurements

For an overall equilibrium check of the specimen, all horizontal and vertical loads were measured. All reactions were monitored through load cells.

The column prestress load was measured by a 900 kN load cell. The lateral force in the two lateral load jacks and the connecting rods at the top of column were measured by means of two horizontal load cells. The horizontal force at the bottom of column was measured by a 90 kN load cell and the net vertical force at the bottom of the column was measured by a 445 kN load cell.

The threaded rods in both the vertical links and the edge restraining system were equipped to act as load cells by installing strain gauges in a full bridge arrangement. The linear range for the edge restraining system load cells, designated as LD1 to LD8, was 30 kN. The range for the vertical links, designated as LD9 to LD16 was 50 kN.

3.7.2 Deflection Measurements

The laboratory floor was used as a reference for the vertical deflection measurements and an unloaded column attached to the strong floor was used as reference for the horizontal deflection measurements. The position of vertical LVDTs is shown in Figure 3.37. The position of horizontal LVDTs and cable transducer is shown in Figure 3.38. The travel of

LVDTs ranges from +75 mm to – 75 mm. The travel of cable transducer ranges from +250 mm to –250 mm.

To measure the deformation of the specimen eleven vertical and four horizontal Linear Variable-Differential Transformers (LVDT) were used. Vertical LVDTs were used to measure the deflection profile of the specimen and horizontal LVDTs were used to measure the rotation and translation of the slab. The horizontal LVDTs were mounted on a wooden frame, attached to the reference column. Aluminum extension arms were attached to the north and south edge of the slab. Wires were strung between the LVDTs and the extension arms at two levels, 150 mm and 880mm below the slab.

A cable transducer was used to measure the lateral deflection of the column relative to the reference column.

3.7.3 Rotation Measurement

Six Rotational Variable-Differential Transducers (RVDT) were used to measure rotations at specific points on the specimen. The positions of RVDTs are shown in Figure 3.39. RVDT1 and RVDT2 were used to measure the rotation of column with respect to slab-column joint. They are placed at a distance of 150 mm from the face of the column. The rotation of the slab with respect to the column was measured by RVDT3 through RVDT6.

3.7.4 Strain Measurements

Eighty-six electrical resistance foil strain gauges with a nominal resistance of 120 Ohm and a gauge length of 5 mm were used to measure strains in the steel reinforcement. At each gauge location the reinforcing bar was ground smooth. Grinding was restricted to a small area to reduce the effect of the strain gauge on the bond characteristics of the reinforcement. After grinding and sanding with emery paper, gauges were attached with an epoxy adhesive recommended for the gluing of strain gauges subjected to cyclic loading.

After soldering of lead wires, all gauges were covered with air drying acrylic agent to provide electrical insulation. A thick patch of silicon sealant was then applied on top of the gauge.

Gauge positions and labels are shown in Figures 3.40 to 3.43.

3.7.5 Recording and Monitoring Data and Loads

A 128 channel data acquisition system attached to a personal computer was used to record electronic data.

3.8 PROCEDURES

3.8.1 Setup Sequence

The specimen was lifted off of the form by means of a crane and positioned into the testing frame. For lifting purposes steel chains and shackles were attached to the specimen by cast-in place hooks. This arrangement permitted the slab to be lifted in its horizontal position. During lifting and positioning, ten strain gauges were monitored.

Once positioned into the test frame, the specimen was supported on temporary supports. All LVDTs were attached to the slab at this point, but no readings taken. The position of the slab was established by survey of sixteen points on the top surface.

The bottom end of the column was attached to the stand-off by means of bolts as shown in Figure 3.13 and Figure 3.14. The top of the column was ground to prevent the tips of lifting hook rebars from sticking out. After grinding, a layer of plaster was applied between the top column surface and the 40mm thick plate to ensure a smooth bearing surface for placing the jack on the top of the plate. A jack was used to post-tension the column.

The lateral load system was then attached to the steel reaction frame and the top of the column as shown in Figure 3.21. All strain gauges, load cells, LVDTs and RVDTs were connected to the data acquisition system.

Before attaching the edge restraining system, all strain gauges were initialized. An initial gauge reading was recorded. After attaching the edge restraining system, shown in Figure 3.28, another set of strain readings was taken.

At the start of each test, the ERS was pretensioned by tightening the 25 mm dia threaded rods against the HSS sections. Following the pretensioning of the ERS, the temporary supports were removed and the slab was allowed to deflect under its own weight. Another set of strain reading was recorded and a second survey of the slab was done. The next step was to hang the 1.9 kN concrete blocks from the slab as shown in Figure 3.3. The blocks were hung one by one in a symmetrical manner to avoid tipping the specimen. Once again strain readings were recorded and a third survey of the slab was done under full gravity load. Once the full gravity load was on the slab, the vertical links shown in Figure 3.31 were engaged.

3.8.2 Sequence of Testing

Before applying any lateral load to the specimen, an initial set of readings of all load cells, LVDTs, RVDTs, cable transducer and strain gauges was taken. The first loading step was to apply the 760 kN prestress to the column. Once the column was loaded, the first half cycle of the lateral load was applied in the southward direction in three increments of 2 mm each, until a displacement of 6 mm at the top of the column was reached. As the bottom end of the column was fixed against lateral movement, this 6 mm displacement corresponded to a story drift of H/500, which is a realistic amount of drift

that can be expected in real structures under service load. Readings of all instruments were recorded after each increment. The column was unloaded in a similar fashion with drift being reduced by 2 mm until the entire horizontal load was removed from the column. For the second half cycle, the direction of lateral load system was reversed from that of the first cycle. That is, the north lateral load jack was activated acting in north direction. The load was applied incrementally until the displacement at the top of the column in north direction reached a value equal to the first half of the cycle in south direction. The column was then unloaded in three increments to bring back to its neutral position.

The procedure for subsequent cycles of loading was similar to that of the first. In general, at least two additional cycles of loading were applied at the same peak displacement of the column, before increasing the displacement to a new value. For the second loading sequence, the column was displaced to 12 mm north and south from the neutral position. For the fourth and all subsequent loading cycles, at least 6 to 8 increments were taken between the zero and the peak deflection.

After the completion of every loading sequence the vertical links were released so that the slab could deflect under its own weight. Before commencing the next loading cycle, vertical links were again tightened. A complete loading history is presented in the next chapter.

Specimen		Age	Compressive Srength	Tensile Srength	Modulus of Elasticity
			f'_c	f'_t	E_c
		Days	MPa	MPa	MPa
A	Slab	28	32.7	2.9	25000
	Slab	78*	32.9	3.1	25800
	Column	78*	45.85	3.9	30500
B	Slab	28*	34.1	3	26300
	Column	28*	40	3.8	28500

* Time of slab tests.

Table 3.1 Concrete Properties

Specimen	Bar Size	Nominal Area	Yield Stress	Ultimate Stress	Modulus of Elasticity
		mm^2	MPa	Mpa	
A	10M	100	425	658	186500
	15M	200	394	549	193500
B	10M	100	415	653	179500
	15M	200	440	649	194500

Table 3.2 Properties of Reinforcing Bars

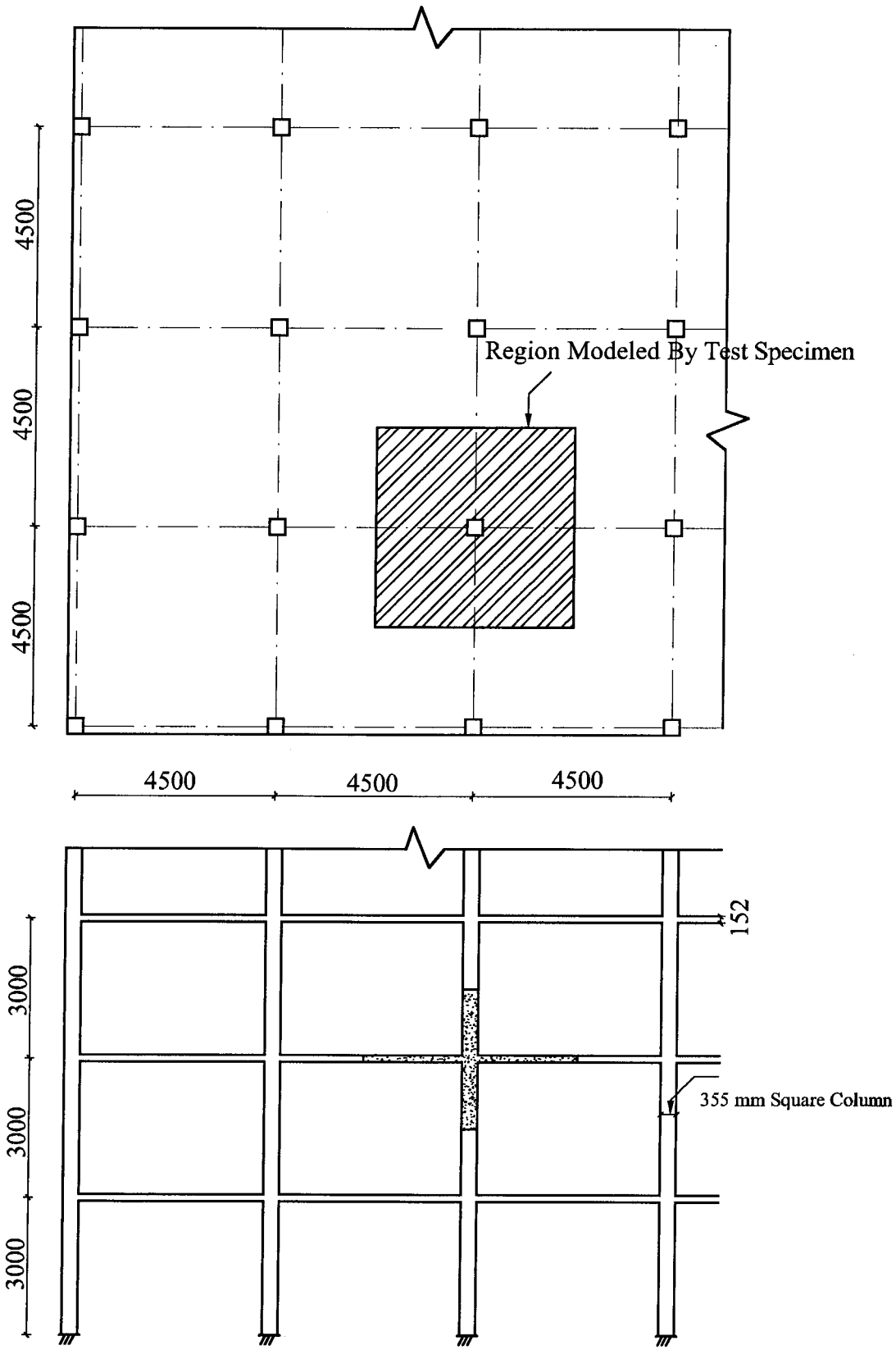

Figure 3.1 Prototype Flat Plate Structure

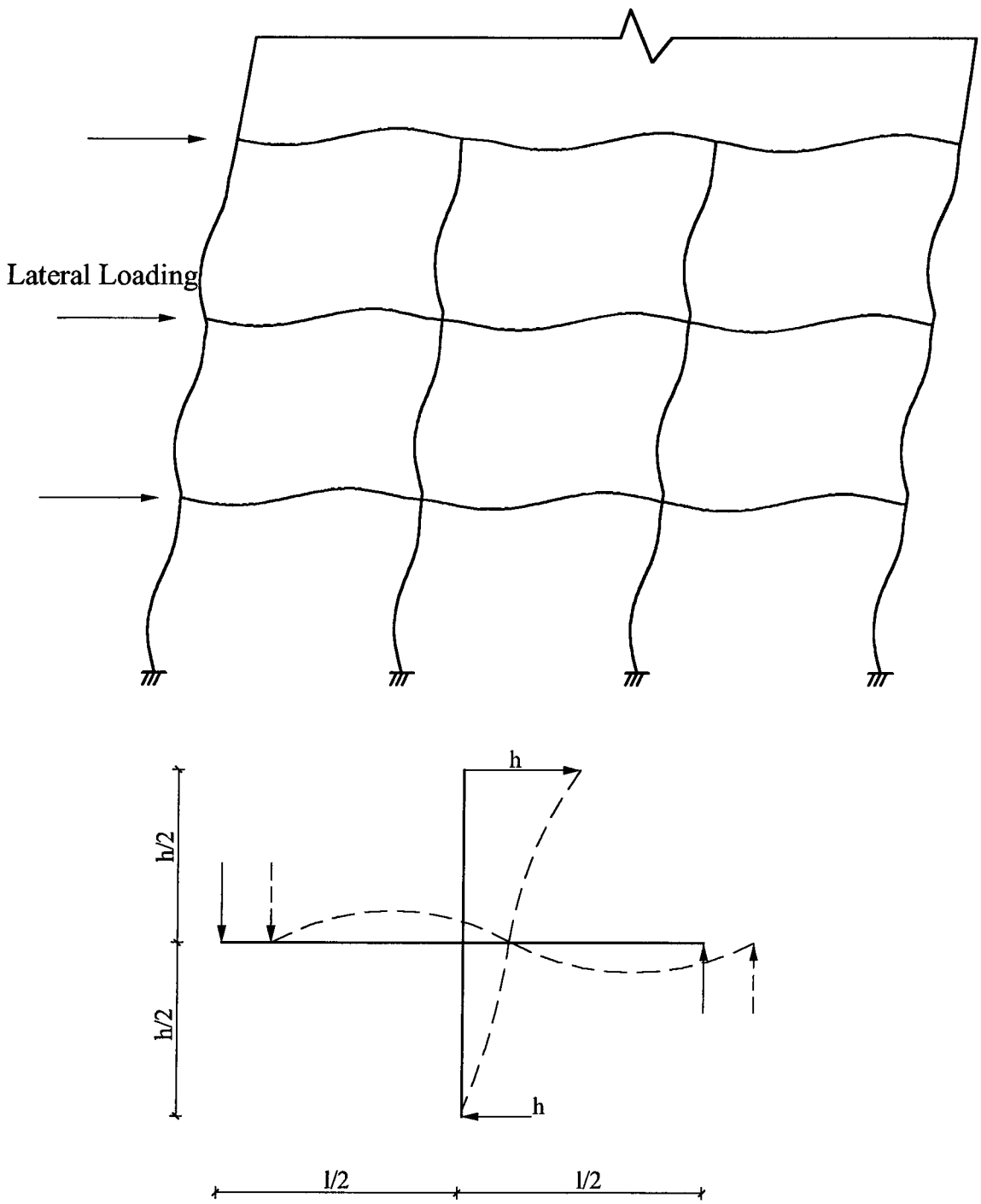

Figure 3.2 Typical Deflectd Shape of Prototype Structure

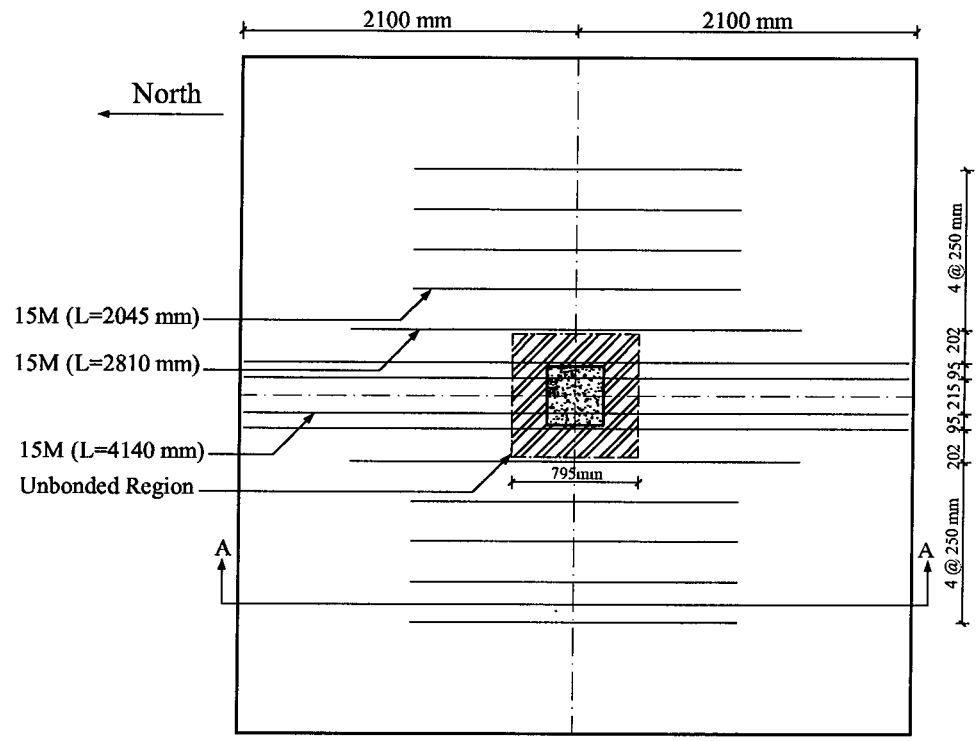

Figure 3.5 Layout of Negative Reinforcement in N-S Direction

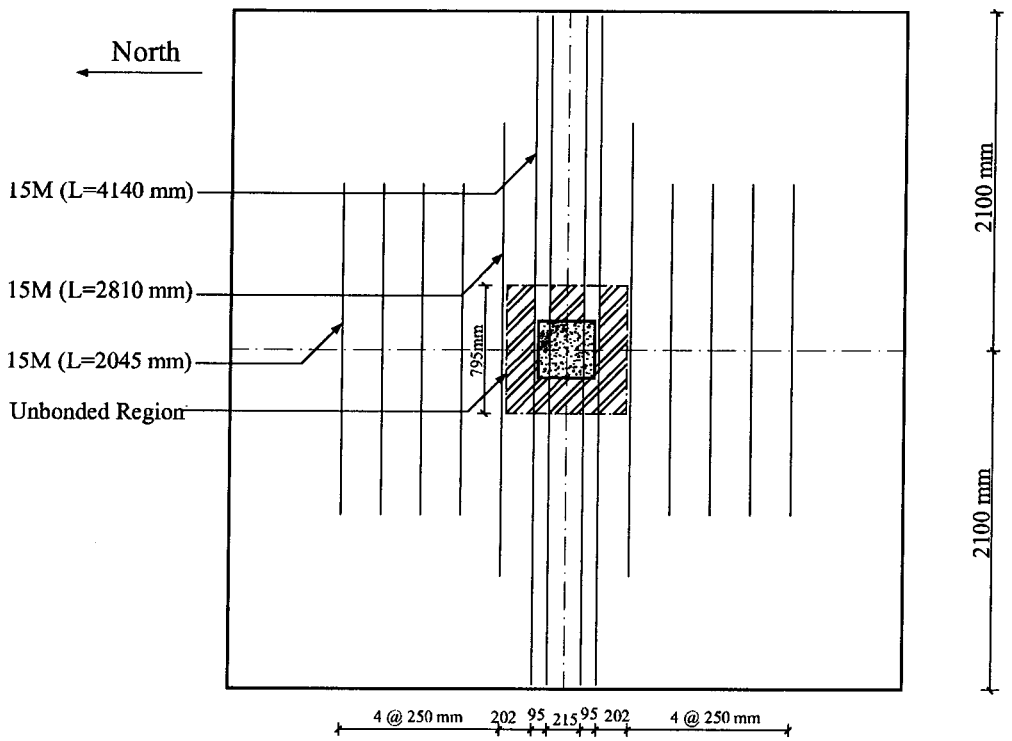

Figure 3.6 Layout of Negative Reinforcement in E-W Direction

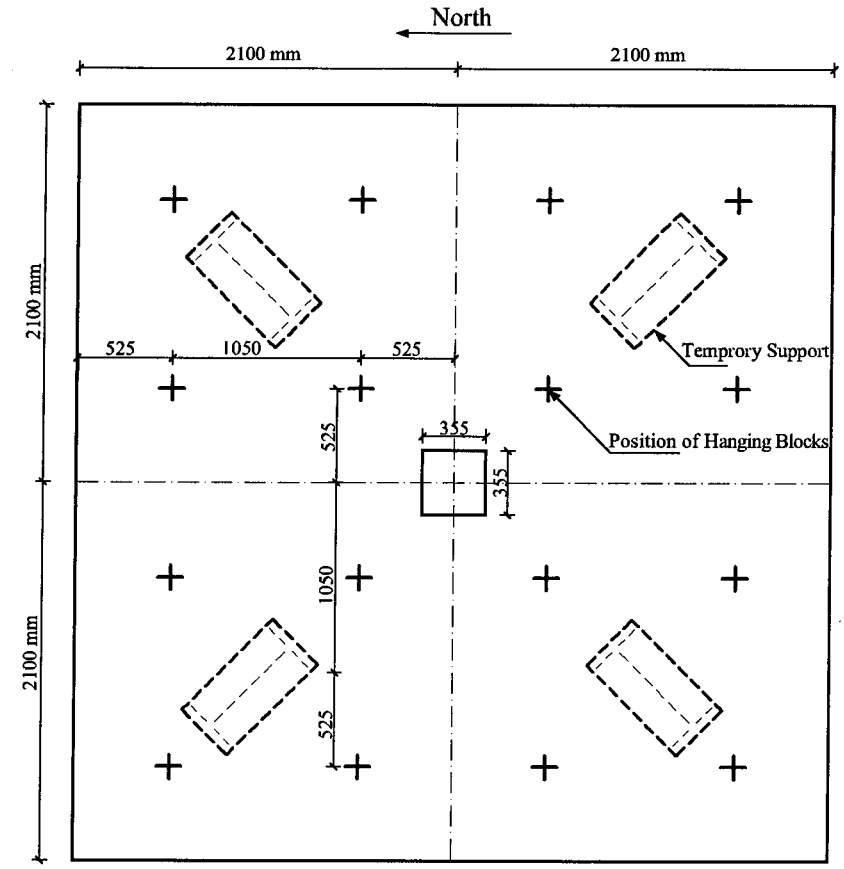

Figure 3.3 Plan of Specimen

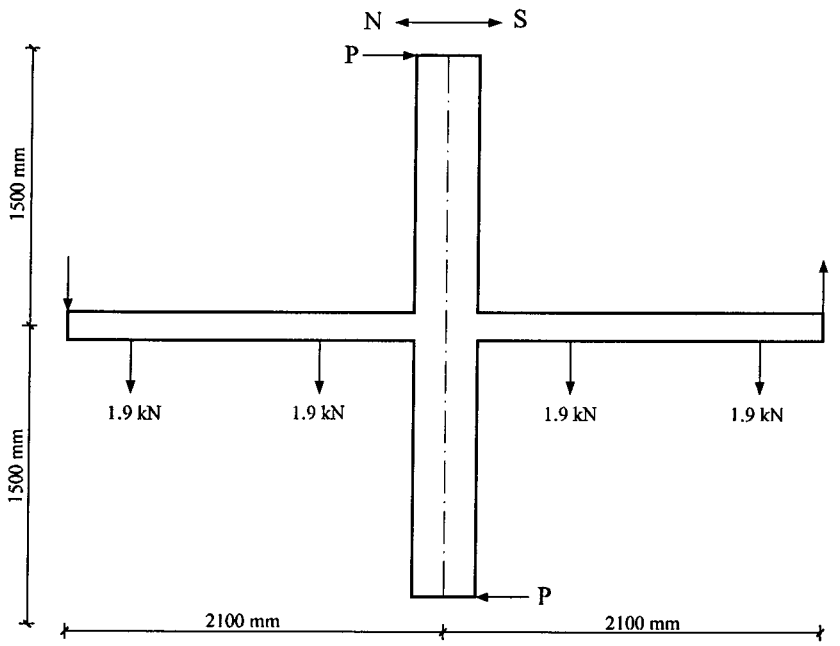

Figure 3.4 Side Elevation of Specimen

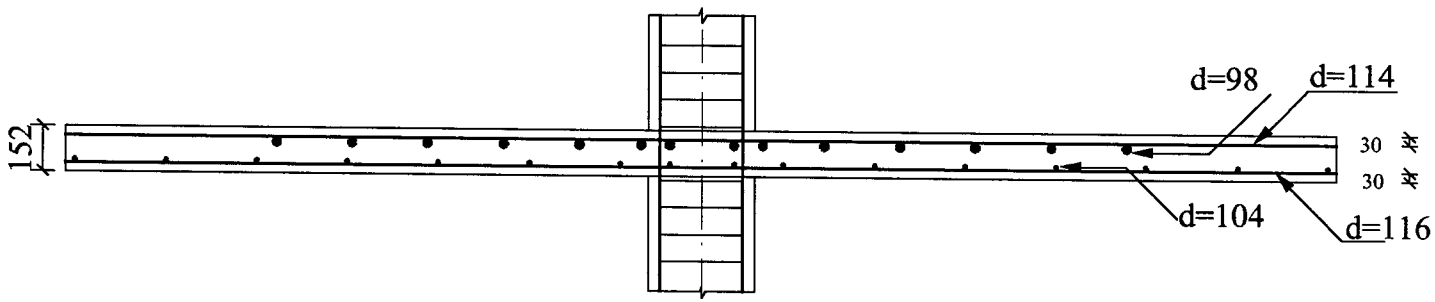

Section A-A of Figure 3.5

Figure 3.7 Detail of Reinforcement of Slab

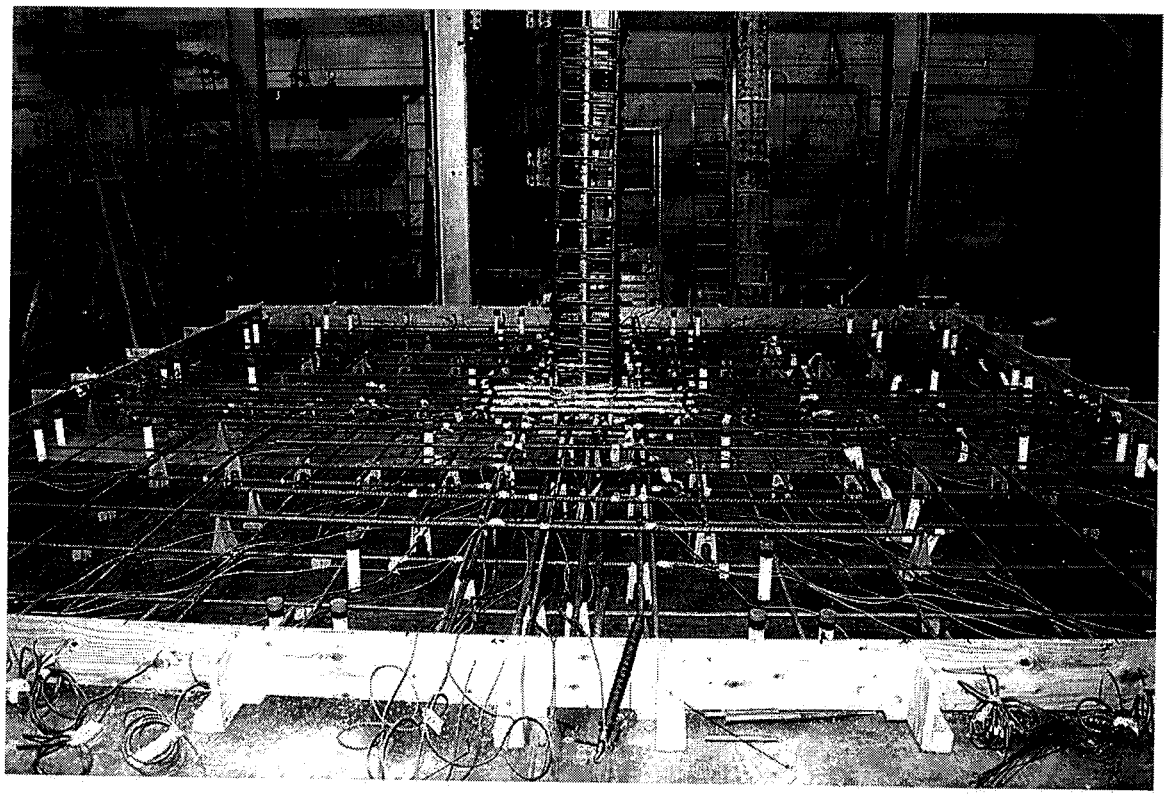

Figure 3.8 Top Reinforcement Layout

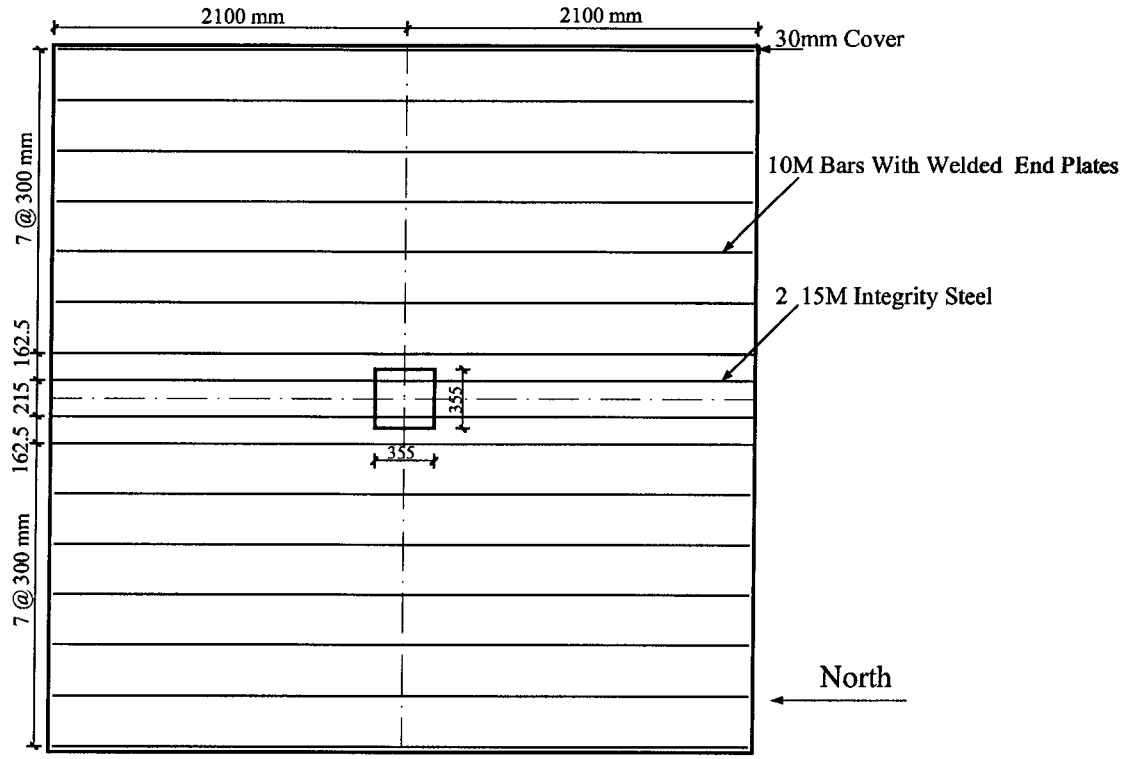

Figure 3.9 Layout of Positive Reinforcement In N-S Direction

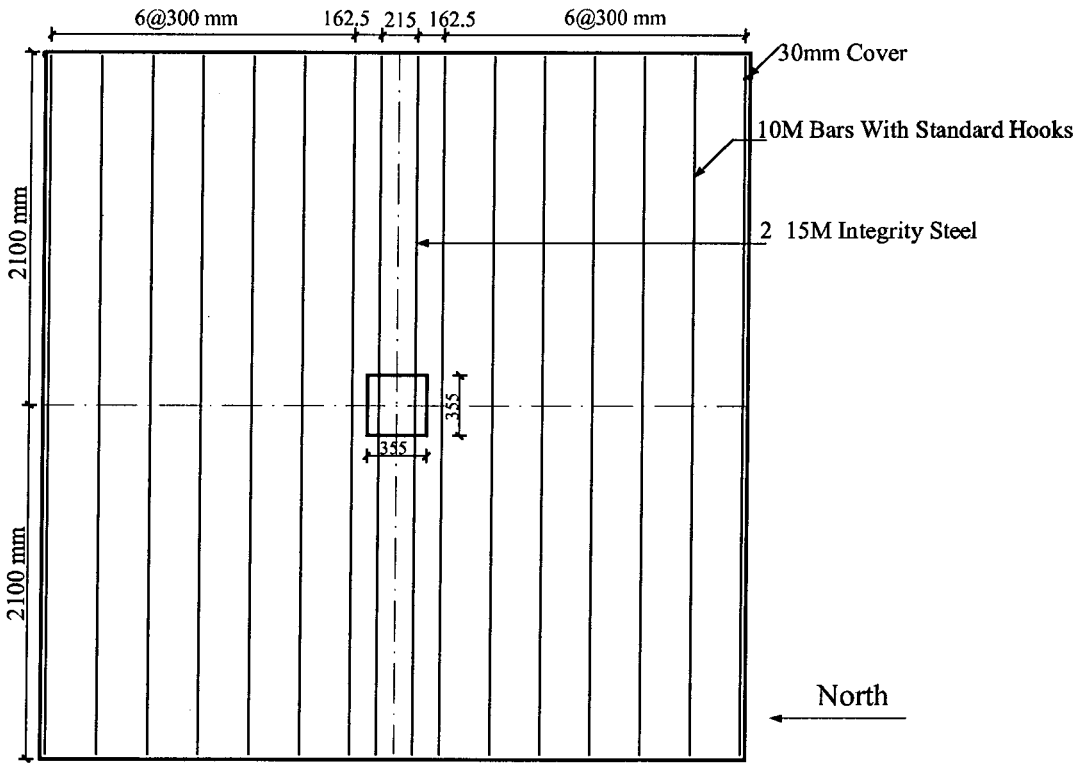

Figure 3.10 Layout of Positive Reinforcement In E-W Direction

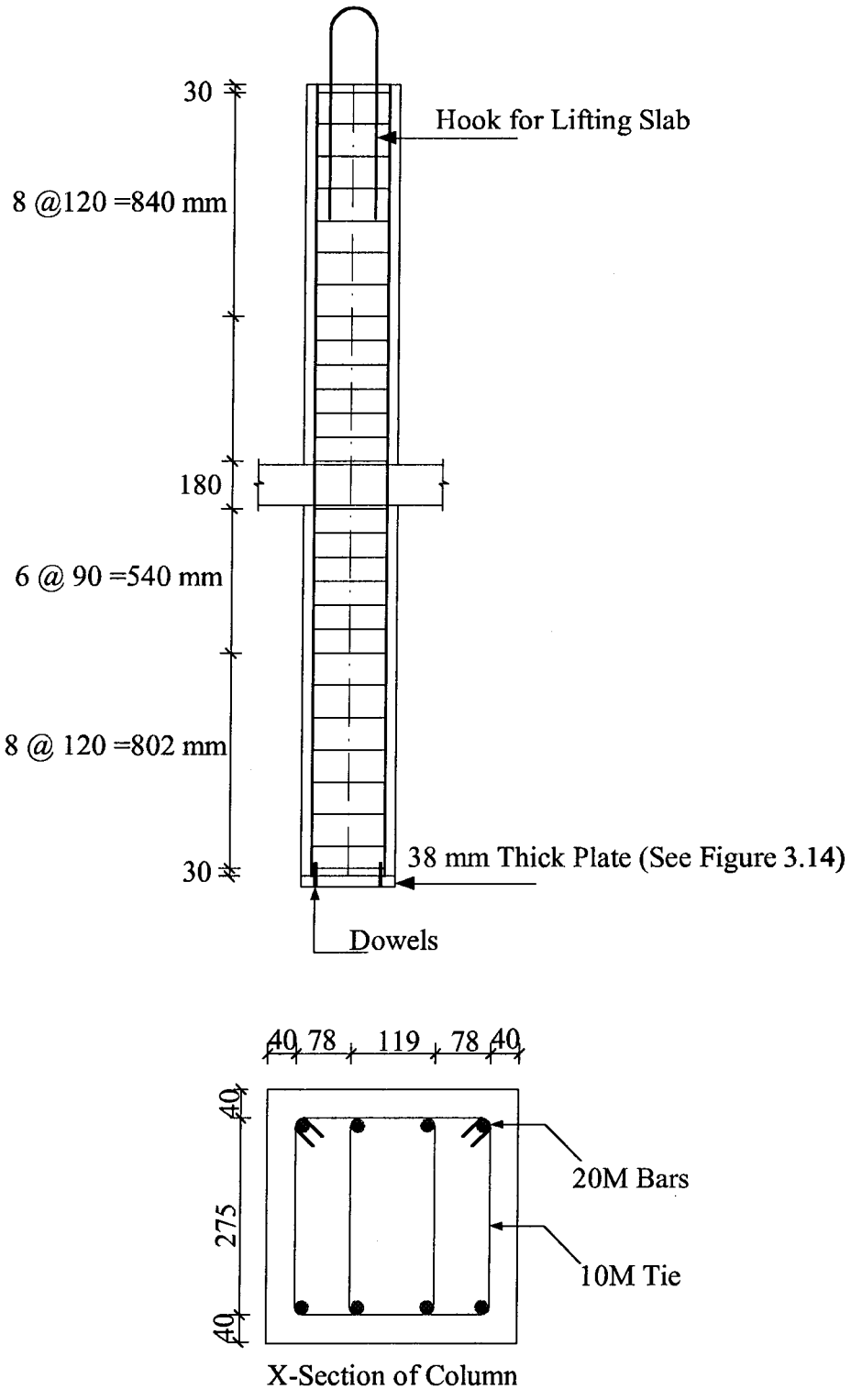

Figure 3.11 Dimension and Reinforcement of Column

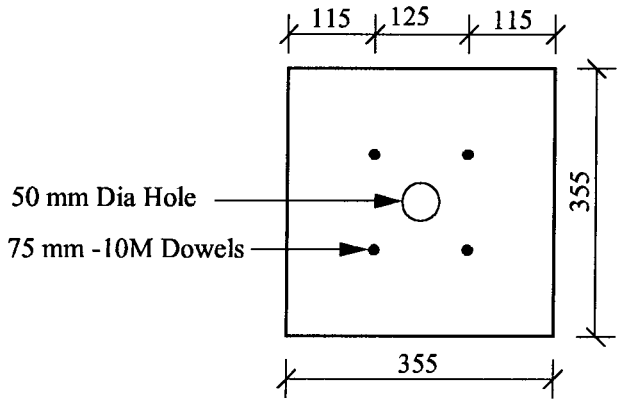

Figure 3.12 38 mm Thick Plate with Dowels

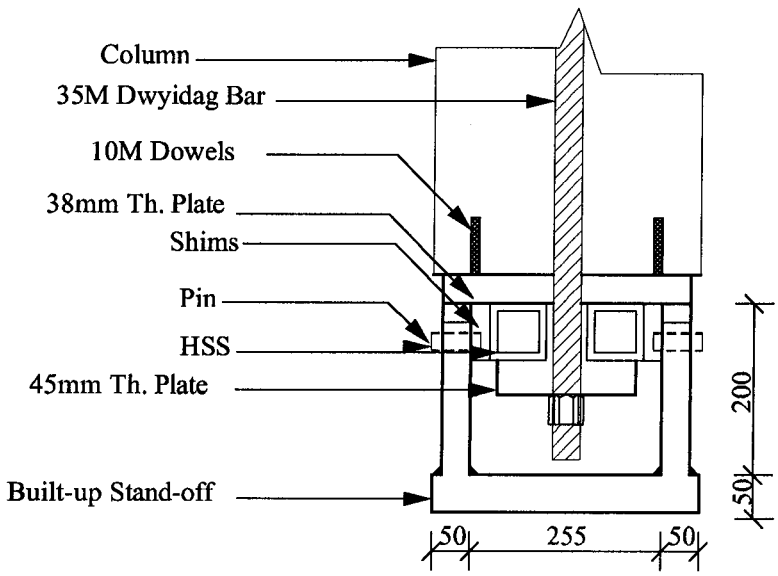

Figure 3.13 Stand Off for Post Tensioning

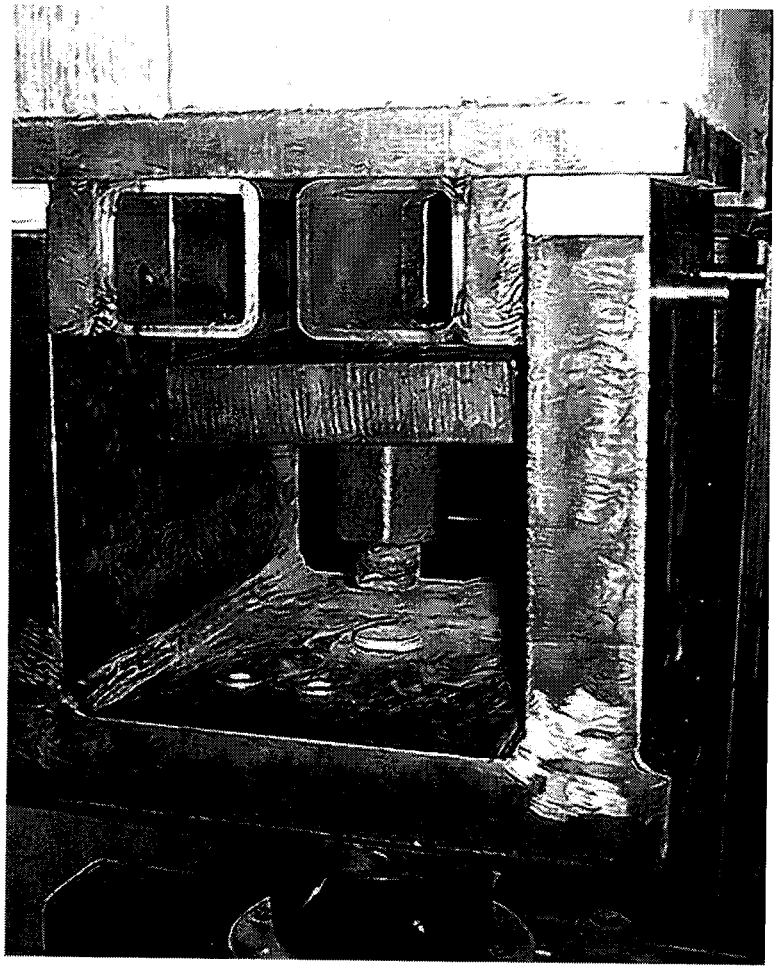

Figure 3.14 Stand Off for Post Tensioning Assembly

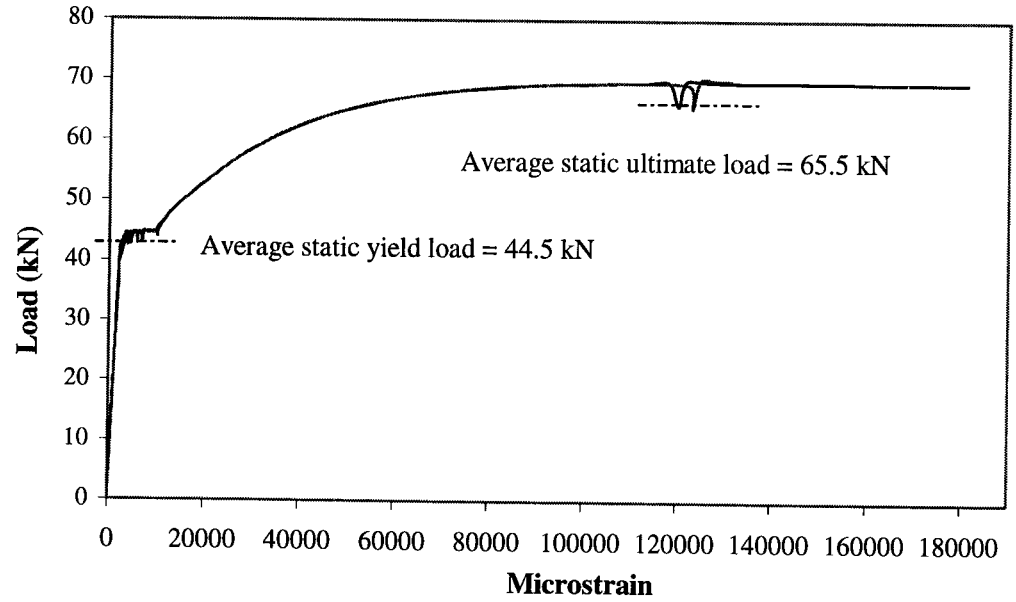

(a) 10M Deformed bars with nominal area of 100 mm^2

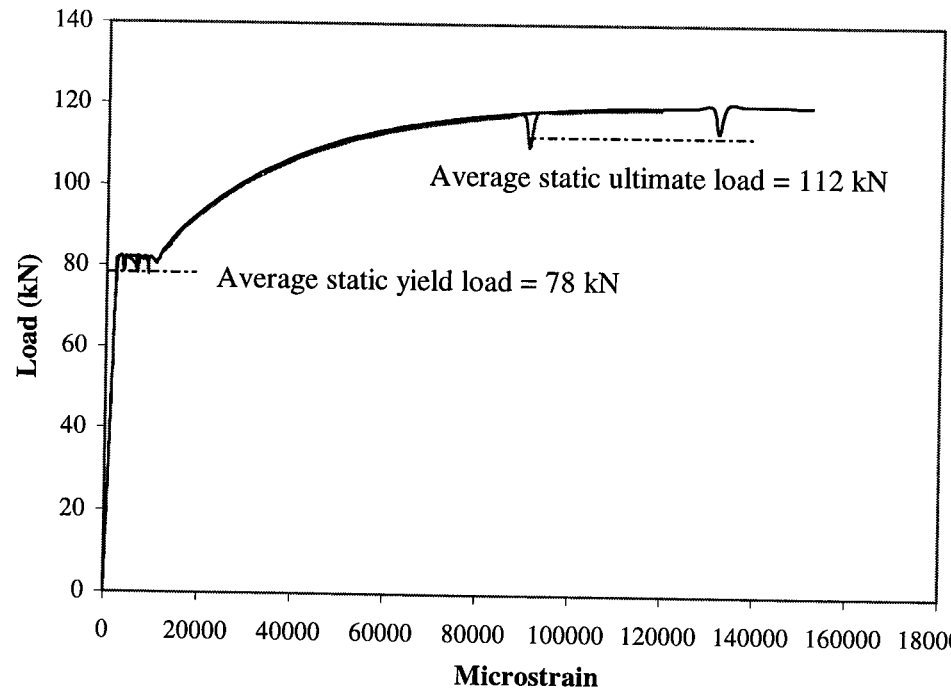

(b) 15M Deformed Bars with Nominal Area of 200 mm^2

Figure 3.15 Typical Force -Strain Curves of Reinforcement of Specimen A

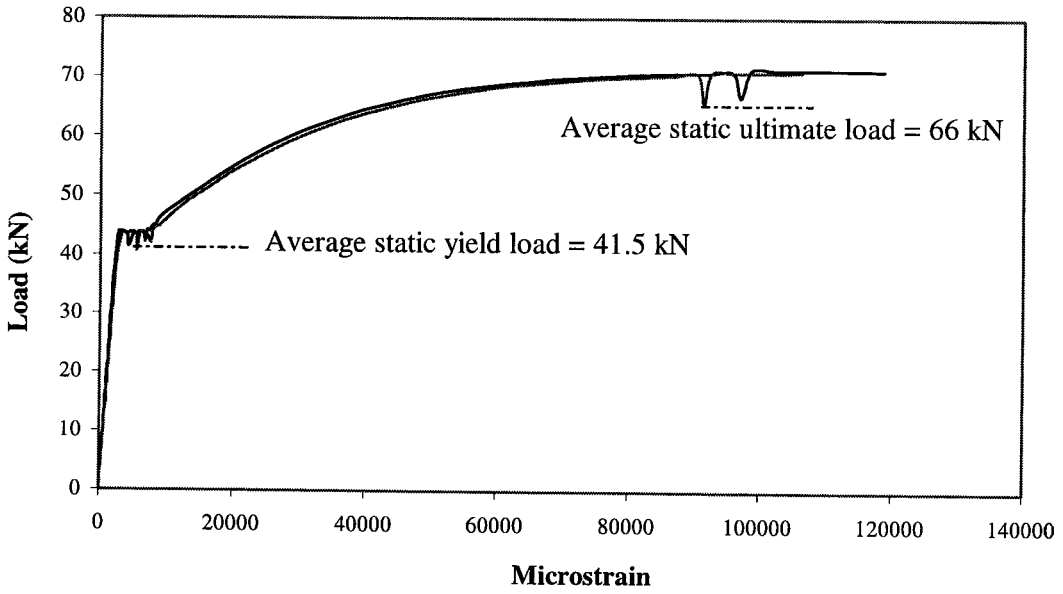

(a) 10M Deformed Bars with Nominal Area 100 m^2

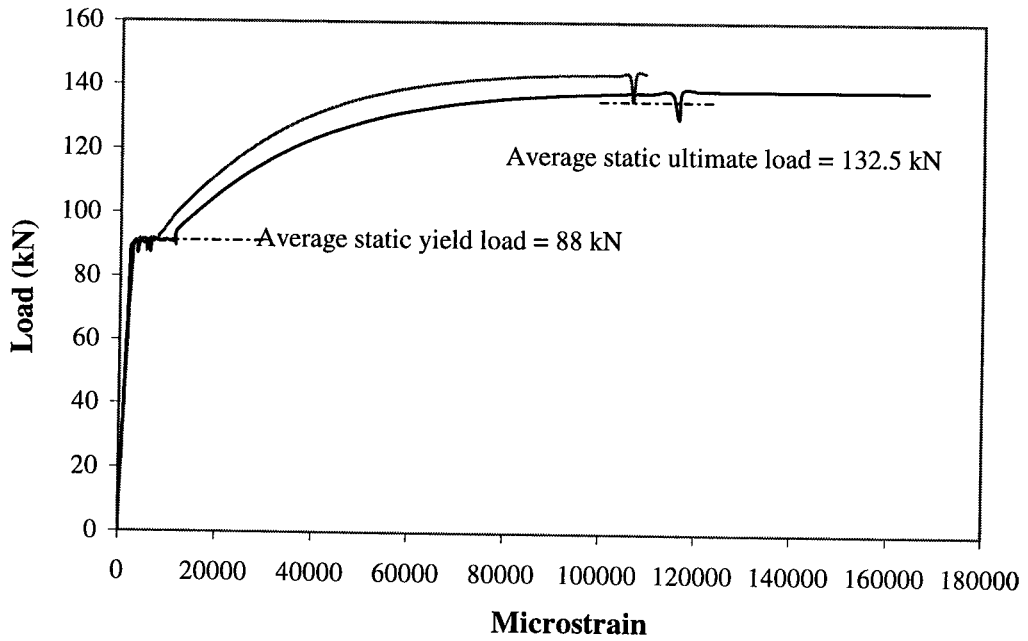

(b) 15M Deformed Bars with Nominal Area of 200 mm^2

Figure 3.16 Typical Force-Strain Curves of Reinforcement of Specimen B

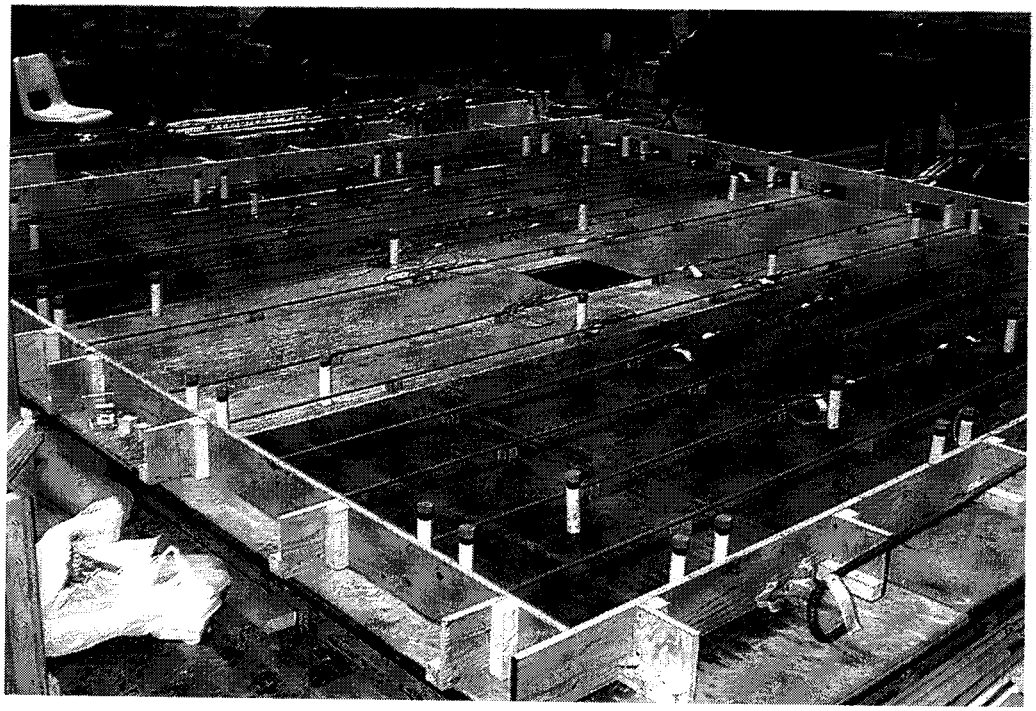

Figure 3.17 Form work of Slab

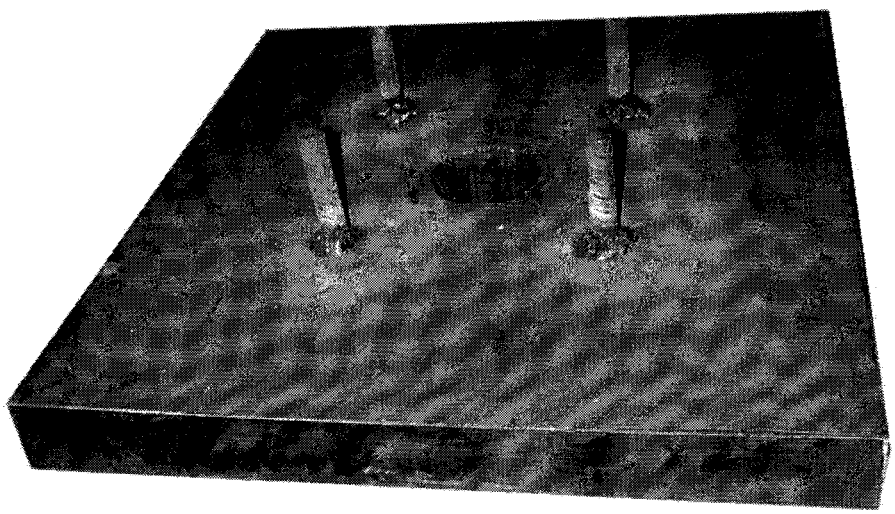

Figure 3.18 Column Base Plate with 10M Dowels

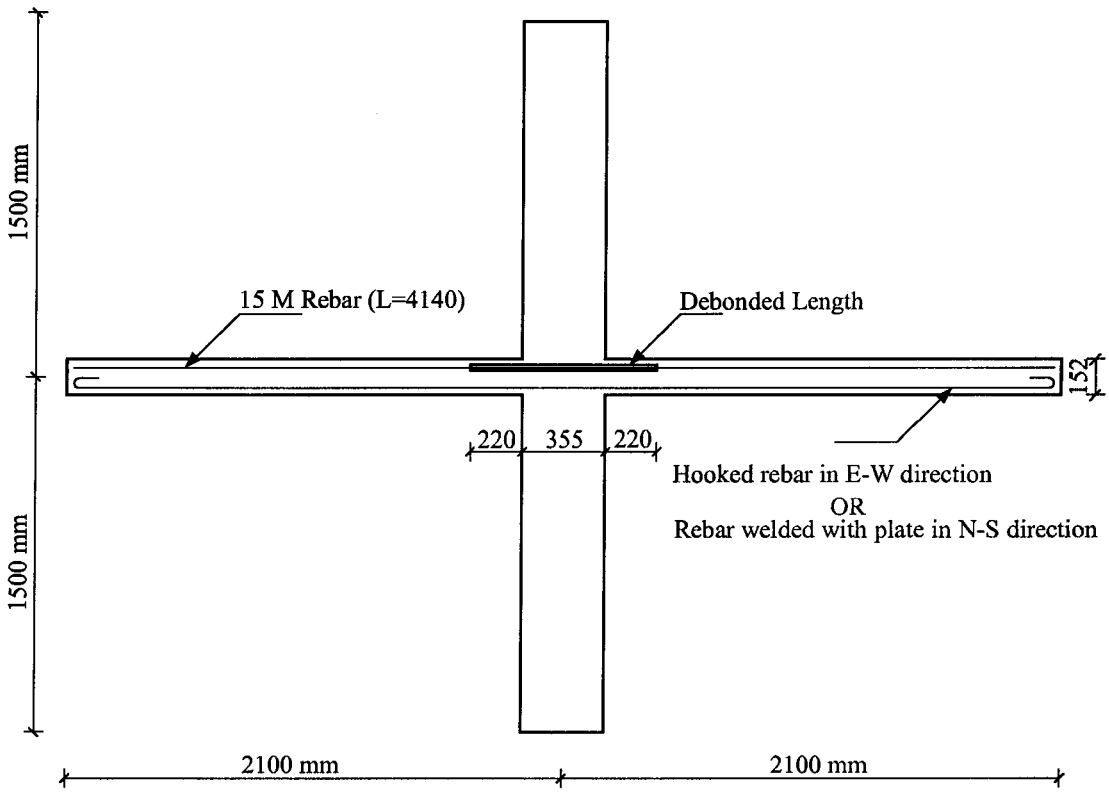

Figure 3.19 Slab-Column Connection with Partially Debonded Rebars

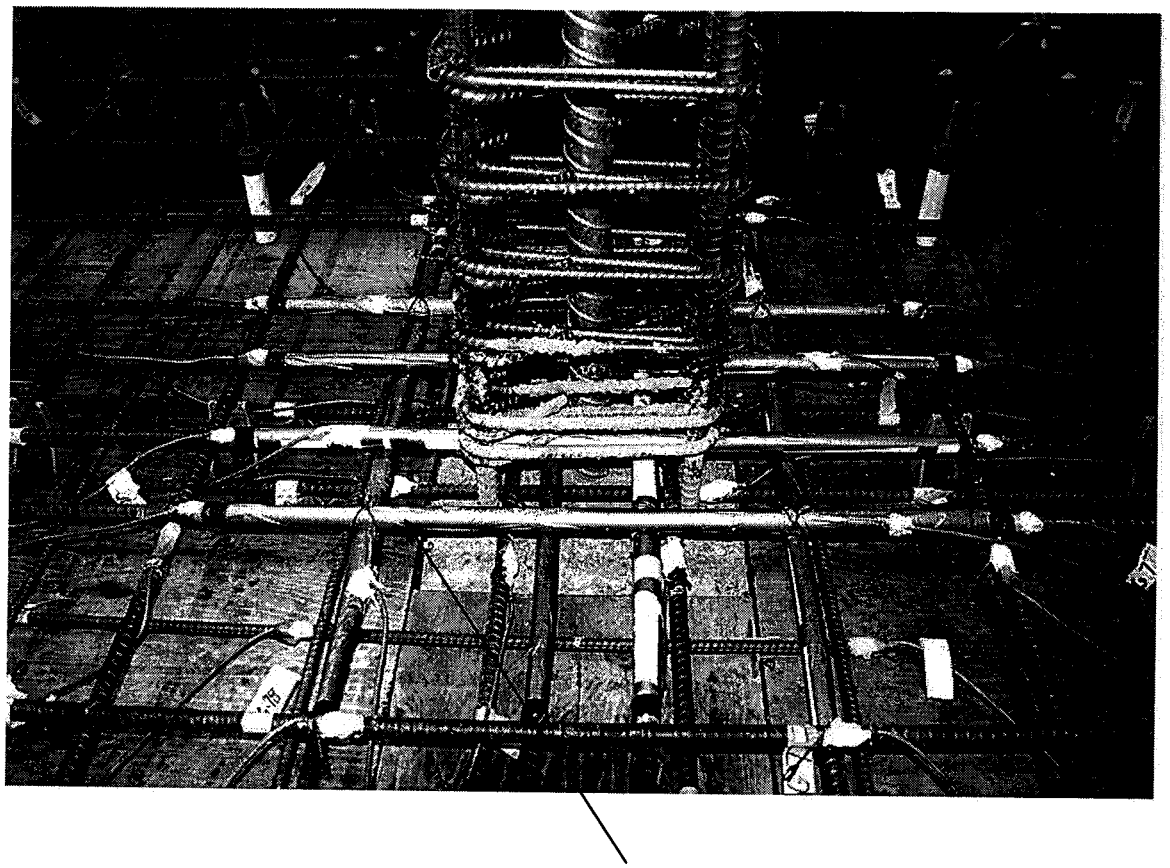

Figure 3.20 Partially Debonded Reinforcement

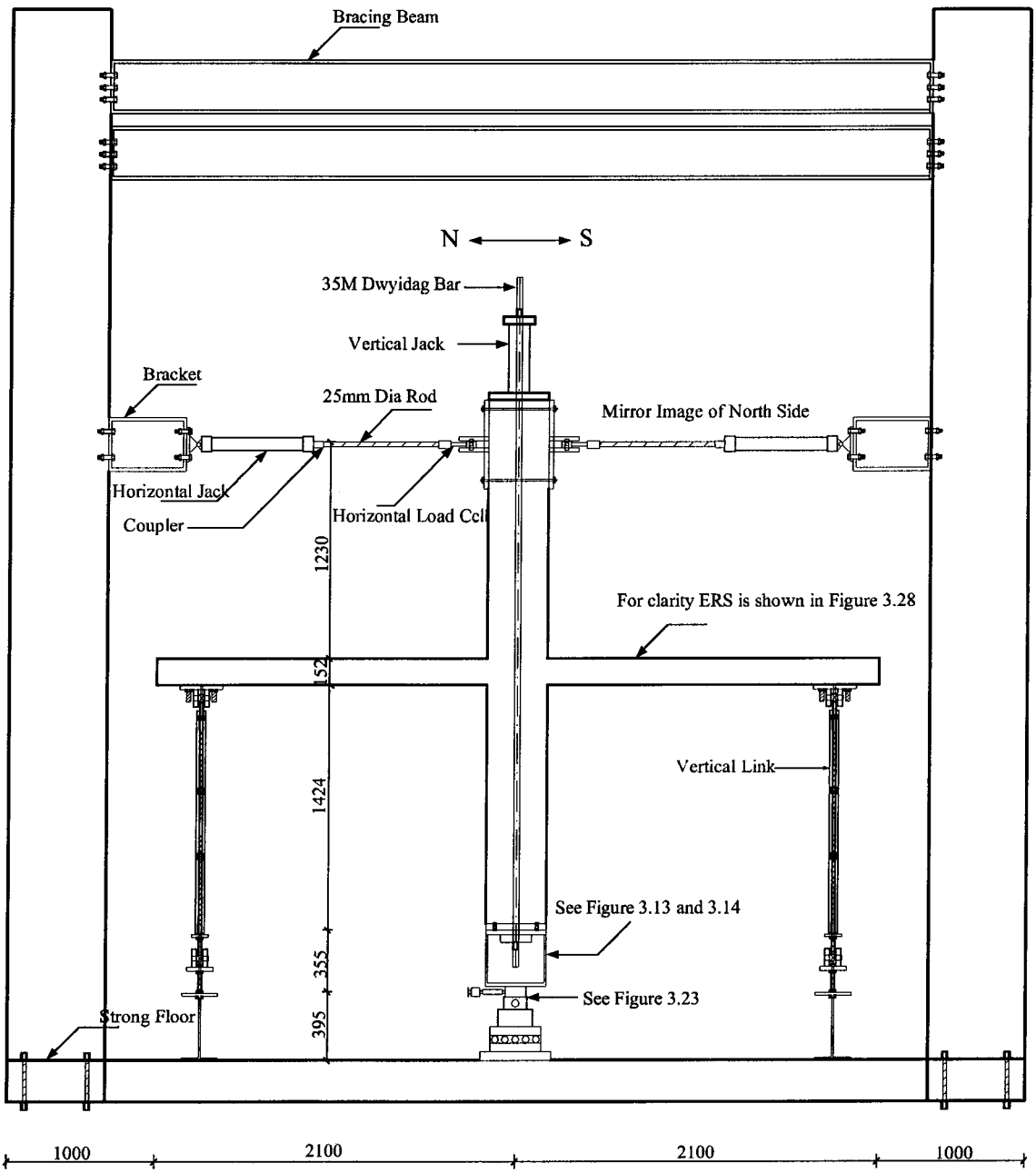

Figure 3.21 Test Frame For Applying Lateral Load

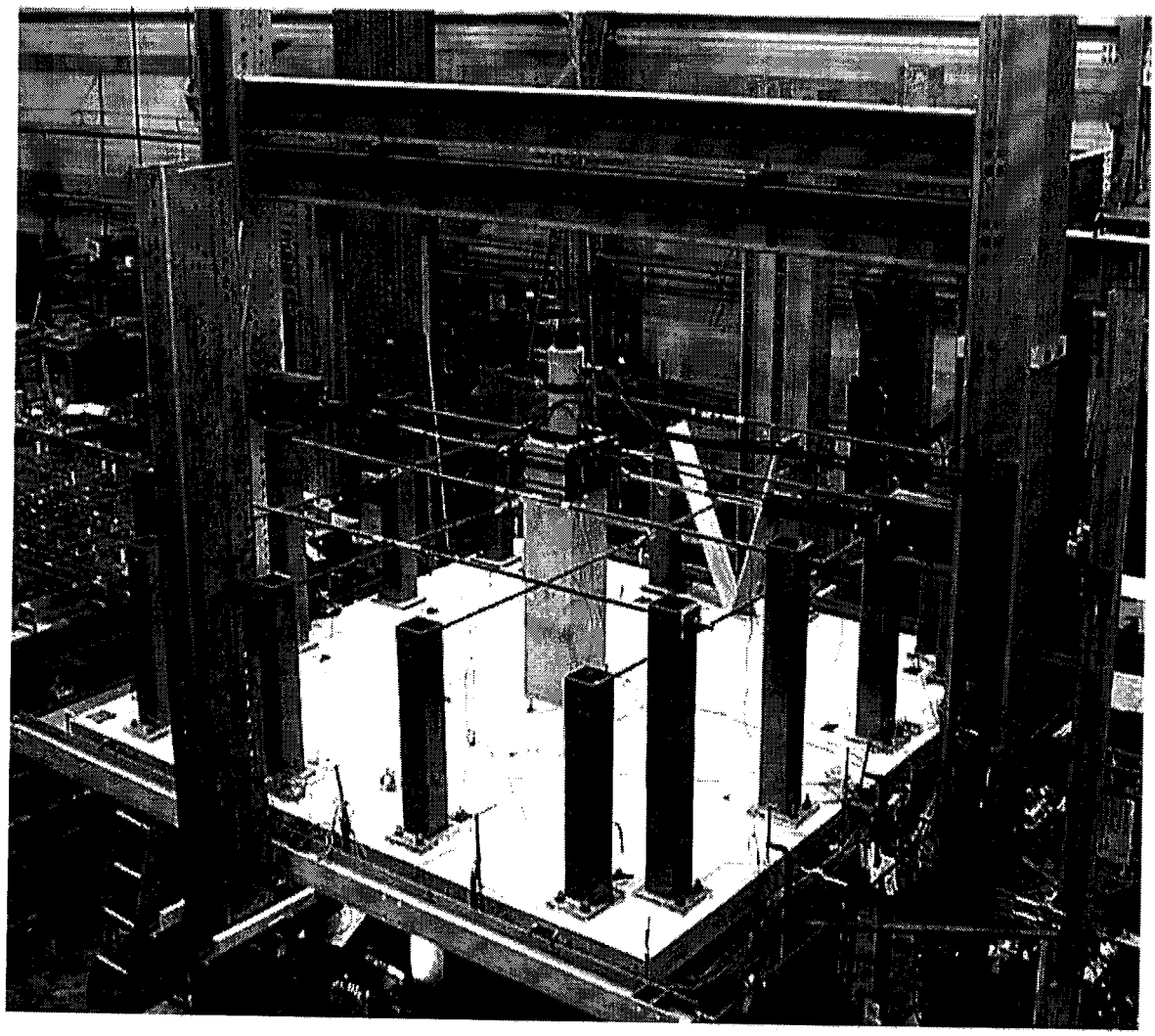

Figure 3.22 Test Setup from S-W Corner looking North East

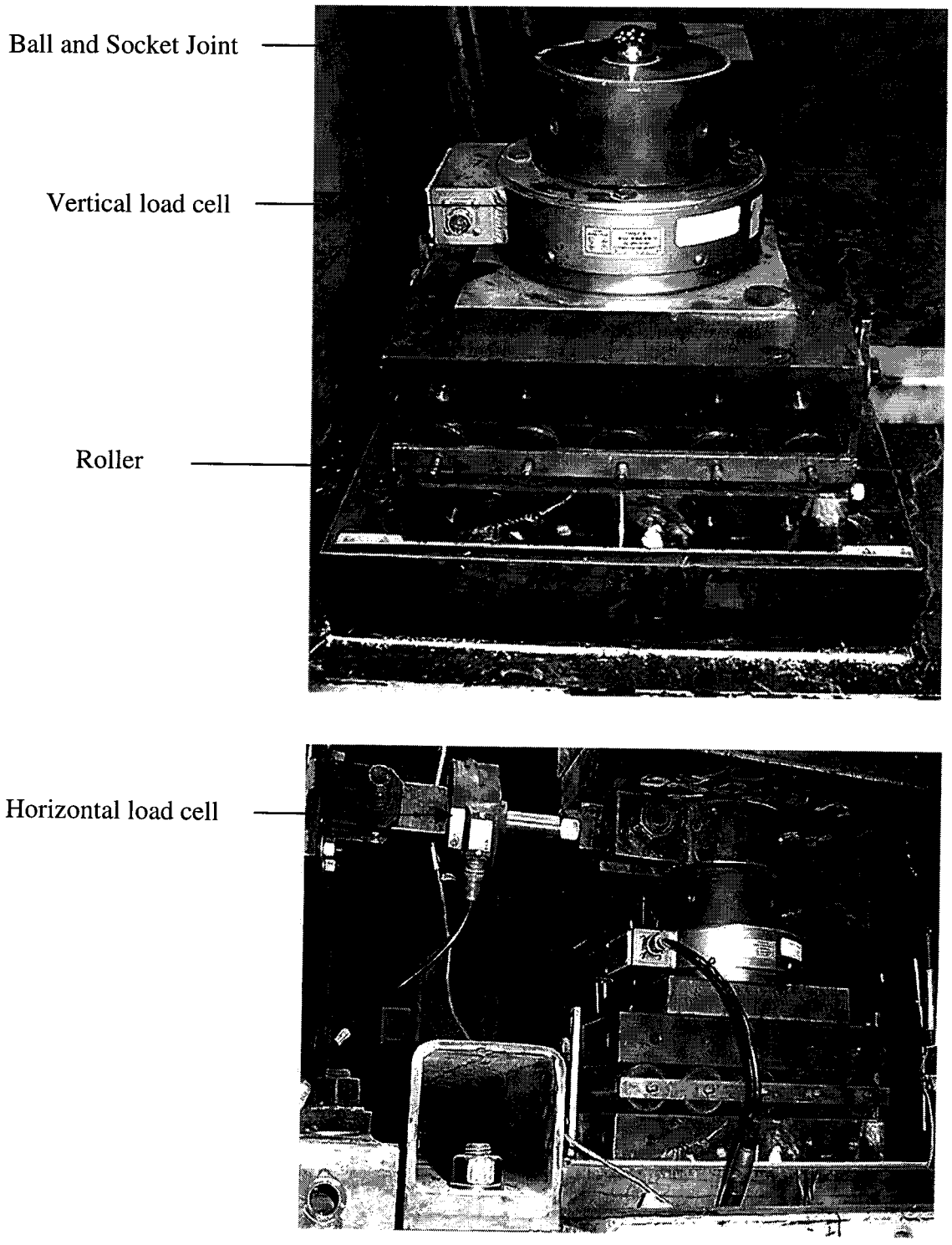

Figure 3.23 Boundary Conditions of Column at Bottom

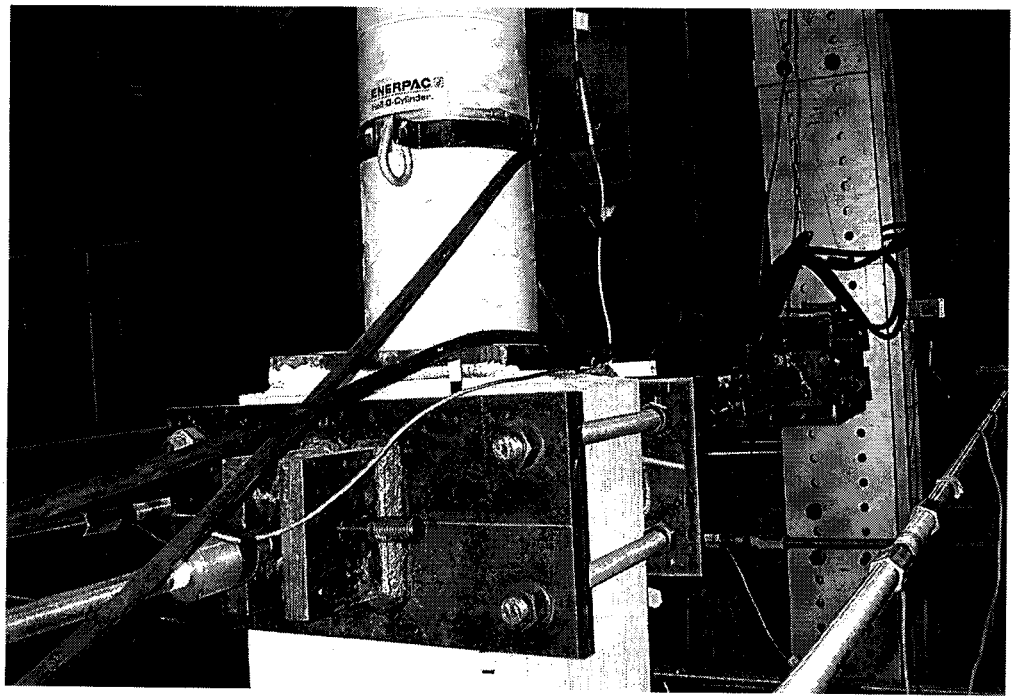

Figure 3.24 Horizontal Load Cell Pin connected to Column

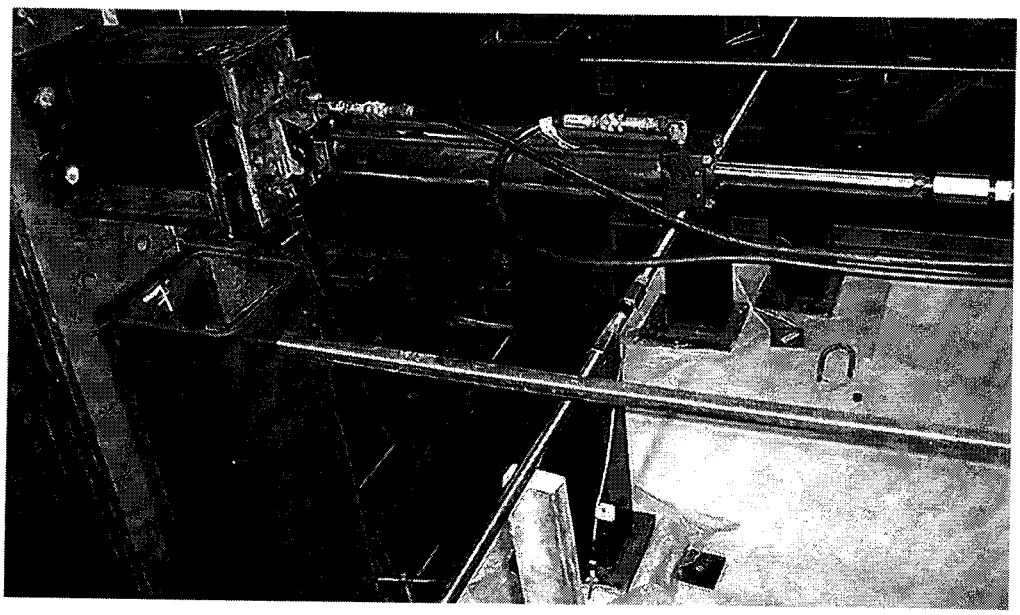

Figure 3.25 Horizontal Jack Attached to Steel Reaction Frame

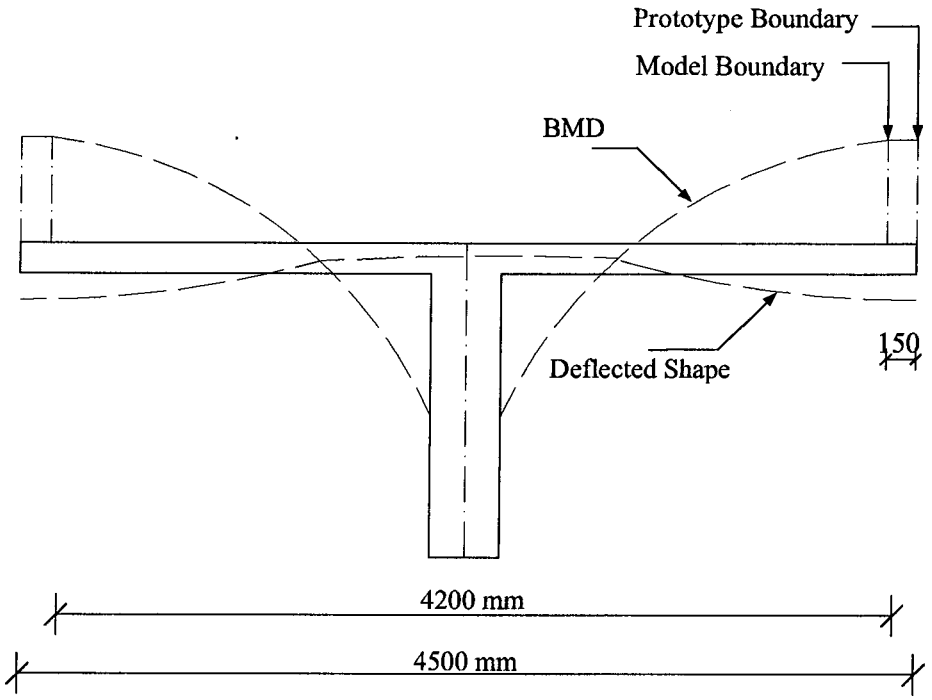

Figure 3.26 Ideal Deflected Shape and Moment Diagram of Structure Under Gravity Loads

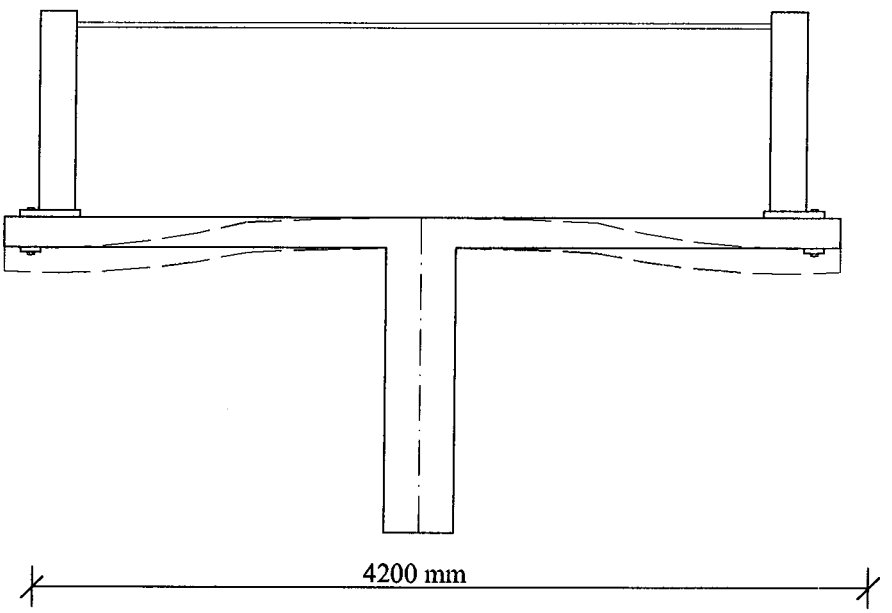

Figure 3.27 Deflected Shape Under Gravity Load

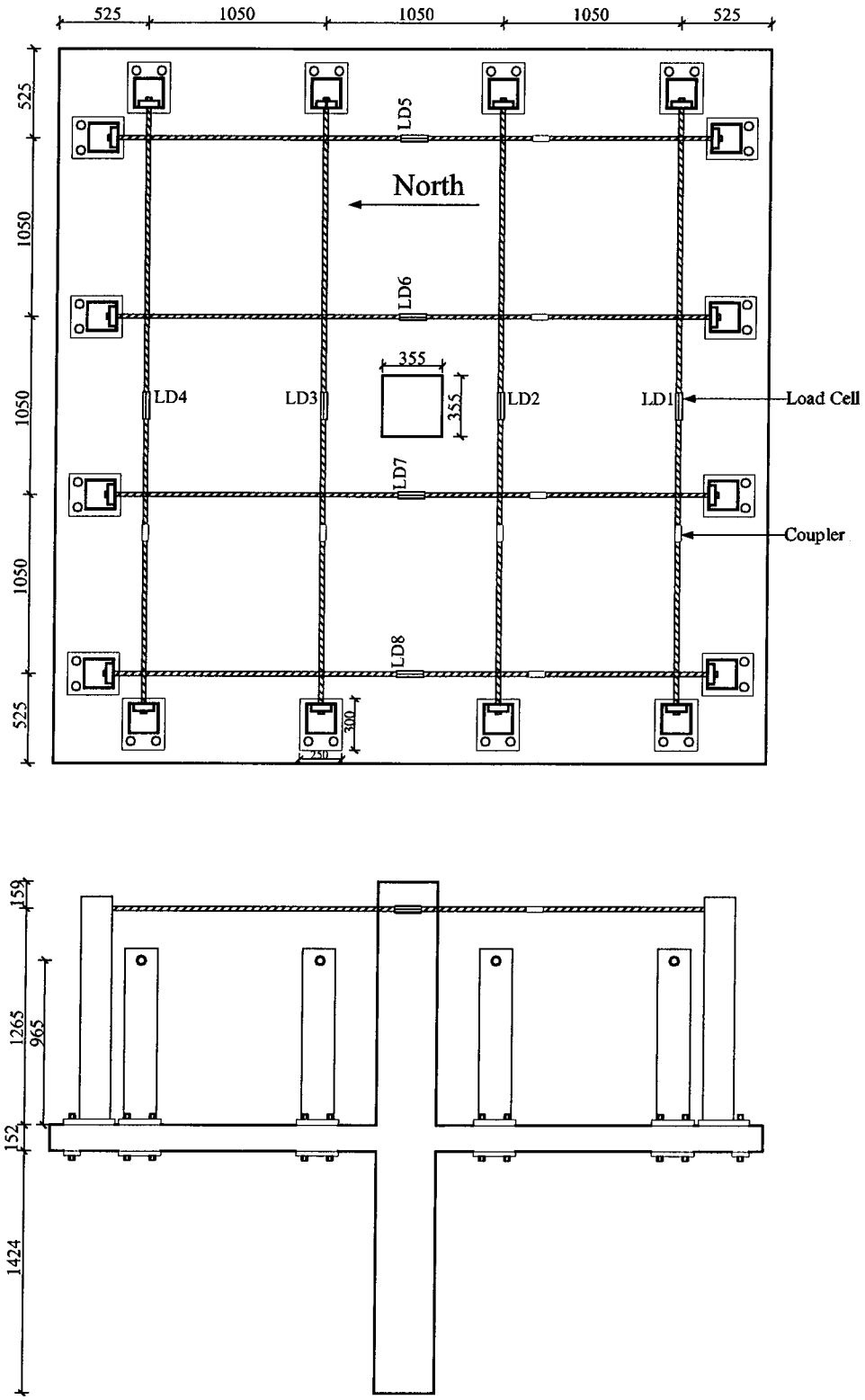

Figure 3.28 Top Edge Restraining System

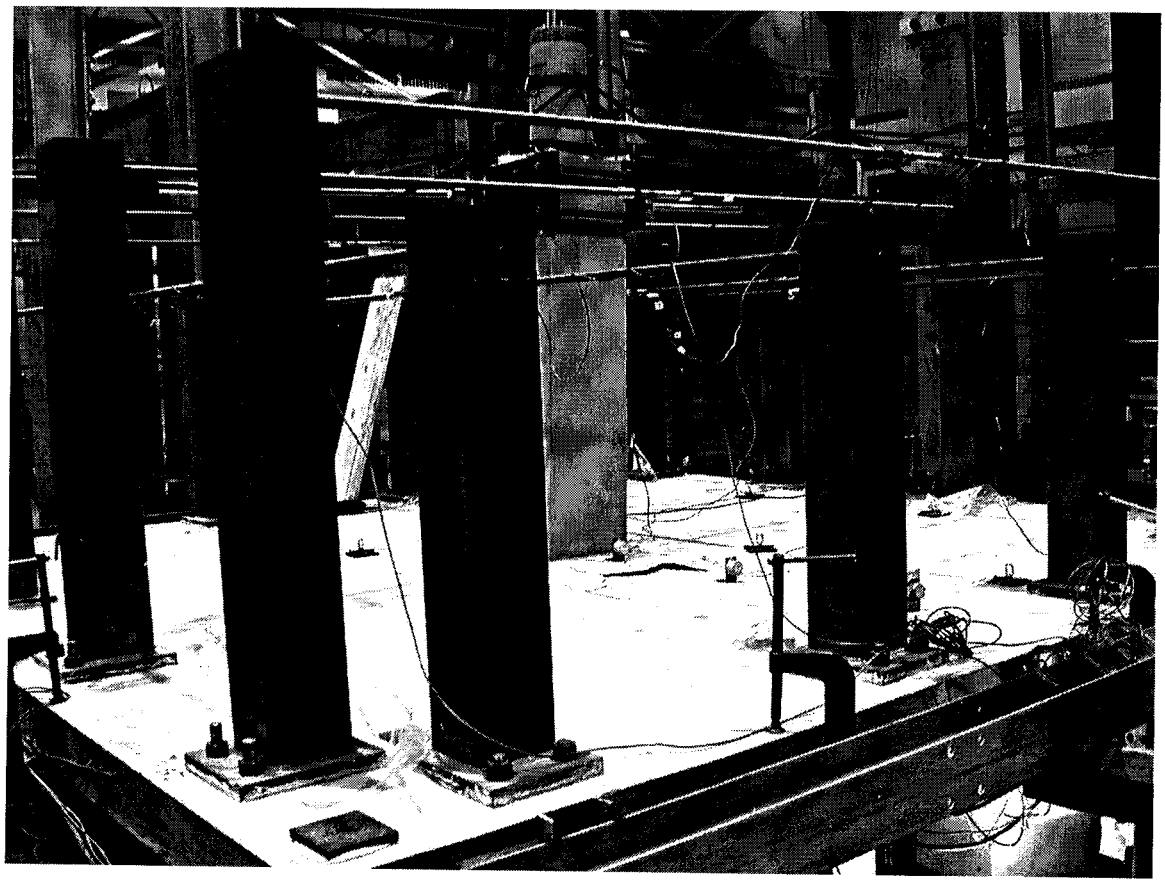

Figure 3.29 Edge Restraining System

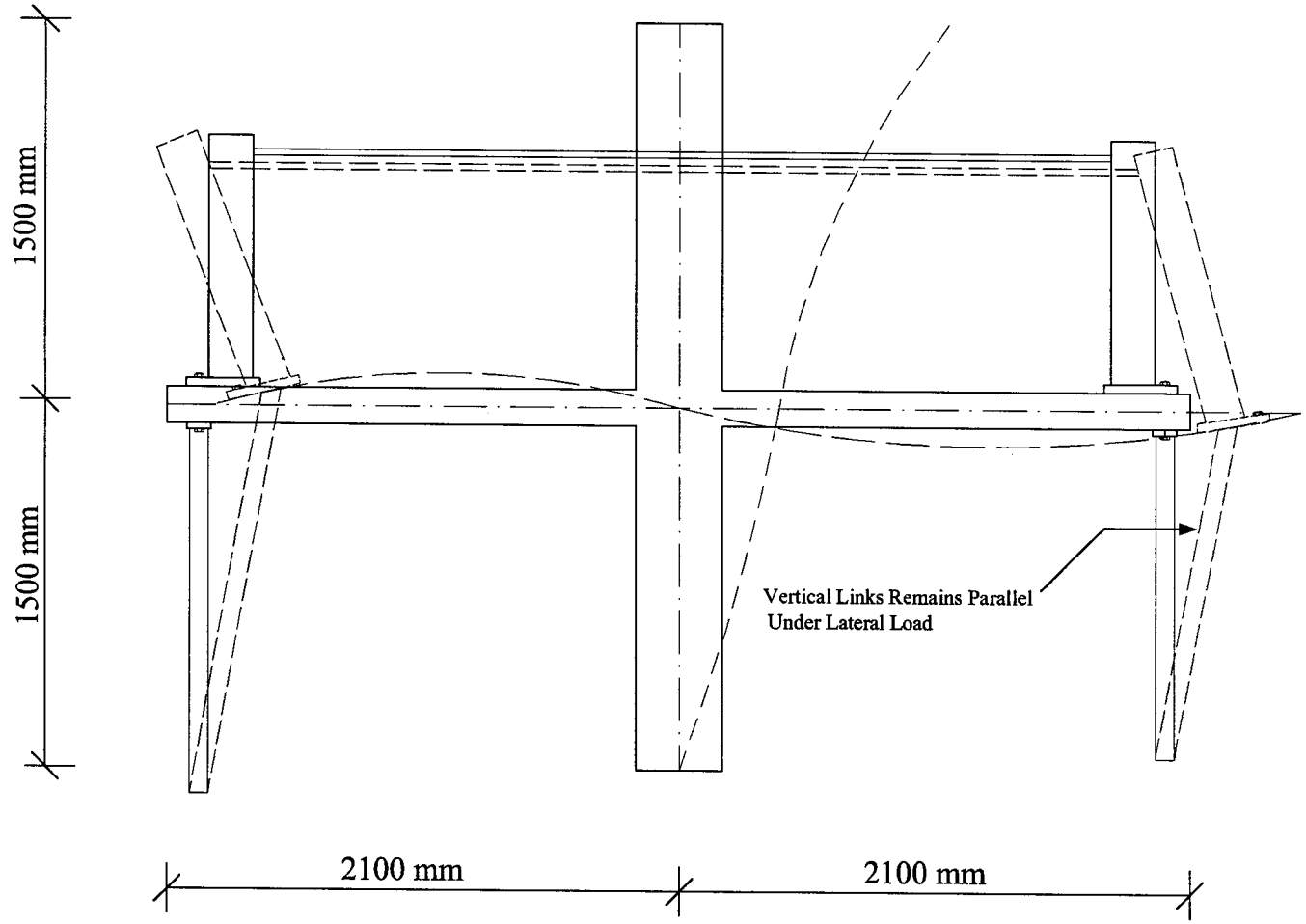

Figure 3.30 Deflected Shape Under Combined Gravity and Lateral Load

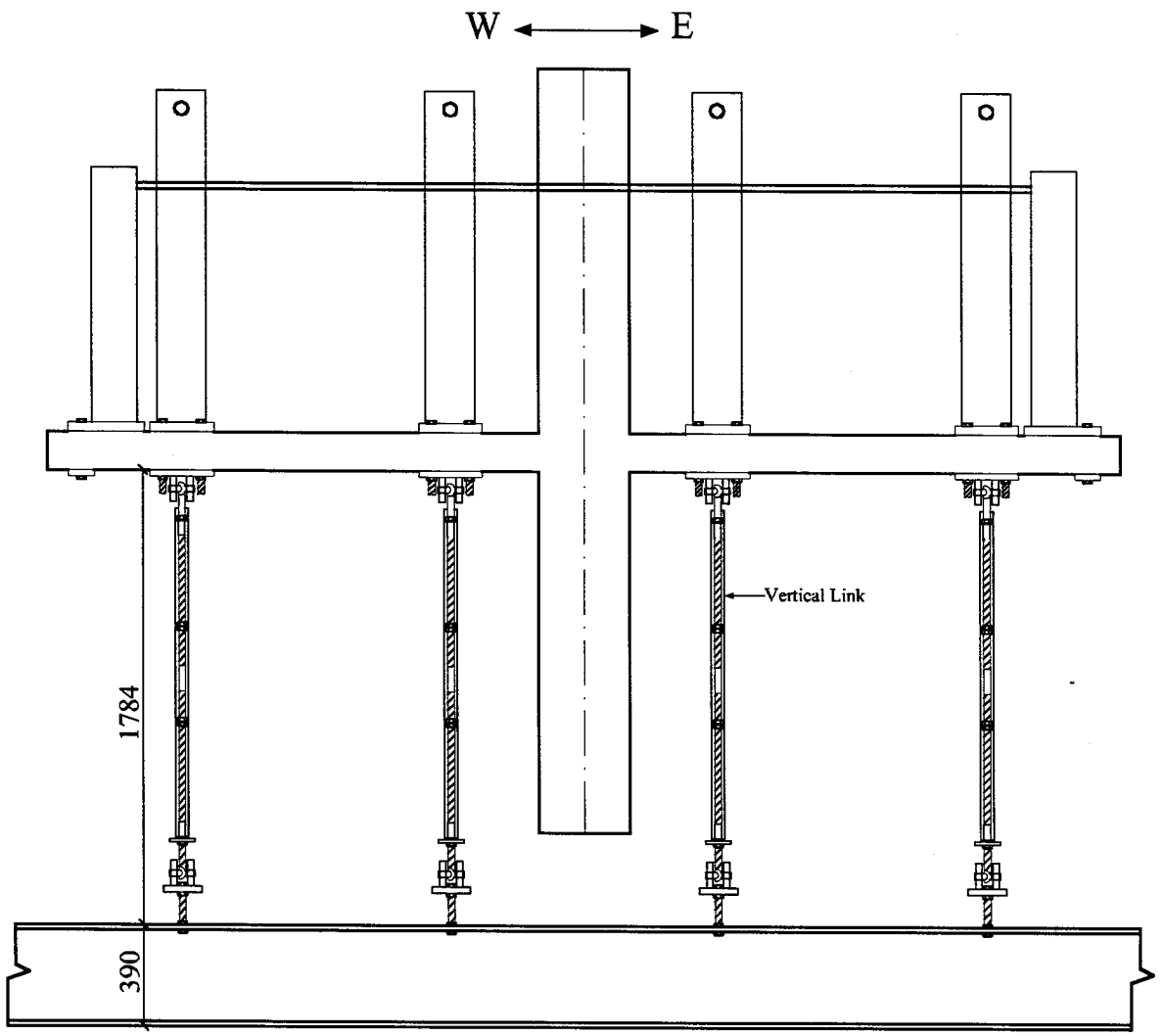

Figure 3.31 Bottom Edge Restraining System

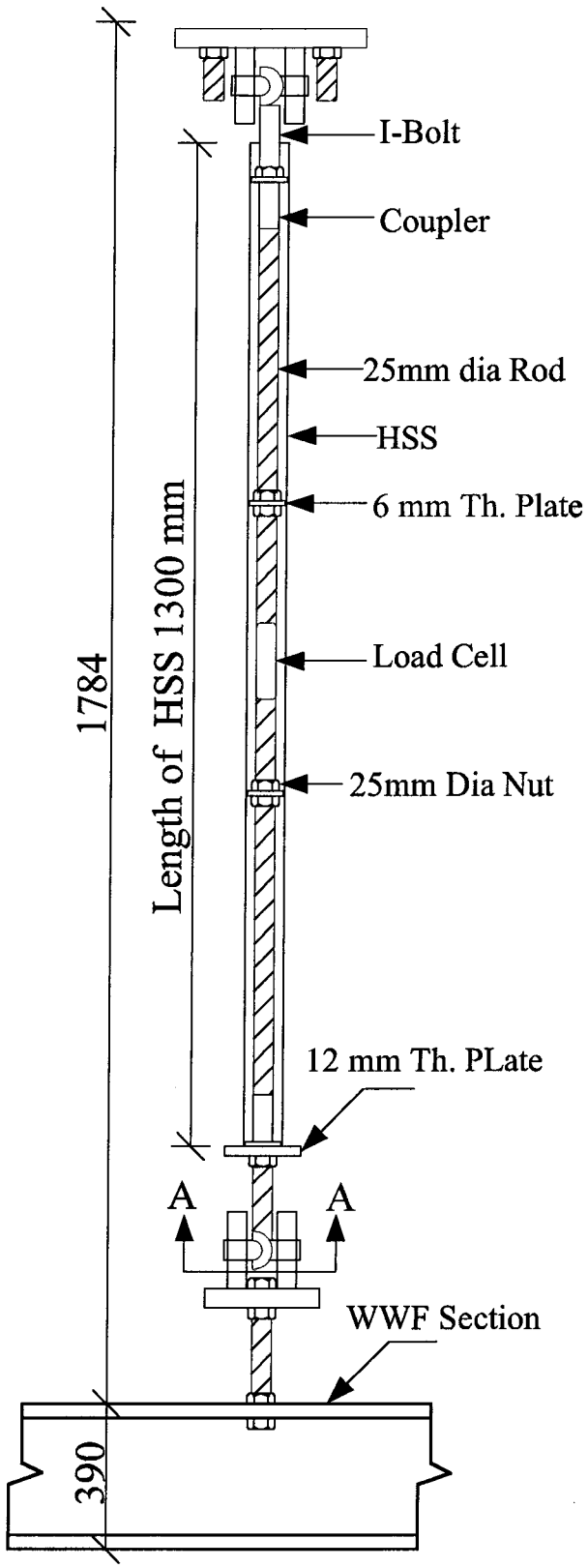

Figure 3.32 Vertical Link

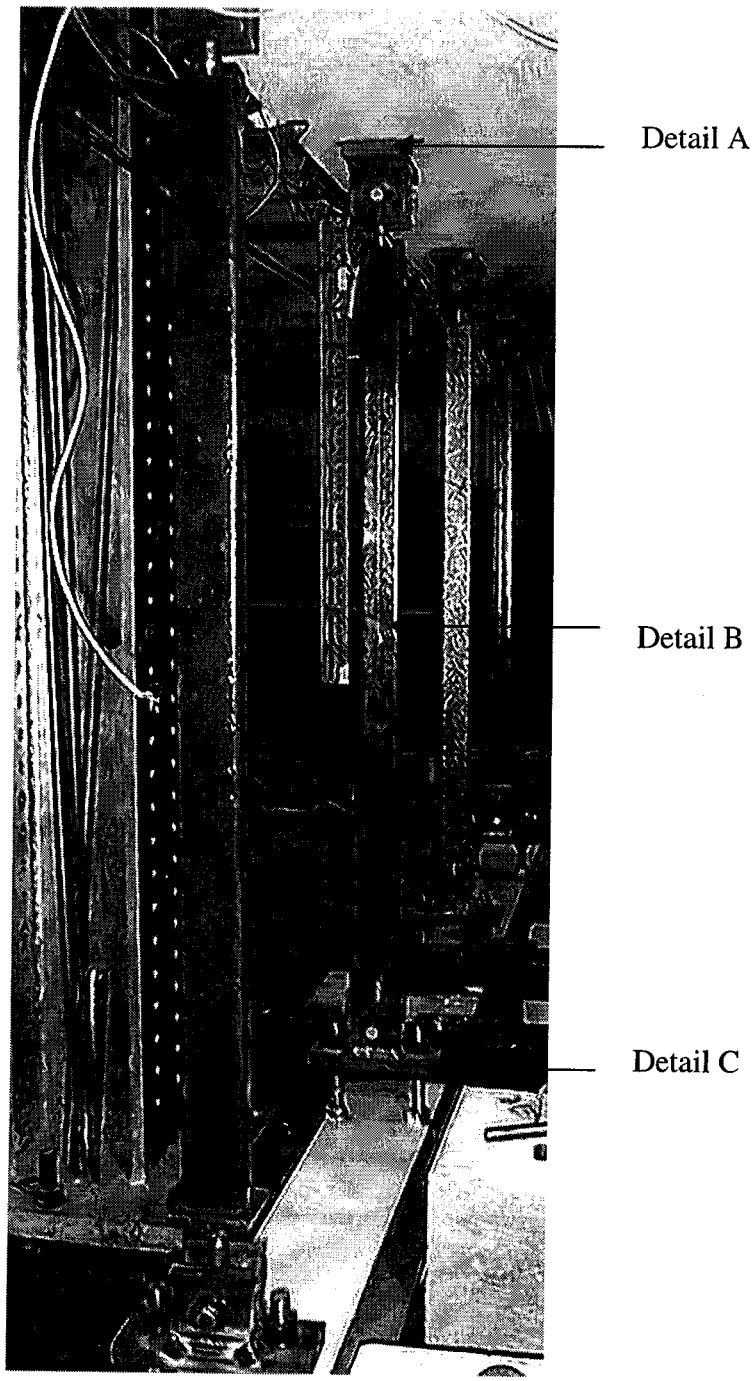

Figure 3.33 Bottom Edge Restraining System

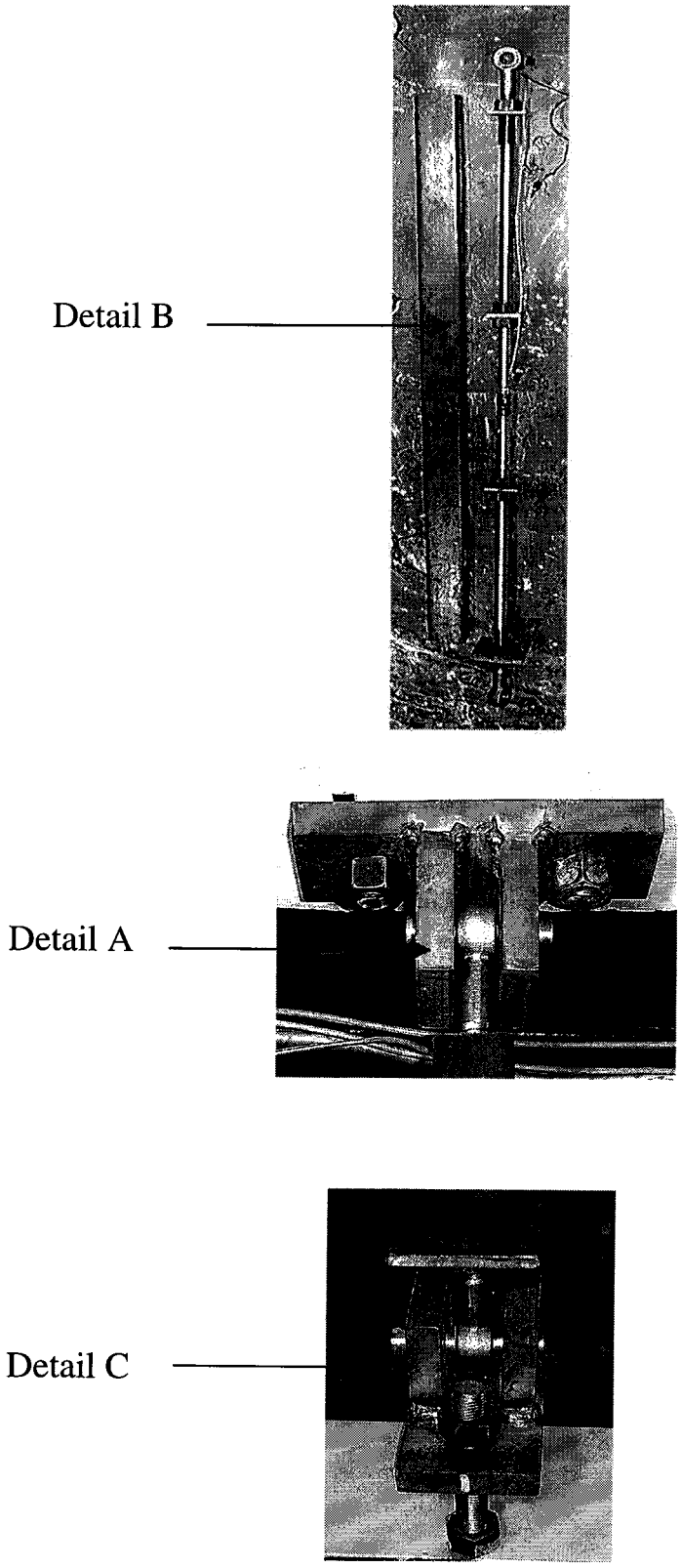

Figure 3.34 Detail Of Vertical Link

Coupler and Chain

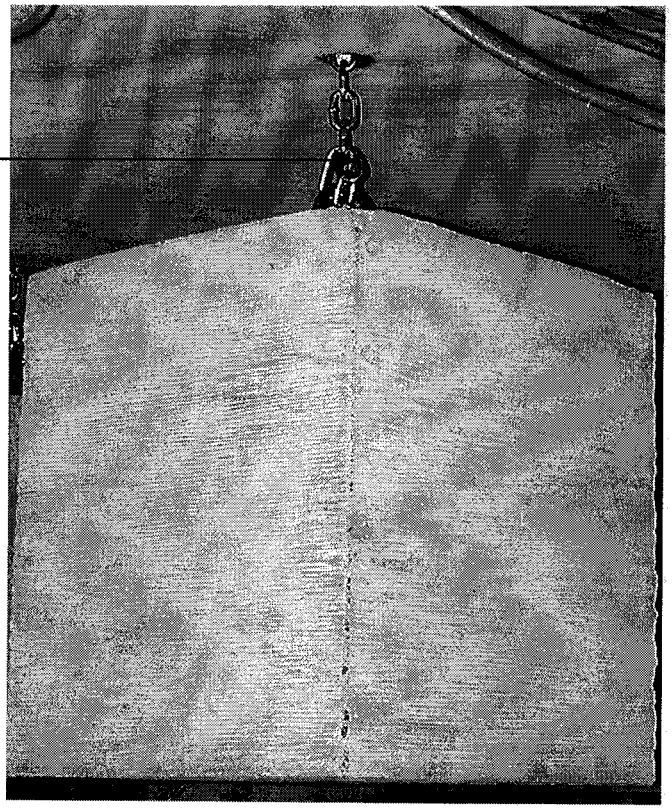

Plate and Pin for
hanging blocks

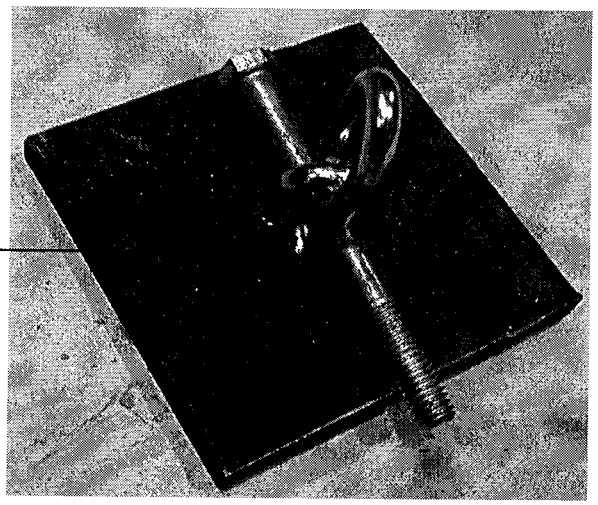

Figure 3.35 Concrete Block Hanged to Simulate Additional Gravity Load

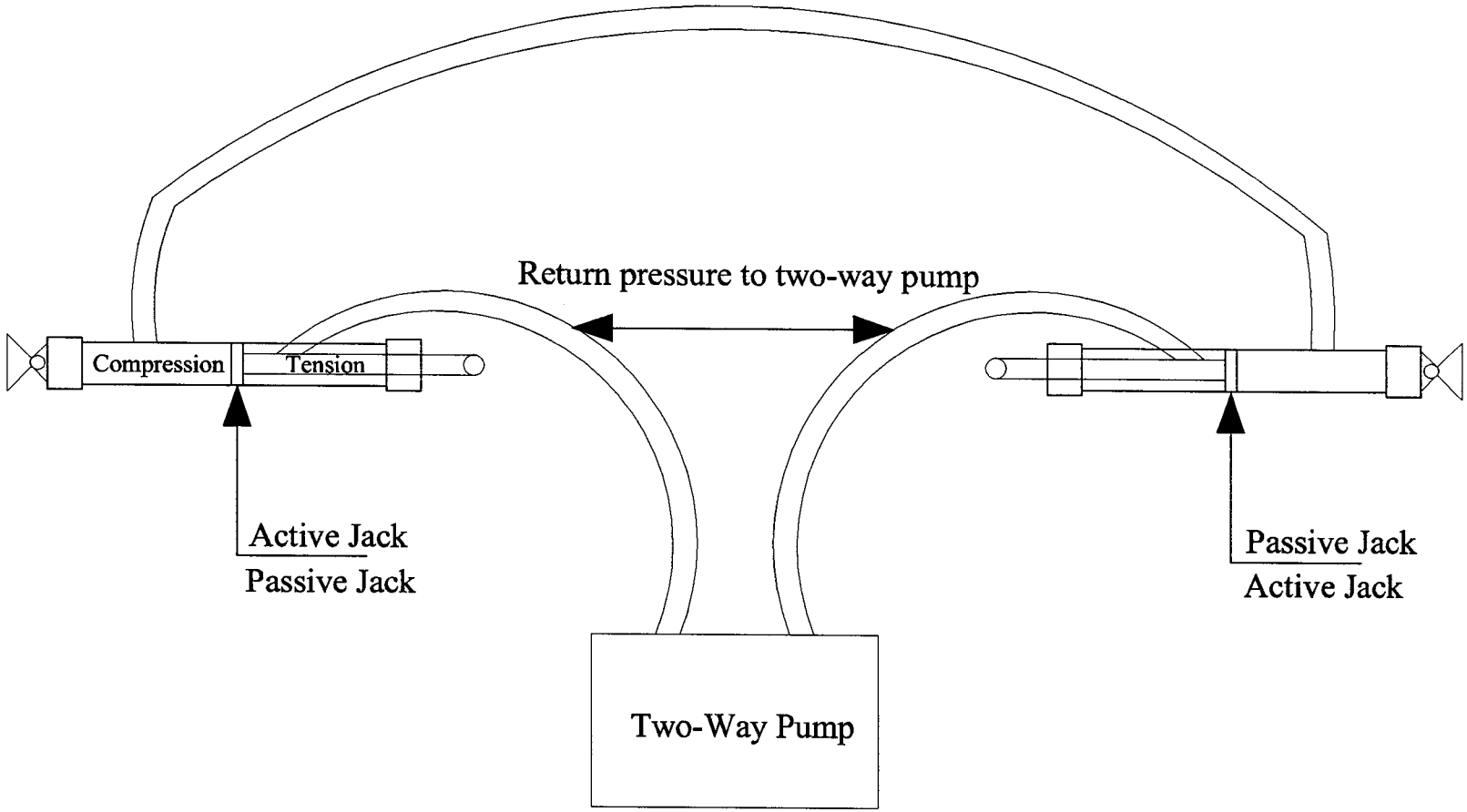

Figure 3.36 Hookup of Horizontal Jacks to Two-way Pump

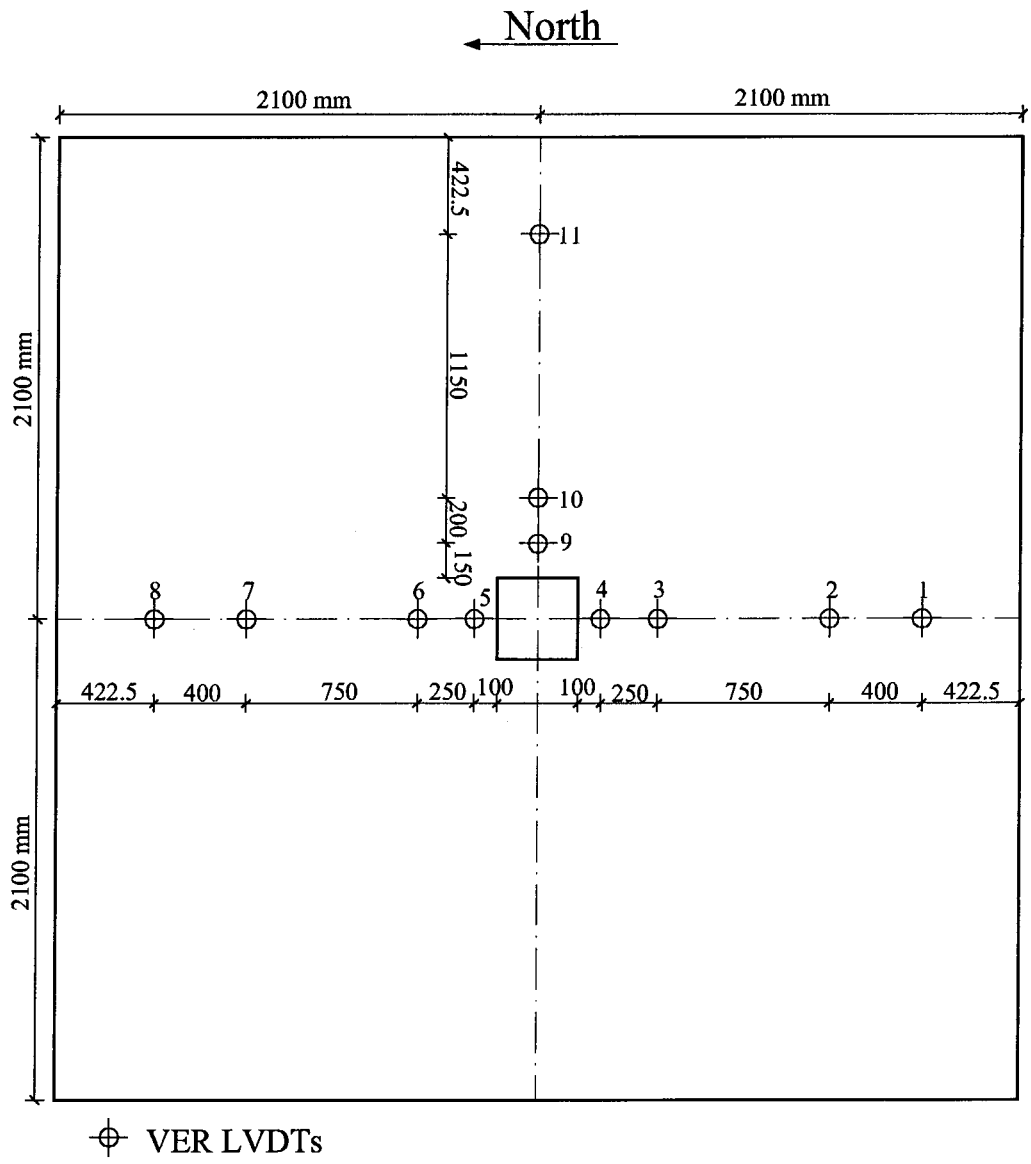

Figure 3.37 Position of Vertical LVDTs

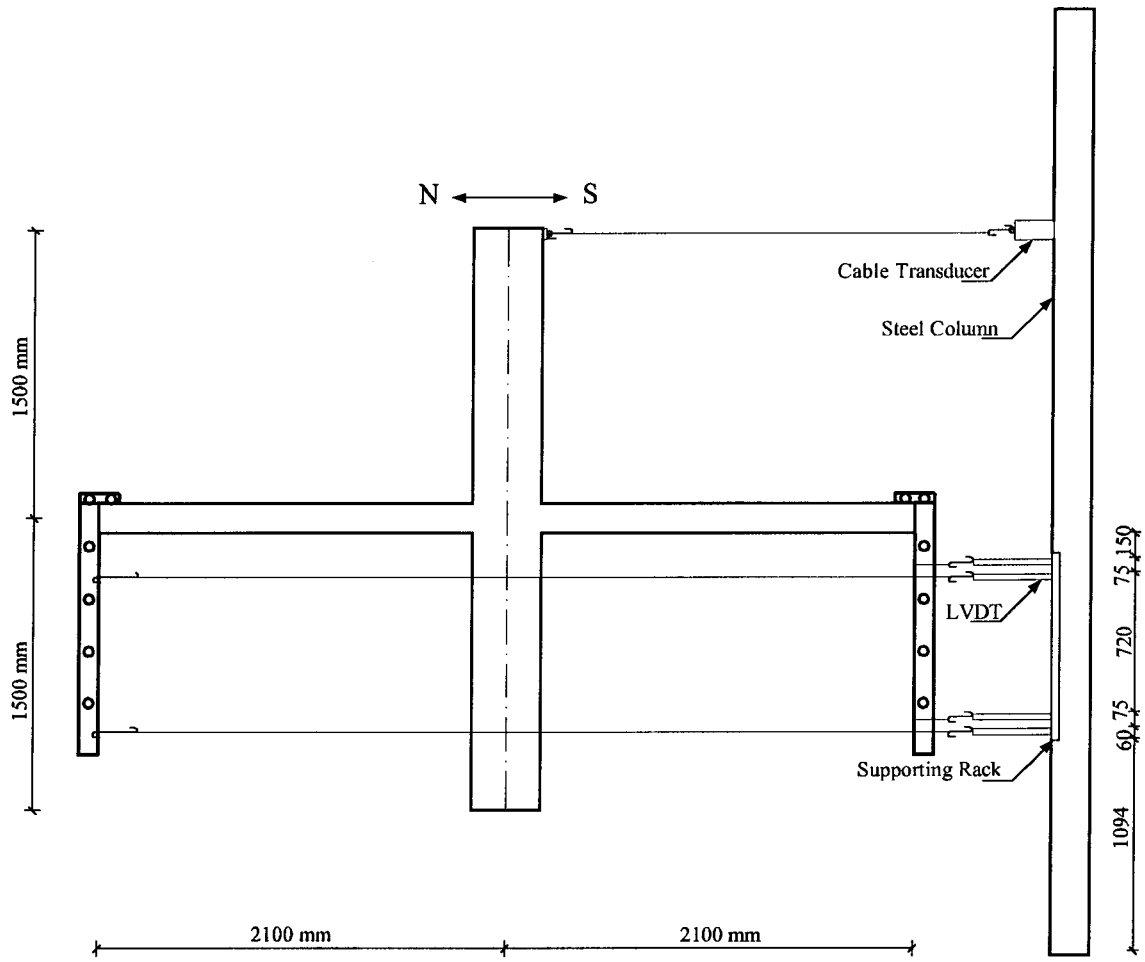

Figure 3.38 Position of Horizontal LVDTs and Cable Transducer

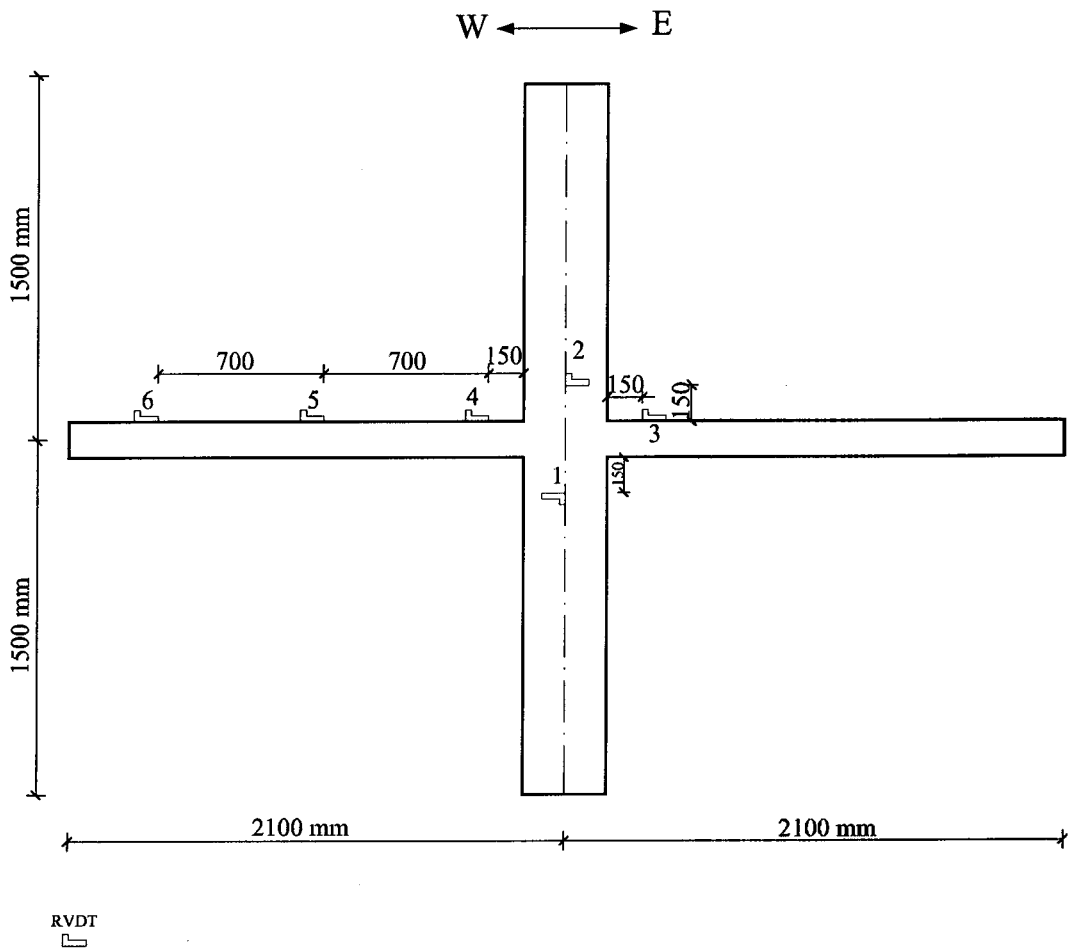

Figure 3.39 Position of RVDTs

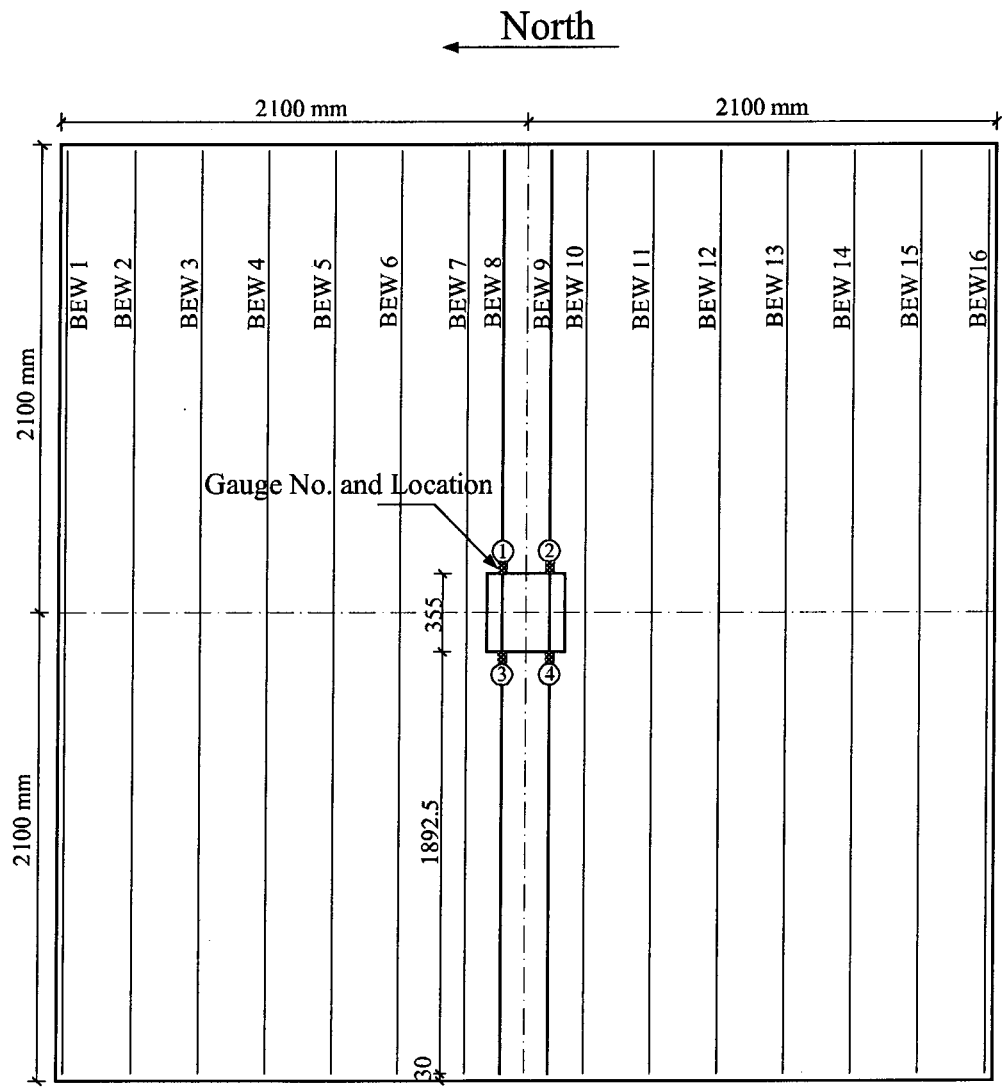

Figure 3.40 Layout of Strain Gauges of Positive Reinforcement in E-W Direction

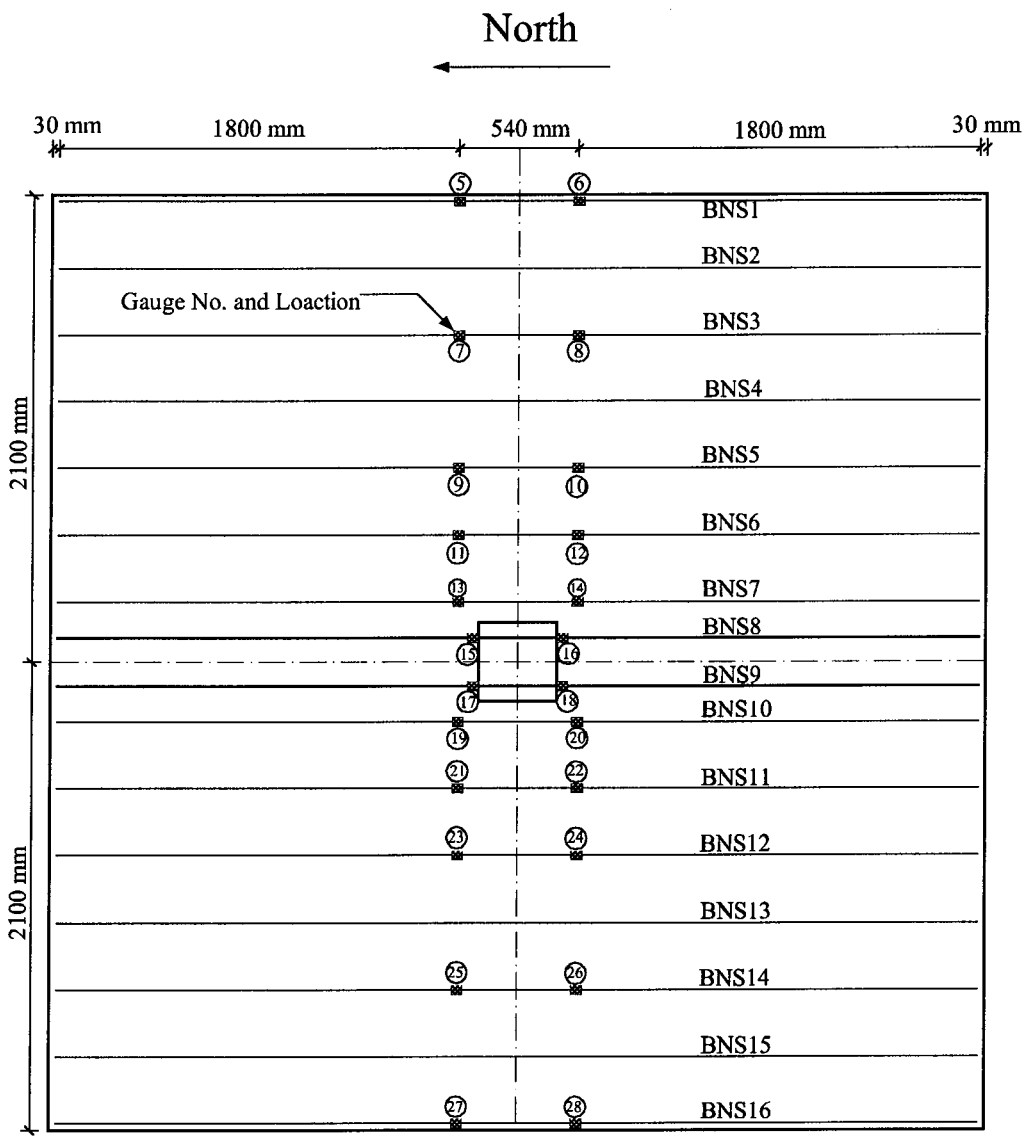

Figure 3.41 Layout of Strain Gauges of Positive Reinforcement in N-S Direction

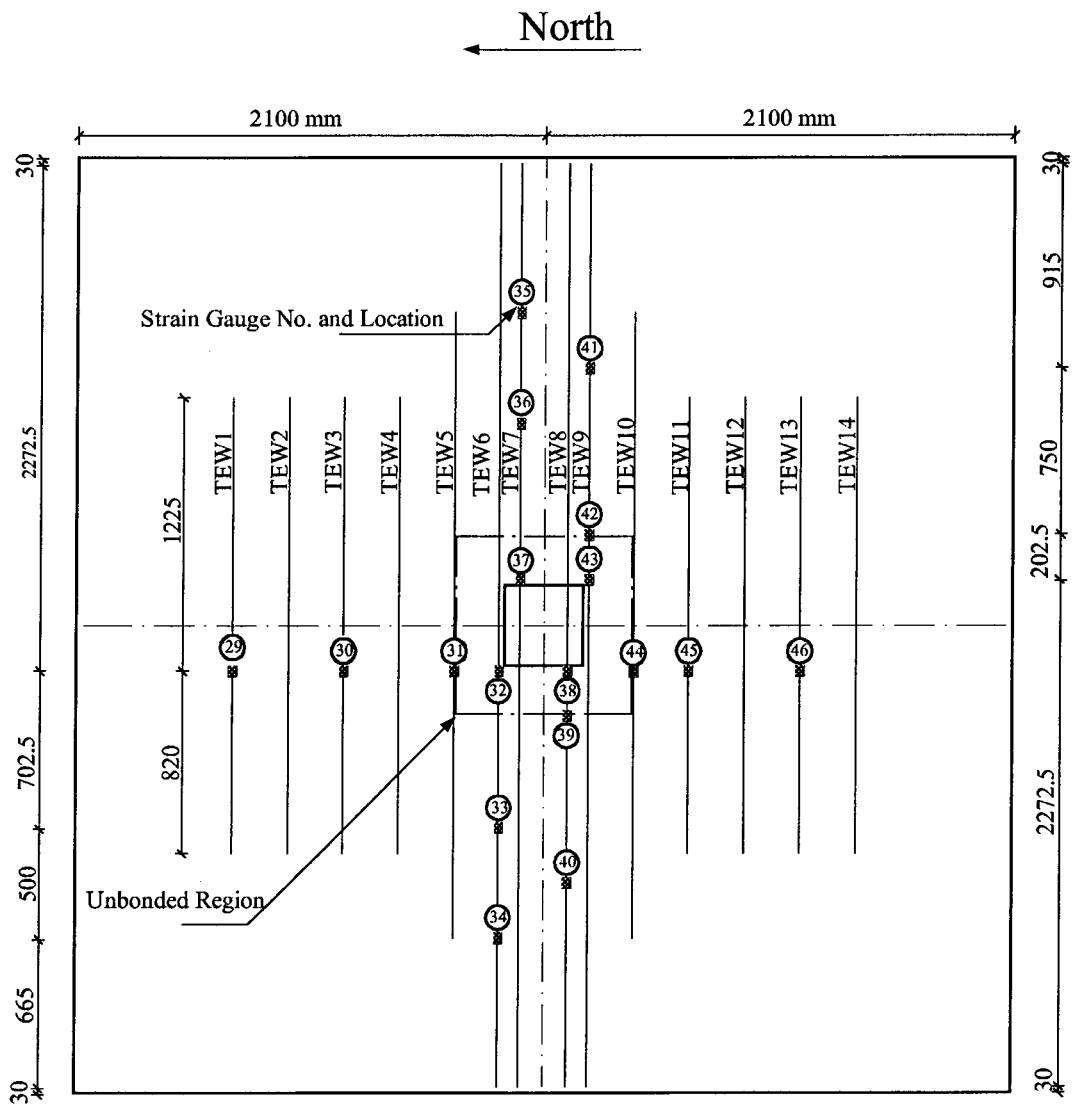

Figure 3.42 Layout of Strain Gauges of Negative Reinforcement in E-W Direction

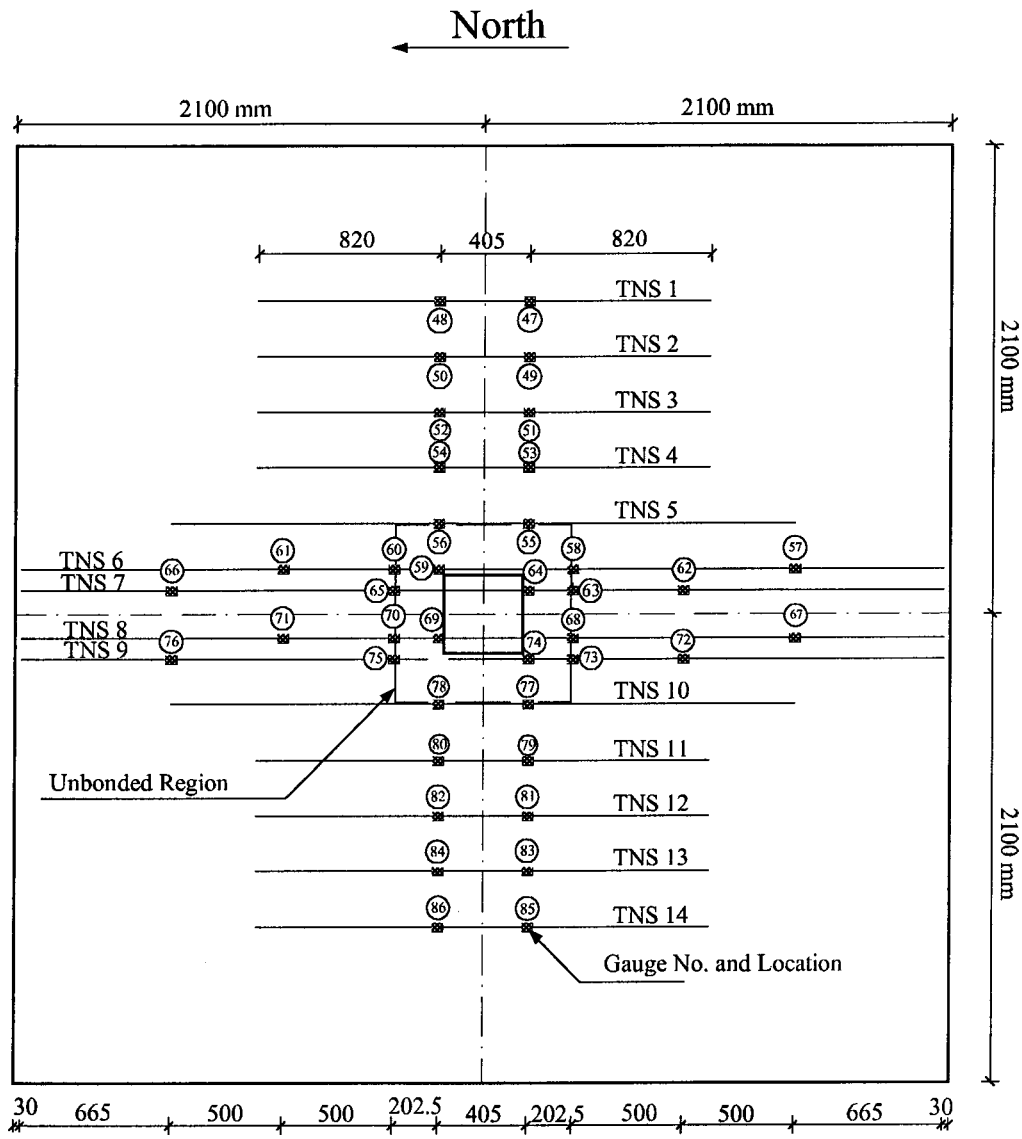

Figure 3.43 Layout of Strain Gauges of Negative Reinforcement in N-S Direction

4. Test Results and Discussion

4.1 Introduction

In this chapter the results from the test data are presented in detail. For each of the two specimens the response is compared with respect to the following observed quantities:

(1) Lateral load versus lateral drift.

(2) Rotation of the column and slab at peak drifts.

(3) Strain distribution at peak drift values.

(4) Bar force profile at peak drift values.

(5) Lateral load-Stiffness relationship.

(6) Vertical displacement of slab along the mid-span at peak values.

The crack pattern of the two specimens observed during the test along with illustrative photographs is also presented in this chapter.

4.2 Lateral Load versus Lateral Drift Relationship (Hysteresis Loops)

The hysteresis loops of SP-A and SP-B are shown in Figures 4.1 and 4.2. Peak drift and load values of two specimens are presented in Tables 4.1 and 4.2.

The loading cycles A through H are labeled on all the curves. Inter-story drifts are given in percent. Lateral loads and drifts are considered positive in the north direction and negative in the south direction.

The load-deflection hysteresis of the two specimens indicates progressive degradation in stiffness with increasing drifts. By comparing Figure 4.1 and Figure 4.2 it can be noted that the hysteresis loops for both the specimens were relatively narrow and spindle shaped up to 1 % drift. For both specimens there is a considerable decrease in connection stiffness at a drift value of 2 % and again at 3 %.

For loading cycles at or below 3 % drift, there is little difference in hysteric behavior between the two specimens. After reaching the ultimate load, the lateral load response of SP-A softened gradually with increasing drift, reaching a value of 30 kN at over 8 % drift. By the end of the test, a sloping failure surface was evident but it was not clear exactly when this formed.

In contrast, the lateral load resistance of SP-B, dropped sharply after ultimate. Failure coincided with the appearance of a diagonal failure surface at the top of the slab.
SP-A reached a higher ultimate load and drift than did SP-B. SP-A sustained a drift of about 4.5 % with a lateral load of 57 kN. This compares to a drift of about 3.5 % and a lateral load of 45 kN for SP-B.

4.3 Lateral Load versus Slab Column Rotation Relationship

Slab and column rotations for each individual specimen at peak drift values are plotted in Figures 4.3 to 4.6. These plots show the rotation of slab and column measured from the RVDTs shown in Figure (3.39). RVDT 6 did not function properly during the test of SP-B, and hence data of RVDT 6 is not reported in Figures 4.5 and 4.6. Due to a technical fault in RVDT 3, the data of RVDT 3 has not been plotted for either specimen.

Rotations of the slab away from the column are much smaller and more uniform than adjacent to the column for both the specimens. For a drift value of less than 30 mm the two specimens exhibited similar behavior.

For SP-A the column and adjacent slab rotations were almost same throughout the test. In SP-B the slab rotation did not follow column rotation. This behavior is quite evident at drift values of 60 mm and 90 mm as shown in Figures 4.6 and 4.7.

For drift values greater than 30 mm the distribution of the slab rotation is more uniform for SP-A compared to SP-B. At a drift value of 60 mm the slab rotation for SP-A was 0.8 degrees whereas for SP-B it was 1.3 degrees. At a drift value of 90 mm it was 1.2 degrees and 1.85 degrees, respectively.

4.4 Strain Distributions in Reinforcement at Peak Load Values

For the purpose of this discussion, the response of the slab reinforcement to lateral load is defined as either active or passive. When loading north, the bottom bars at the north face and the top bars at the south face are considered active while the bottom bars at the south face and the top bars at the north face are considered passive. The reverse applies when loading south.

4.4.1 Bottom Reinforcement

Strain distribution of bottom bars for the north and south edges of each specimen are shown in Figures 4.7 through 4.14. For bottom bars only the strain profile of selected bars (BNS 7 to BNS 10) is shown, the rest of the data is presented in Tables 4.3 and 4.4.

Passive and active strains were much higher in SP-A than SP-B. For SP-A, the first yielding in the bottom bars BNS8 and BNS9 passing through the column region was observed at a drift of 60 mm applied in the south direction. At the end of the 60 mm drift cycle all four bottom bars BNS 7 to BNS 10 reached the yield point but the stress in remaining bottom bars did not reach the yield point. In contrast to SP-A, none of the bottom bars of SP-B reached the yield point.

For SP-A bottom bars passing through the column region were more highly strained than those outside the column. For SP-B bars through the column tended to have lower strains than bars outside the column.

4.4.2 Top Reinforcement

The strain profile of top bars running parallel to N-S direction is shown in Figures 4.15 to 4.22. Complete results are presented in Tables 4.3 and 4.4.

As was the case for bottom reinforcement, passive steel strains are much higher on average in SP-A than in SP-B. Some passive strains were compressive in SP-B but all were tensile in SP-A.

Average active strains are comparable but the peak values in SP-B are higher than in SP-A. Strains for the bars passing through the column are higher for SP-B than SP-A whereas strains away from column are lower for SP-B than SP-A.

At a drift value of 90 mm, the strain range in bar (TNS 8) passing through the column is 1650 μ-strain and 8450 μ-strain for SP-A and SP-B respectively. Strain ranges for bars away from column were smaller for SP-B than SP-A. At a drift value of 90 mm, strain range in rebar (TNS 10) away from the column is 3850 μ-strain and 2200 μ-strain for SP-A and SP-B respectively.

4.5 Bar Force Profile at Peak Load Values

The bar force distributions for the top north-south reinforcement are shown in Figures 4.23 to 4.30.

As shown in Figure 4.25, at failure, yielding of top steel extended to four bars on either side of the column for SP-A. In contrast, Figure 4.29 shows that for SP-B only the bars through and just outside the column reached the yield point at failure.

Figures 4.24 and 4.25 show that for SP-A, all top steel was effectively engaged in resisting the lateral moment.

In SP-B bar forces are the highest in the bars passing through and near the column. From bar force distribution profile it can be seen that bar forces become smaller in the outlying bars. In SP-A the loss of bar forces in the outlying bars is less pronounced, and the bar distribution profile remains constant towards the edge of the slab.

4.6 Lateral Load Stiffness Relationship for Peak Drifts

The stiffness of the slab subjected to lateral load deteriorates gradually with increasing drift values. The decrease in stiffness is generally attributed to cracking of slab concrete. CSA A23.3-94 describes the elastic frame model for calculating the stiffness of the slab. The elastic frame method uses gross section properties for calculating member stiffness

and is appropriate for gravity load analysis only. For members subjected to gravity and lateral load, flexural cracking tends to concentrate near the connection while the slab away from the column remains uncracked. This pattern of cracking suggests that modifications are required to correctly account for reduction in stiffness due to cracking of the slab. Vanderbilt and Corley (1983), on the basis of their research, suggested that for slabs subjected to lateral loads, the slab-beam stiffness should be reduced to 1/3 of the gross value section.

Figure 4.31 shows how the stiffness parameter K is calculated from the measured data. Figure 4.32 shows a plot of stiffness parameter K versus the lateral drift for each specimen. For comparison, the stiffness calculated using the gross section properties and the 1/3 reduction factor suggested by Vanderbilt and Corley is also plotted in Figure 4.32.

The test results of the two specimen show the measured stiffness deteriorated gradually with increasing drift, although the decrease in stiffness is slightly less in SP-A than in SP-B.

At a drift value of 1% the stiffness of both the specimens is the same. After 1% drift, the stiffness of SP-B deteriorates faster than SP-A but the difference is so slight as to be negligible.

The value of stiffness at the end of the test was approximately one third of the uncracked value at the beginning of the test.

4.7 Edge Expansion

The overall expansion at mid-depth of the slab along the continuous edge of at mid-height of the slab of the along the continuous edge in the loading direction was measured using horizontal LVDTs.

The overall expansion of SP-A and SP-B is plotted in Figures 4.33 to 4.36.

No marked difference is observed between the two specimens. The trend is for expansion to increase with the drift. This is attributed to accumulated damage in the vicinity of the connection.

4.8 Slab Deflection Profile:

Due to a technical fault with LVDTs for SP-A, the slab deflection profile could not be plotted.

The slab deflection profile for peak drift values of SP-B is shown in Figure 4.37 and Figure 4.38. For reference, the typical service deflection limit of L/360 is also shown.

The measured deflections of SP-B remained below the nominal limit, prior to the development of the punching failure. After punching the vertical displacement exceeded the nominal limit.

4.9 Crack Propagation:

After the hanging of dead weights small hairline cracks were observed and marked along the column centerline extending towards the slab edge in both specimens. At the end of every lateral load cycle cracks were measured and marked on the specimens.

Primary flexural cracks on the top surface of the slab for SP-A first formed around the periphery of column at a drift of 12 mm. The first crack on the bottom surface of the slab was noted at a drift of 24 mm. The maximum crack widths measured were 0.6 mm at a drift of 18mm, 1 mm at a drift of 30 mm and 2 mm at a drift of 60 mm. At a drift of 90 mm, the crack at the slab-column junction opened up to 4 mm.

Apart from the large cracks mentioned above, secondary cracks were very small and none of them exceeded 0.2 mm.

For SP-B the first primary crack due to lateral load was observed at a drift of 12 mm. The maximum crack widths measured were 0.8 mm at a drift of 18mm, 1 mm at a drift of 30 mm, 1.25 mm at a drift of 90 mm. Secondary cracks were hairline with none exceeding 0.25 mm prior to failure.

While the surface crack patterns of the specimens were similar, SP-B had a greater number of cracks than SP-A. Conversely the cracks in SP-A were slightly wider than in SP-B.

Photographs of the two specimens showing the crack pattern after failure are shown in Figure 4.39and Figure 4.40.

Specimen	Cycle	Drift	Loading Direction	Lateral Load	Column Drift
		(mm)		(kN)	(mm)
A	**A**	**0-6**			
	A-1		S	-9.19	-5.7
			N	8.42	5.99
	B	**0-12**			
	B-1		S	-9.28	-5.48
			N	14.96	11.68
	B-2		S	-13.91	-10.69
			N	11.89	9.77
	B-3		S	-17.39	-13.15
			N	8.39	7.08
	C	**0-18**			
	C-1		S	-22.78	-18.02
			N	20.86	18
	C-2		S	-22.61	-18.19
			N	20.51	18.61
	D	**0-24**			
	D-1		S	-28.99	-24.25
			N	27.2	24.64
	D-2		S	-24.05	-24.11
			N	27.56	24.25
	D-3		S	-22.73	-24.32
			N	26.69	24.25
	E	**0-30**			
	E-1		S	-30.09	-30.29
			N	31.56	30.42
	E-2		S	-29.67	-30.54
			N	30.55	30.21
	E-3		S	-28.84	-30.46
			N	30.87	30.25
	F	**0-60**			
	F-1		S	-46.16	-61.08
			N	45.09	60.08
	F-2		S	-40.55	-61.02
			N	43.78	60.41
	F-3		S	-38.86	-60.43
			N	42.55	60.7
	F-4		S	-38.48	-60.73
			N	41.71	60.09
	F-5		S	-38.22	-60.26
			N	40.11	60.38
	F-6		S	-37.46	-60.48
			N	39.88	60.4
	G	**0-90**			
	G-1		S	-50.79	-86.79
			N	50.66	91.16
	G-2		S	-49.38	-90.58
			N	46.84	91.45
	G-3		S	-49.4	-94.55
			N	46.62	90.72
	H	**0-Failure**			
	H-1		S	-57.11	-133.85

Table 4.1 Peak Drift and Lateral Load Values at Different Load Cycles

Specimen	Cycle	Drift	Loading Direction	Lateral Load	Column Drift
		(mm)		(kN)	(mm)
B	**A**	**0-6**			
	A-1		S	-5.28	-6.11
			N	9.49	6.18
	A-2		S	-6.34	-6.06
			N	9.87	6.67
	A-3		S	-6.73	-6.37
			N	9.27	6.45
	B	**0-12**			
	B-1		S	-13.44	-11.94
			N	17.3	12.18
	B-2		S	-13.78	-11.86
			N	16.85	12.18
	B-3		S	-14.51	-12.25
			N	16.26	11.94
	C	**0-18**			
	C-1		S	-17.23	-20.78
			N	25.12	18.89
	C-2		S	-18.14	-18.04
			N	23.63	18.4
	C-3		S	-19.41	-18.9
			N	23.37	18.58
	D	**0-24**			
	D-1		S	-23.22	-24.13
			N	29.63	25.04
	D-2		S	-23.08	-24.15
			N	27.27	24.09
	D-3		S	-24.15	-25.07
			N	27.84	24.69
	D-4		S	-22.33	-24.15
			N	27.28	24.69
	E	**0-30**			
	E-1		S	-29.07	-30.42
			N	31.91	30.178
	E-2		S	-27.25	-29.97
			N	31.79	30.49
	E-3		S	-28.19	-30.57
			N	30.69	29.94
	F	**0-60**			
	F-1		S	-43.95	-62.64
			N	44.57	59.55
	F-2		S	-38.87	-59.6
			N	42.68	60.01
	F-3		S	-39.79	-62.04
			N	41.25	59.73
	F-4		S	-36.6	-59.9
			N	40.31	60.17
	F-5		S	-36.27	-59.97
			N	40.02	60.63
	G	**0-90**			
	G-1		S	-46.92	-90.65
			N	49.96	92.873
	G-2		S	-43.32	-89.75
			N	45.73	90.14
	G-3		S	-41.86	-90.09
			N	44.53	90.31
	H	**0-Failure**			
	H-1		S	-45.62	-110.28

Table 4.2 Peak Drift and Lateral Load Values at Different Load Cycles

Loading Stage	Loading Direction	Peak Drift	Lateral Load	GA-1	GA-2	GA-3	GA-5	GA-6	GA-7	GA-8	GA-9	GA-10	GA-11	GA-12	GA-13	GA-14	GA-15
		(mm)	(kN)														
Virgin Slab				-0.4	3.7	715	1	-1.4	-0.6	-0.6	-0.6	-2.2	-0.6	-1.1	-1.2	-2.8	0.4
After Mounting ERS				98.9	-216	664	151	33.2	-476	-112	-17.9	32.5	173.6	81.8	83.8	232.6	-41.9
After Prestressing of ERS				140.3	-3.9	352	149	12.9	-479	-108	-35.5	32.5	110.9	7.8	73.2	233.9	-93.1
After Hanging Dead Weights				139.7	-5.3	456	150	12.7	-479	-107	-35.1	32.9	110.6	7.6	74	233.9	-93.1
	S	-5.7	-9.19	103.6	200	679	127	-12.3	-530	-130	-60.2	97	149	182.3	80.2	333.3	156.8
	N	5.99	8.42	90.7	267	644	129	-15.8	-523	-137	-45.4	81.7	163.2	165.9	93.9	309.4	-73.4
	S	-13.2	-17.39	120.7	452	720	109	-21.7	-538	-130	-44.6	97	175.9	298.4	101.6	388.4	372.6
	N	11.69	14.96	88.4	253	655	142	-5.3	-511	-133	-26.7	87	186.1	175.8	127.4	301.2	0.8
	S	-18.2	-22.61	182.7	169	747	112	-16.7	-523	-114	-25	130.9	230.2	388.6	118	658.4	532.2
	N	18.62	20.51	49	428	790	120	-26	-500	-130	-6.3	112.1	281.8	338.3	183.5	494	202.8
	S	-24.3	-28.99	221.5	154	741	112	-13	-510	-101	-10.5	152.4	256.3	603	120.5	917.3	640.2
	N	24.25	27.56	21.2	424	719	622	-32	-429	-170	21.3	146.5	382.8	187.4	284.2	490.7	444.9
	S	-30.5	-29.67	298.1	-76.9	817	830	-8.7	-389	-133	27.8	193.4	360.9	547	246.3	941	810.3
	N	30.43	31.56	33.6	336	813	771	-26.8	-388	-158	47	146.9	419.3	210.8	391.2	517.1	680.8
	S	-61.1	-46.16	332.1	-54	753	1653	20.4	-95.8	-74	62.5	354.3	426.5	1010.7	539.8	1618.9	1466.2
	N	60.08	45.09	248.4	571	740	1871	0.4	16.8	-127	160	197.2	657.9	297.5	1248.7	828.8	1888.4
	S	-86.8	-50.79	341.1	125	723	2138	38.1	23.2	-45.3	126	509	480.4	1250.5	826.5	1802.6	1947.3
	N	91.16	50.66	385.6	859	794	2290	-12.7	81	-67.8	343	250.2	966.3	399.7	1586.9	1597.5	2815.3
	S	-134	-57.11	379.9	562	762	2494	136	132	589	245	1104.5	737.2	1848.8	1747.4	2637.4	2136.3

Table 4.3 Strain Gauge Readings in Reinforcing Bars Of SP-A
(Strain 10^{-6})

GA-18	GA-19	GA-20	GA-21	GA-22	GA-23	GA-26	GA-27	GA-28	GA-29	GA-30	GA-32	GA-33	GA-34	GA-35	GA-38	GA-39
-0.7	-1	0.8	-128.7	3.6	-1	2.5	-0.8	1	-11.1	-5.3	-2.5	-0.8	-2.2	1.6	-1.9	-0.2
298.4	-288.9	109.1	215.5	151.9	-43.7	-156.9	-72.2	35.1	-9.6	-7.3	107.1	194.1	-126.7	-933.3	-15.9	-19.3
263.4	-338.4	142.5	252.4	133.6	-73.5	-181.4	-70.4	40.1	22.9	43.6	188.9	192.4	-124.9	853.5	84.1	84.3
263.1	-337.1	141.8	226.3	132.7	-73.1	-181.4	-70.5	40.3	23.5	45.1	188.6	192.6	-124.5	853.7	84.6	85.2
428.2	-252.8	230.5	706.6	166.2	35.5	-110.1	234.1	41.2	57.7	159	224	140.6	94.1	-491.9	137.2	135.6
575	-251.2	229.1	677.3	157.2	40.9	-119.2	236.8	35.8	55.2	139	223.3	139	82.4	-490.6	137.4	166.7
411.9	-186.9	303.4	483.7	189.3	76.6	-63.8	404.9	42.3	74.9	206	263.4	135.6	180.8	-1098	190.2	160.7
616.6	-219.7	235	722.5	162.5	51.5	-107	218.6	44.3	40.9	113	197	131.8	65	-489.7	116.1	151.2
632.2	-150.5	402.6	-400.4	253.2	100.4	-23.8	585.8	78.8	83	231	283.9	155.8	201.9	-1109	232.5	180.6
903.5	-106.6	317.2	-424.4	205	109.3	-37.5	563.3	74.6	58.3	157	233.3	128.9	62.5	-1108	236.4	290.6
883.6	-132.4	552	-548.8	398.5	113.2	-3.6	677.2	91.6	87.1	253	300.2	157.1	143.4	-1114	251.9	179.6
1199.5	-20.6	382.9	-742.7	258.8	125.4	-37.5	573	36.1	56	162	211.8	90.1	35.4	-1129	269.3	346.7
1061.3	-33.5	653.8	-34.5	478.6	112.2	16.8	853.8	78.1	90.5	290	324.6	149.7	47.3	-1146	305.6	209.8
1335.4	73.5	419.1	20.1	278.9	163.5	-6	786.6	63	62.6	166	215.3	109.2	-83.3	-1145	307	380.9
2146.8	234.7	1223.2	-757.6	911.5	151.8	63.3	1376.7	964	113.4	367	447.4	149.9	109	-1141	405.5	210.8
1960.9	840.1	624.7	-794.2	392.4	556.4	172.9	1426.2	1164.4	77.6	203	298.7	151.8	-121.1	-5905	470.1	559
2504.2	874.8	1518.3	422	1063.8	258.6	666.3	1505.1	1701.7	139.9	436	599.5	250.8	161.5	-3685	631.5	340.7
1990.9	1144.4	916.7	2210.9	473.8	812.5	505	1347.1	1544.2	106.3	248	422.8	256.6	-78.4	-3671	664.6	779.5
3732.3	2292.8	2514.3	-85.7	1313.4	327.3	1020.4	1263.1	2033.8	169.9	480	603.9	418	284.1	-3886	818.3	449.1

Table 4.3 Continued

GA-40	GA-41	GA43	GA-45	GA-46	GA-52	GA-53	GA-55	GA-56	GA-57	GA-58	GA-59	GA-60	GA-64	GA-65	GA-67	GA-70	GA-73
-2.2	1.8	-0.2	1.7	-3	2.1	0.9	-0.4	-0.8	-0.3	0	2.3	-0.6	0.1	0	-0.6	0.2	2.2
-19.7	-17.7	35.4	-13.6	71.5	160.9	166.5	54.6	61.4	5.1	82.3	61.6	310.2	-16.8	112.5	-14	12.7	-20.4
-36.6	-34.9	163.7	60.6	136.7	225.1	297.1	288.1	163.5	-35.9	186.6	168.5	419	132.4	323.4	-37.6	117.2	88.2
-36.5	-34.8	164	61.8	137.8	225.2	297.2	288.2	163.9	-36.1	186.7	168.3	419.3	132.9	324	-38.2	117.8	89
-47.2	-47.6	257.2	141.3	180.3	387.3	462.9	293.6	704	-91.3	375.9	346.7	565.4	255.9	694	-63.2	295	253.8
-45.8	-54.5	268.2	182.8	208.2	335.7	744.1	847.1	280.5	-94.2	385.8	292.7	565.5	306.4	631.9	-59.9	285.5	251.4
-50.7	-41.1	303.1	171.2	219.5	471.9	409.6	225.4	1033.9	-98.6	465.6	467.6	648	311.8	732.6	-75.6	384.5	331.1
-42.3	-53.3	249.5	180.4	200	283.8	739.8	893.5	170.1	-89.7	355.2	244.1	528.4	275.6	564.6	-54.3	241.5	219.2
-48.4	-22.3	296.1	181.6	289.1	583.2	370.8	184	1176.3	-101.8	536.6	552.1	734	351.6	778.3	-79.7	463.9	395.1
-57	-59.6	396.5	317.3	395	306.7	1048.1	1256.5	356.4	-100.1	568.2	395.3	715.7	545	721.1	-75.2	388.4	405.4
-45.6	-5.3	276.4	176	288.2	668.5	342.6	165.2	1341.1	-107.5	593.5	645.6	798.7	398.2	835.8	-80.6	541	444.7
-76.7	-78.1	472	418	501.9	421.5	1315.3	1572.6	486.8	-117.3	735.1	507.4	847.3	772.7	812	-64.4	478.2	564.2
-43.5	18	305.2	260	381.8	839.7	405.7	220.6	1525.9	-113.4	739.9	779.8	948.8	507.3	908.7	-40	703.2	568.2
-70.1	-84.9	513.4	522.6	585.3	420.3	1408.5	1693.2	511.4	-112.2	845.3	565.3	916.1	911.7	888	-23.6	521.3	673.6
-7.8	81.1	278.3	277	448	1037.2	581.5	347.9	2139.6	-142	1142.5	1408.6	1438.8	941.6	1251.4	-67.7	1325.5	948.3
-6.9	-97.3	738	696.5	756.8	392.7	1884.3	2315.3	888.8	-95.3	1506.9	1050.3	1317.7	1771.2	1154.6	9.6	884.7	1389.5
63.5	175	433.7	450	600.5	944.2	765.1	906.6	2563.3	-161.4	1565.4	2076.7	1937.1	1369	1712.1	-104.7	1463.9	1375.1
101	-67.1	1093	987.2	1020.5	345.7	2131.3	3413.5	1251.4	-99.8	2181.1	1640.9	1750.1	2631.2	1614.9	-27.7	1049.8	2043.7
146.6	348.5	584.3	570.1	657	1022.2	1003.5	1967.6	2805	-170.6	2125.2	4467.7	2687.1	1892.3	2402.7	-97	1835	1924

Table 4.3 Continued

GA-76	GA-77	GA-78	GA-79	GA-80	GA-81	GA-82	GA-83	GA-84	GA-85	GA-86
1.2	-0.3	-1.7	0.4	-0.8	-0.8	0.7	-0.6	-2.6	-1.2	-1.3
134.1	163	108.3	133.1	-30.7	-54.9	-2	41.8	165.4	-87.5	-2.8
123.1	465.6	388.1	305.2	199.3	22.9	114.3	103.9	224.5	-36.1	44.3
122.5	469.5	386.4	306.9	198.8	23.5	114.1	104.5	223.8	-35.6	44
39	382.5	1151.4	487.7	876	233.2	973.7	272.1	912	-18	837.3
34.3	886.7	603.7	735.1	516.3	367.3	753.8	330.9	832.8	6.4	757.9
42.4	292.4	1290.1	498.9	1168.6	234.8	1289.7	281.6	1188.5	-27	1096.5
34.3	914.8	403.7	729.9	326.9	340.1	553.6	305.4	696.5	-12.8	569.5
47	254.3	1380.3	502	1259.4	236.1	1339.3	318.7	1253	2.4	1171.7
37.2	1224.9	261	998.9	521.2	572	786.4	509.7	959.9	84.6	878.7
51.4	237	1529.2	525.2	1410	230.1	1477.5	315.9	1356.2	-0.2	1284
43.8	1483.2	214	1212.7	576.3	768.4	802.6	664.1	993.6	193.2	934.6
72	267.7	1556.2	628.9	1468.3	272.3	1523.7	371.1	1411.1	49.5	1370.2
52.9	1589.1	262.5	1304.5	585.4	853	760.5	732.7	972.2	246.7	919.4
91.4	453.9	2103.9	825	1960.7	467.5	1927.1	438.4	1745.1	84.9	1789.1
46.7	2375.7	598.6	1863.6	829.4	1412.1	724	1478.4	952.9	1239.3	853.1
138.7	751.7	3062.8	1115.6	2432.9	888.9	2213.1	836.7	1873.3	600.7	1943.3
85.9	3038.6	1485.5	2161	1047.7	1601.1	814.9	1673.2	1071.8	1420.6	874.6
161.8	1574.5	2601.1	1232.6	2494.6	949.3	2265	789	1790.8	570.6	1923.6

Table 4.3 Continued

Gauges Lost

Ga-4	Ga-16	Ga-17	Ga-24	Ga-25	Ga-31	Ga-36
Ga-37	Ga-42	Ga-44	Ga-47	Ga-48	Ga-49	Ga-50
Ga-51	Ga-54	Ga-61	Ga-62	Ga-63	Ga-66	Ga-68
Ga-69	Ga-71	Ga-72	Ga-74	Ga-75		

Loading Stage	Loading Direction	Peak Drift	Lateral Load	GA-1	GA-2	GA-3	GA-4	GA-5	GA-6	GA-7	GA-8	GA-9	GA-10	GA-11	GA-12	GA-13
		(mm)	(kN)													
Virgin Slab				2.8	-0.3	-4.4	-2.9	0.4	-1.7	-0.2	0.3	-0.4	-0.6	-0.8	2.3	-0.8
After Mounting ERS				6.6	12.4	4.2	-1.5	4.9	-0.6	-1.2	5.1	7.8	6.7	3.4	15.7	4.6
After Prestressing of ERS				261.3	217.8	911.7	142.5	-23.1	-27.4	146.6	205.1	14.1	-6.8	-3	187.5	182.6
After Hanging Dead Weights				283.9	247	895.2	147.2	-27.5	-31.5	141.2	198.6	5.7	-17.9	-13.5	177	166.7
Lateral Load	S	-6.4	-6.73	311	281.8	931.3	209.2	-30.1	-29.9	136.6	209.2	1.7	-10.6	-20.9	203.6	154.3
	N	6.67	9.87	308.7	295.3	928.4	211.3	-26.4	-33.5	141.2	199.4	18.4	-27	7.7	167.6	206.6
	S	-12	-14.5	330.4	299.2	925.3	219.8	-29.4	-27	137.5	216.6	1.6	4.2	-28.1	236.8	139.1
	N	12.2	17.3	311.4	358.8	920.3	234.6	-24.3	-34.6	145.7	196.1	33.2	-29.6	31.4	164.7	245.4
	S	-21	-17.2	365.3	300.6	927.6	220.7	-38.6	-35.1	129.7	209.7	-0.7	7.9	-34.1	250.9	132.9
	N	18.9	25.12	337.3	434.9	912.6	279.9	-30.9	-43.1	145.7	189.4	60.6	-31.8	83.4	155.8	537.7
	S	-25	-24.2	415.5	302.5	939.1	316.4	-45.1	-37.1	128.5	223.9	11.5	37	-41.1	311.8	117.5
	N	25	29.63	361.9	486.5	950.8	363.7	-39.7	-49.9	145.7	186	92.6	-37.2	125.1	147.4	683.7
	S	-31	-28.2	453.9	299.5	880.5	525.2	-67.4	-33.4	175.8	243.1	41.3	90.8	-43.2	427.1	152.1
	N	30.2	31.91	398.3	510.9	905.5	457.4	-55.9	-47.9	177.6	194.4	134.6	-34.6	136.1	172.5	693.9
	S	-63	-44	429.4	320.1	918.7	510.1	552.9	45.1	403	329.6	49.8	327.3	-30.6	949.1	241.2
	N	59.6	44.57	450.6	370.6	950.9	604	933.2	29.1	432.8	355.5	249	-0.6	618.4	186.5	1113.6
	S	-91	-46.9	548.7	369.3	859.1	488	892.6	210.9	474.1	399.6	80.8	541.7	30.6	1244	488.1
	N	92.9	49.96	533.7	511.4	911.6	630.6	1262.5	98.6	544.6	467.3	380	112.9	911.8	259.1	1377.9
	S	-110	-45.6	552.5	385.9	895.7	497.3	950.7	256.9	485.6	437.2	133.6	634.6	76.9	1322.7	930.6

Table 4.4 Strain Gauge Readings in Reinforcing Bars Of SP-B (Strain 10^{-6})

GA-14	GA-15	GA-16	GA-17	GA-18	GA-19	GA-20	GA-21	GA-22	GA-23	GA-24	GA-25	GA-26	GA-27	GA-28	GA-29	GA-30
1.2	-1.2	-0.9	-2.1	-2.2	-3.8	-5.1	-2.6	-1.1	-193.5	-0.7	-0.4	-1.9	-1.1	-4.1	3.6	-773.7
5.2	8.6	11.2	2.6	0.3	-0.5	-5.8	9.2	1.2	-572.6	1.6	-0.3	-1.3	31.8	-1.4	9.8	732.6
96	344.9	-18.8	186.8	5.8	276.9	20.7	-827.8	15.9	-7.3	44	80.7	15.2	-22.7	9.6	40.6	68.8
75.6	341.2	-25.9	178.8	2.5	274	10.3	-912.4	8.8	-19.7	40.5	73.1	7.2	-28.2	4.4	46.2	84.9
111	406.3	-8.5	225.1	14.7	271.4	34.9	-1215	30.8	-31.3	56.9	71.7	13.1	-34.3	8.6	68	178.1
54.5	400.6	-0.6	225	33.9	308.4	-8.6	-1174	10.5	-16.7	47.8	77.8	9.9	-30.2	5.3	59.7	147.2
159.5	476.7	13.7	311.2	21.9	263.5	73.3	-1257	53.7	-31.5	71.4	71.5	19.1	-34.6	12.1	85.8	268.6
45.4	429.5	67.4	264.2	74.5	331.6	-18.4	-1190	10.2	-5.2	51.7	83.6	11	-28.3	4.2	61.6	168.6
223.4	563.6	66.6	410.4	45.8	267.5	102.4	-1221	71.6	-34.2	70.5	64.4	12.5	-46	2.6	109.3	357.6
41.3	634.1	191.7	495.8	126.6	431.3	-37.1	-1095	23.8	21.3	82.4	88.2	0	-34.6	-7.8	81.6	208.4
483.2	642.9	190.3	518.2	200.2	192	191.1	-1283	113.7	-13.3	152.2	82.2	173.5	-36.5	31.5	132.3	461.4
38.7	744.9	261.5	634.2	168.3	465.7	-46.1	-1067	35.7	63.3	169.6	110.6	160.7	-26.3	7.1	89.6	236
609	803.7	254.2	432	227.6	226.1	253.9	-1253	145.9	-12.8	166	93.6	255.8	-49.1	41.2	172.1	539.7
40.2	840.3	297.7	506.8	216.8	648	-38.8	-972	50.7	76.7	190.7	129.3	267.1	-39	18.7	117.7	242.6
1200	1031.9	532.2	593.4	339.3	260.2	677.1	-1284	277.4	10.7	330.5	127.8	303.5	-9.7	731	245.7	798
121.2	791.6	304	669.6	183.1	875.6	-16.3	-691.6	84.3	510.8	194.7	175.1	437.5	-8.4	393	165.4	300.1
1463.5	796.5	376.5	821.9	369.7	395.7	915.6	-1285	413.7	209.5	616.4	168	398	-3.7	1013.5	292.7	821.6
791.6	1089	397.7	1771.6	197.7	1117.9	127.5	-283.6	183.4	1001.2	242.2	191.8	513.6	2.7	781.3	220.2	333.6
1294.1	825.6	478.6	1027.3	663.1	365	1089	-1196	495.6	344.1	641.6	196.5	423.9	1.4	1071.8	369.8	944.8

Table 4.4 Continued

GA-32	GA-33	GA-34	GA-36	GA-37	GA-38	GA-39	GA-40	GA-41	GA-42	GA43	GA-44	GA-46	GA-47	GA-48	GA-49	GA-51
-1.7	-1.8	-2.5	-6473	-15.5	-2	-1	-1.5	-1.1	-0.4	1.4	-10.2	-1.4	-2.3	35.9	-4.7	2.8
2.6	3.2	0	-13196	-13.6	9.6	10.1	11.1	2.5	3.1	16.8	-55.3	2	-0.1	663.5	0.6	22.2
90.3	-33.6	28.5	-14.3	241.2	57.8	-17.5	260.1	6.8	33.2	46.9	14.6	-6.1	51.9	79.3	206.1	44.4
113.4	-38.4	26.3	-11.7	362.7	94.3	-24.5	259.2	7.3	21.5	148.9	18.6	3.2	69	100.7	226.9	62.7
220	-44.6	26.6	19.9	447.7	193.3	27.1	273.3	16.9	30.3	194.5	42.4	11.5	91.9	127.2	254	76
180.4	-36.6	28.6	18.9	449.5	287.1	-10.9	271.2	13.7	3.1	233.6	57.6	22	102.8	122.3	264.6	99.9
284.5	-50.8	24.7	20.9	488	153.5	92.1	275.4	20.1	63	187.8	49.2	36.7	89.6	131.9	257	66.2
168.1	-33.1	27.5	18.4	463.4	299.5	-2.3	270	9.8	0.5	282.6	85.2	55	112	118.5	280.3	118.7
390.4	-55.7	22.2	73	607.1	152.2	172	276.7	22.3	104.4	190.3	47.8	42.9	101.2	160	272.1	69.9
177.9	-17	26.5	60.2	537.2	353.3	74.1	269.4	8.5	44.6	397.9	125.8	184.6	154.1	144.7	335.2	180.5
474.7	-49	26.9	85.7	691.4	135.1	302	297	39.4	161.7	201.4	44.7	147.7	153	217	314	101.4
182.8	5	33.1	57.6	608.1	303.9	130.3	278.1	11.5	83.9	470.8	156.8	271.1	213.2	180.2	392	231.1
583.1	-45.3	22.2	92.8	703.1	151.6	410.5	331.9	54.1	177.1	186.9	-5.2	168.3	193.2	704.1	372.9	172.5
209.6	28.8	31.5	49.6	630.9	256	207.3	317.7	25.9	119.1	488.9	126.5	328.3	264.9	549.9	488.4	331.8
792.3	-42.8	25.4	119.2	707	187.1	566.1	324.6	54.1	230.4	176	2.1	201.1	219.3	1353.8	406.7	274.8
304.6	150.4	44.2	100.5	581.4	261.8	247.1	326.1	40.9	310.2	655.6	22	559.6	395	887.5	746.2	616.2
979.4	20.2	48.1	64.7	1017	299.3	705.2	344.7	65.7	399.9	304.9	10.7	227.5	306.4	1378.9	549.5	485.4
572.2	276.5	59.8	100.9	799.4	389.2	446	353.3	77.8	662.8	634.9	25.2	636.6	698.5	1071.1	999.5	868.7
806.7	82	80	52.7	1187.3	399.5	772.7	380.8	90.2	389.8	381.5	68.1	254.2	414.9	1366.9	610.2	585.3

Table 4.4 Continued

GA-52	GA-53	GA-54	GA-55	GA-56	GA-57	GA-59	GA-60	GA-61	GA-63	GA-64	GA-65	GA-67	GA-68	GA-69	GA-70	GA-71
0.2	-0.8	5.5	-0.3	-1.4	-1.3	0.5	-0.1	-3.7	3.7	-0.5	*Ga N A	-1.3	-3.4	*Ga N A	0.7	-1.8
4.2	8.8	3.6	-37.1	15.3	2.4	7.3	5.7	6.8	25.7	0	*Ga N A	1.4	2.3	*Ga N A	1.2	2.8
51.6	9.4	65.4	374.5	70.1	86.4	87.6	364.3	24	-0.8	183.5	*Ga N A	258.5	25.4	*Ga N A	36.6	-7.4
70.1	40.8	102.1	430.5	88.7	84.5	317.2	365.3	16.8	8.6	308.3	*Ga N A	119.2	57.9	*Ga N A	45.2	-16.6
152.9	47.8	237.5	483.7	164.8	71.4	530.7	400.9	16.4	26.9	271.1	107.8	109.2	71.9	293.6	140.3	-37
128.9	87.6	198.5	618.8	94	70.2	326.3	366.8	7.3	91.8	618.3	10.6	109	175.7	35.1	39.1	-43.3
180.9	31.6	298	414.6	238.8	75.2	693.7	426.2	10.5	-14.7	88.1	301.3	111.2	25.5	595.4	266.2	-46
131.2	121.5	202.2	718.3	77.9	72.6	236	345.4	-5.4	218	850.1	-25.6	105.8	344.8	-46.3	-24.9	-58.9
222.6	31.8	398.2	409.7	329.9	73.1	791.1	475.8	18.4	-60	19.5	553.7	112.9	-30.6	829.8	421.3	-37.5
163.5	284.3	270.5	861.1	147.4	72.4	145.6	332.5	-9.7	485.4	1237.2	-72.3	119.9	687.5	-102.7	-88	-73.9
280	96.1	538.4	442.5	506.5	75.8	904.8	543.4	35.1	-103.9	-28.6	867.6	130.1	-64.8	1168.6	598	-39.3
196.4	428.5	381	967.1	225.4	73.7	137.9	323.2	-15.8	665	1474.1	-113.8	130.6	963.5	-120.4	-126.9	-88.1
478.7	130.1	784.7	508.2	628.3	88.9	1087.2	775.3	64.6	-162.2	-51.2	1233.3	191.5	-109.3	1489.3	803.4	-43.2
325.2	566.9	542.3	1117.3	237.2	83.5	120.1	359	6.7	797.6	1724.5	-147.8	195.7	1236.2	-157.8	-149.4	-99.7
867.8	221.1	1273.6	661.5	1142.8	63.4	1784.6	1244.8	105.2	-241	-31.2	2085	180.1	-257.9	2465.7	1502.5	1.8
536.4	1059.9	1000	1554.9	578.6	81.6	333.4	339.2	-5.4	1452.6	4032.5	-213.2	195.5	2224.1	-13.6	-193.3	-132.2
981.5	421.9	1528.9	1259.2	1498.1	52.3	1530.3	1419.6	256.8	-279.7	1241.6	2431.1	172.5	-342	7318.9	1671.7	421.6
795.7	1654.2	1417.1	1947.7	1282.5	83.5	866.6	314.5	14.9	1648.8	4298.1	-417.4	213.9	2525.9	3333.1	-388	-99.3
1057.6	568.9	1610.6	1706.8	1698.8	37.8	1277.6	1288	380.7	-407.1	580.5	2499.9	178	-686	6078.5	1500.6	598.7

Table 4.4 Continued

GA-72	GA-73	GA-74	GA-75	GA-76	GA-77	GA-78	GA-79	GA-80	GA-81	GA-82	GA-83	GA-84	GA-85
-0.3	-1.7	0.8	-1.2	-1.5	0.1	-3.2	-1.7	2.4	-1.5	1.4	0.2	1.4	-1.4
1	5.5	5.8	4.5	9.8	5.1	-0.5	2.7	4.9	2.6	5.2	8.9	5.4	3.9
31.9	96.5	-8.9	119.8	-59	36.6	119.2	67.5	71.1	33.8	41	-0.6	135.6	358.3
22.5	121.9	12.9	149	-100.8	148	141.8	157.1	89.2	76	59.9	24	154.9	381.9
4.3	134.8	-40.4	259.5	40.5	217.8	218.3	294.6	161.7	131.5	108.1	73.1	201.2	434.9
14.9	217.4	146.8	145.1	121.7	364.8	136.5	360.9	130.9	163.2	90.3	89.5	188.7	443.8
-1.5	93.8	-122.2	350.9	-32.5	161.8	319.3	287.8	213.1	138.9	143.2	101.1	217.3	440.2
21.1	298.8	264.9	89.5	81.3	489	116.8	436	133.3	216.5	99.4	134.3	188.4	457.5
-12	62.2	-151.8	445.4	217.1	145.5	540.9	329.8	316.3	143.4	190.5	117.8	252.6	460.3
32.6	543.6	438.7	50.6	225.3	770.5	134	648.9	164.7	403.5	161.4	380.5	210.5	559.4
-22	65.3	-189.7	560.8	-586.9	174.2	770.9	477.5	431	302.1	222.5	455.8	285.5	910.2
38.9	710.7	529.4	24.7	6.6	1076.7	138.1	923.2	187.2	703.2	191.8	813	223.1	1019.9
-36.1	82.3	-177.9	653.3	512.9	215.4	982	502.9	516.3	238.6	279.5	471.9	306.4	773.8
41.8	872.6	569.9	-59.4	472.3	1313.6	129.2	1036.1	181.7	736.2	274.8	932.1	219.6	972.7
-89.9	10.5	-116.3	1333.1	465.4	281.2	1531	520.6	780.9	186.1	375.8	515.5	433.6	772.4
123.7	1603.3	838.8	-78.8	439.8	2114.8	300.8	1373.5	320.8	915.2	398.3	1123.8	344.7	1291.2
-63.1	139.1	15.7	1727.9	452.3	657.4	1907.3	656.2	1020.3	199.8	351.2	643.3	489.3	878.5
456.5	2135.5	1252.9	-9.1	356.2	2564.1	716.4	1812.6	554	1015.3	375	1228.8	473.5	1508.7
-1.9	315.9	329.1	1875.1	455.8	1020	1918	768.5	1179.7	223.5	289.1	665.9	568.2	903.5

Table 4.4 Continued

Gauges Lost	Ga-31	Ga-35	Ga-45	Ga-50
	Ga-62	Ga-66	Ga-86	

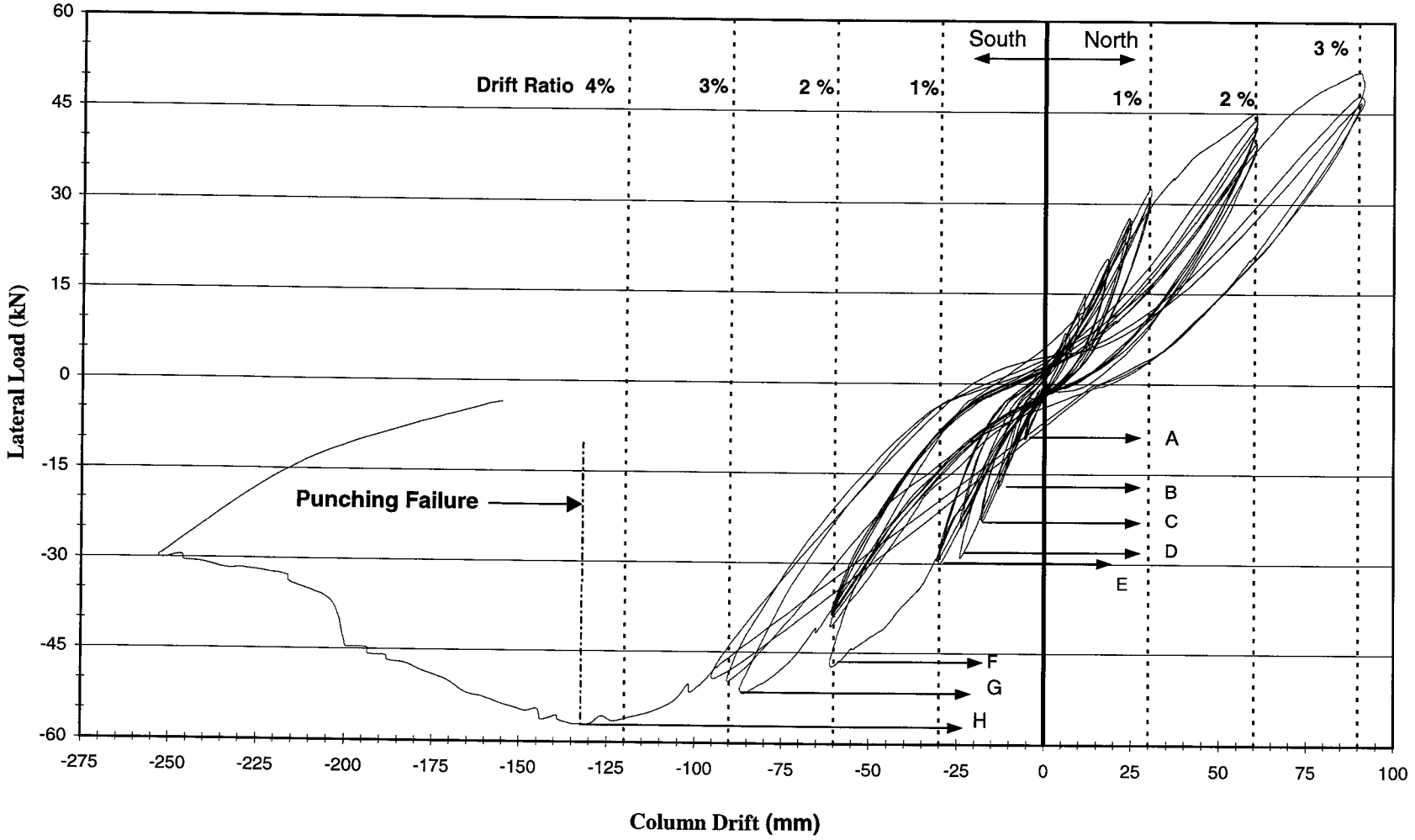

Figure 4.1 Lateral Load Vs Column Drift Hysteresis of SP-A (Partially Debonded Reinforcement)

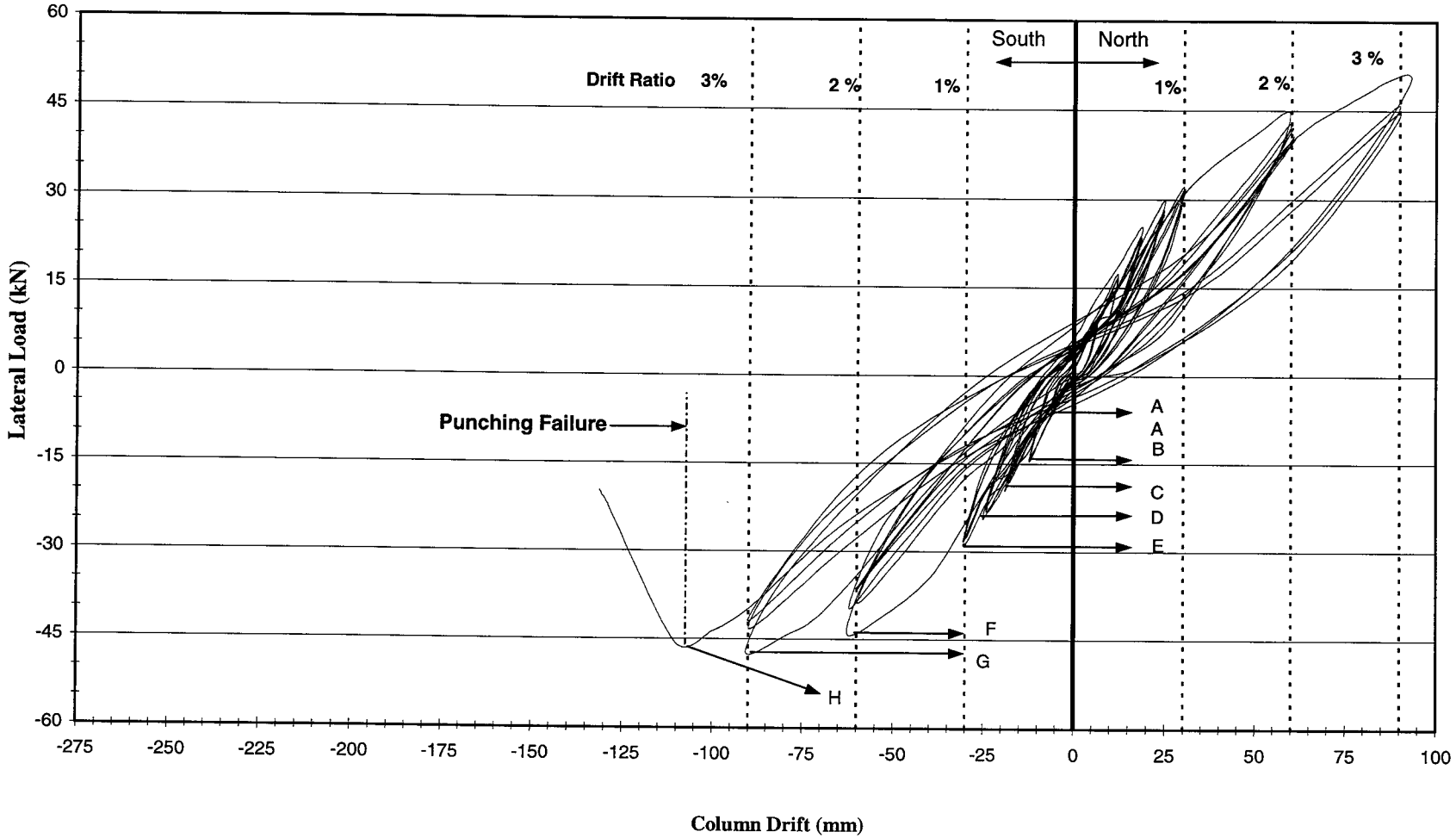

Figure 4.2 Lateral Load vs Column Drift Hysteresis of SP-B (Fully Bonded Reinforcement)

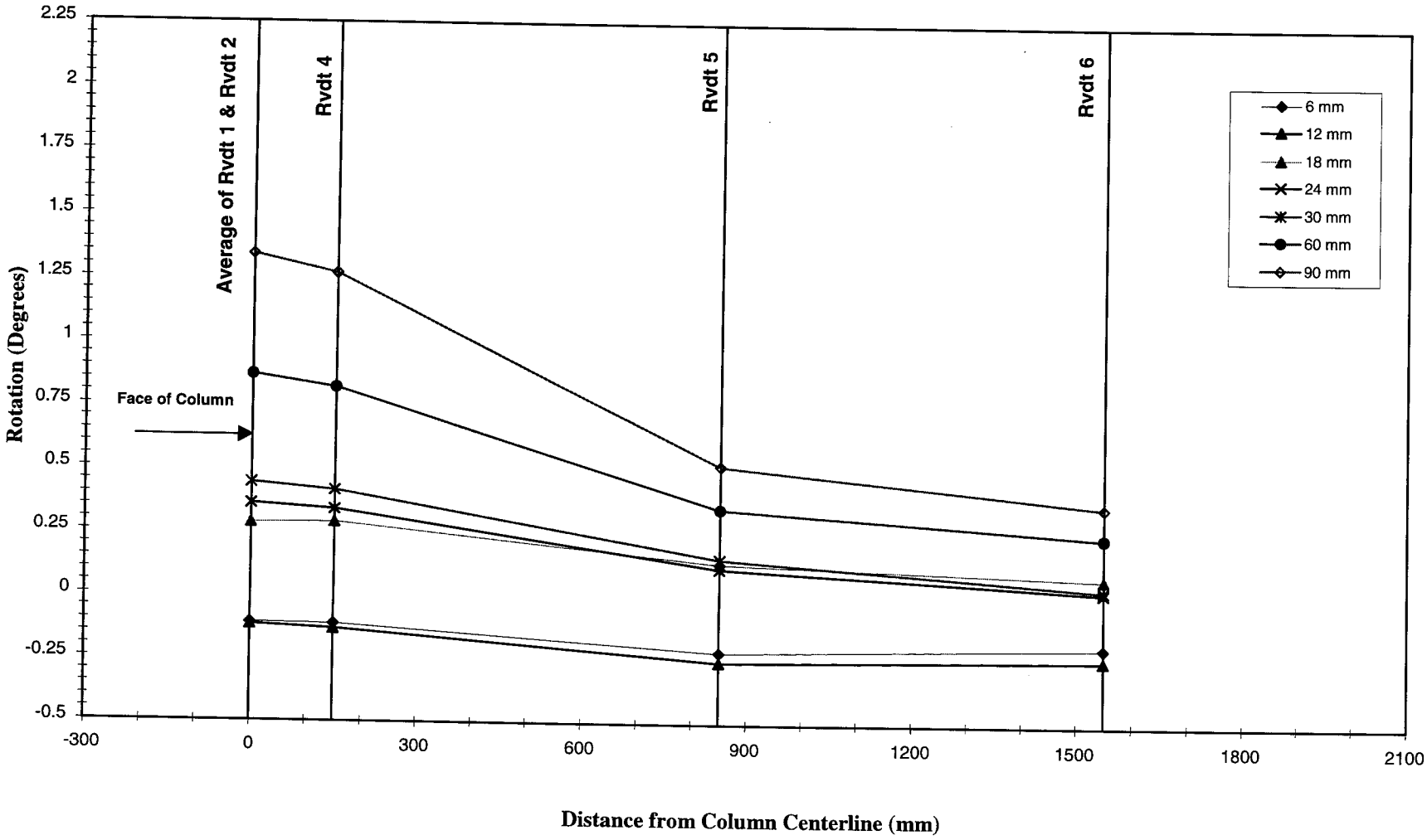

Figure 4.3 Slab-Column Rotation of SP-A at Peak Drift Values - Loading North

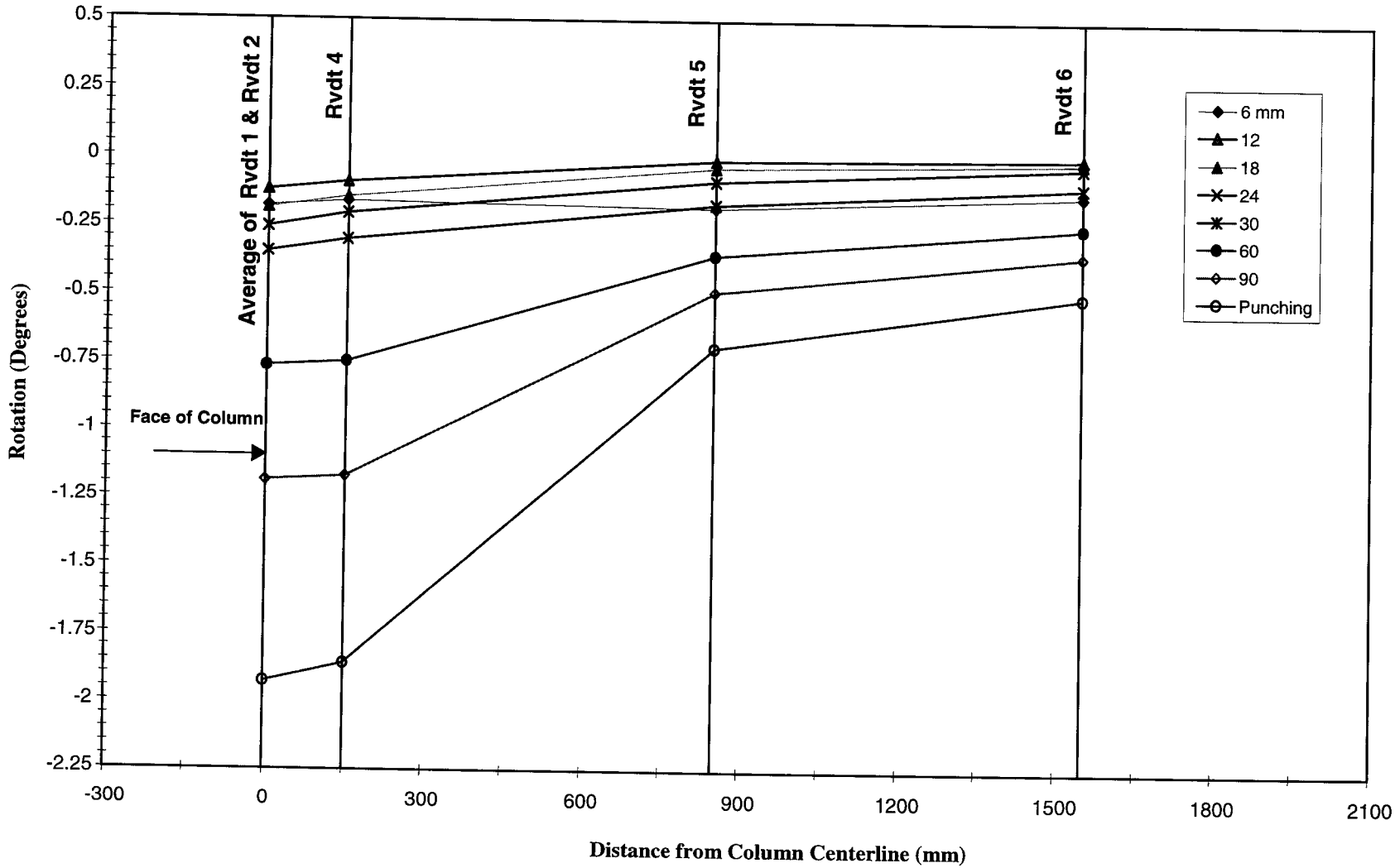

Figure 4.4 Slab-Column Rotation of SP-A at Peak Drift Values - Loading South

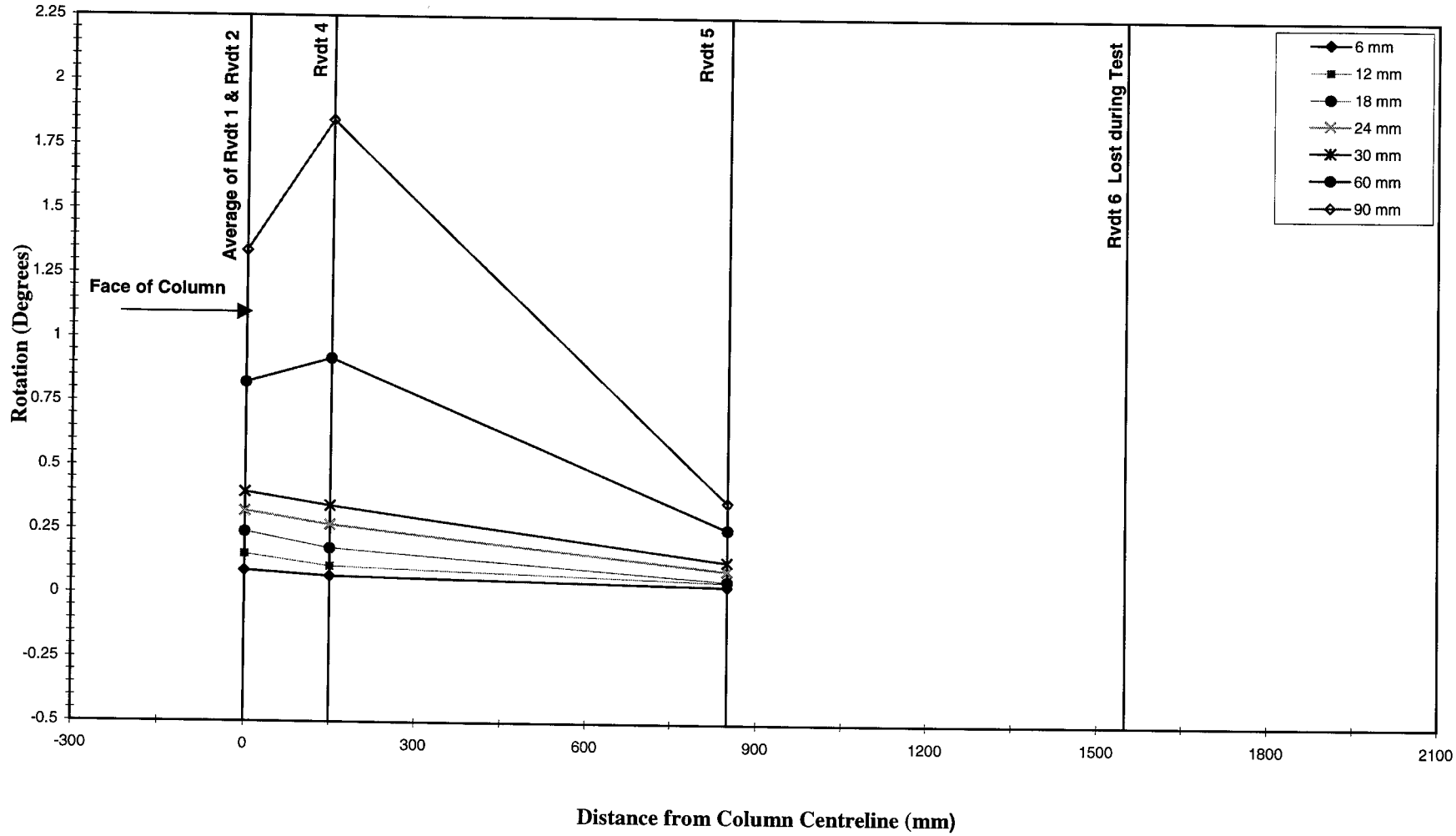

Figure 4.5 Slab-Column Rotation of SP-B at Peak Drift Values- Loading North

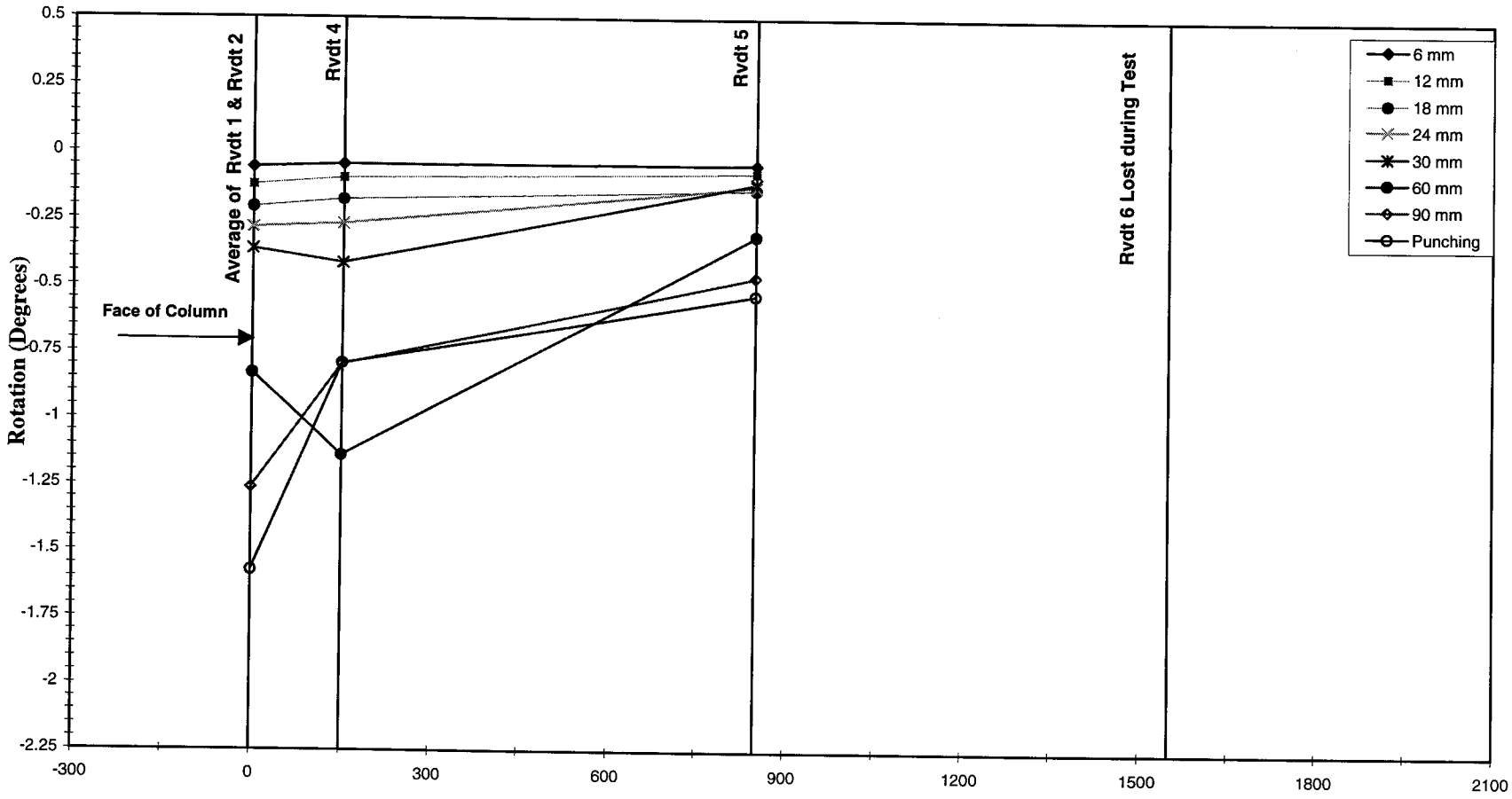

Figure 4.6 Slab-Column Rotation of SP-B at Peak Drift Values- Loading South

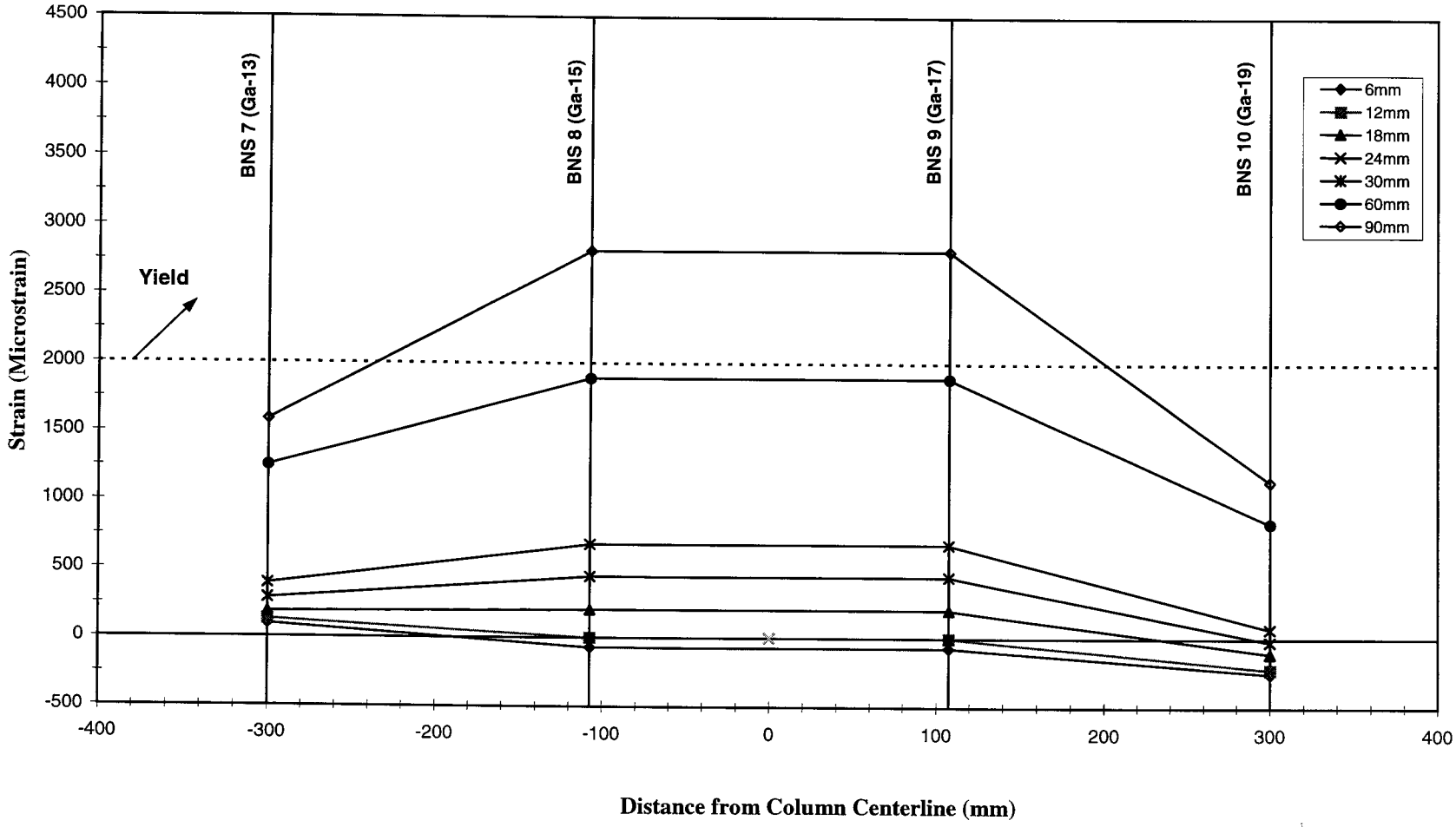

Figure 4.7 Strain profile of N-S bottom bars of SP-A at north face of column- Loading North

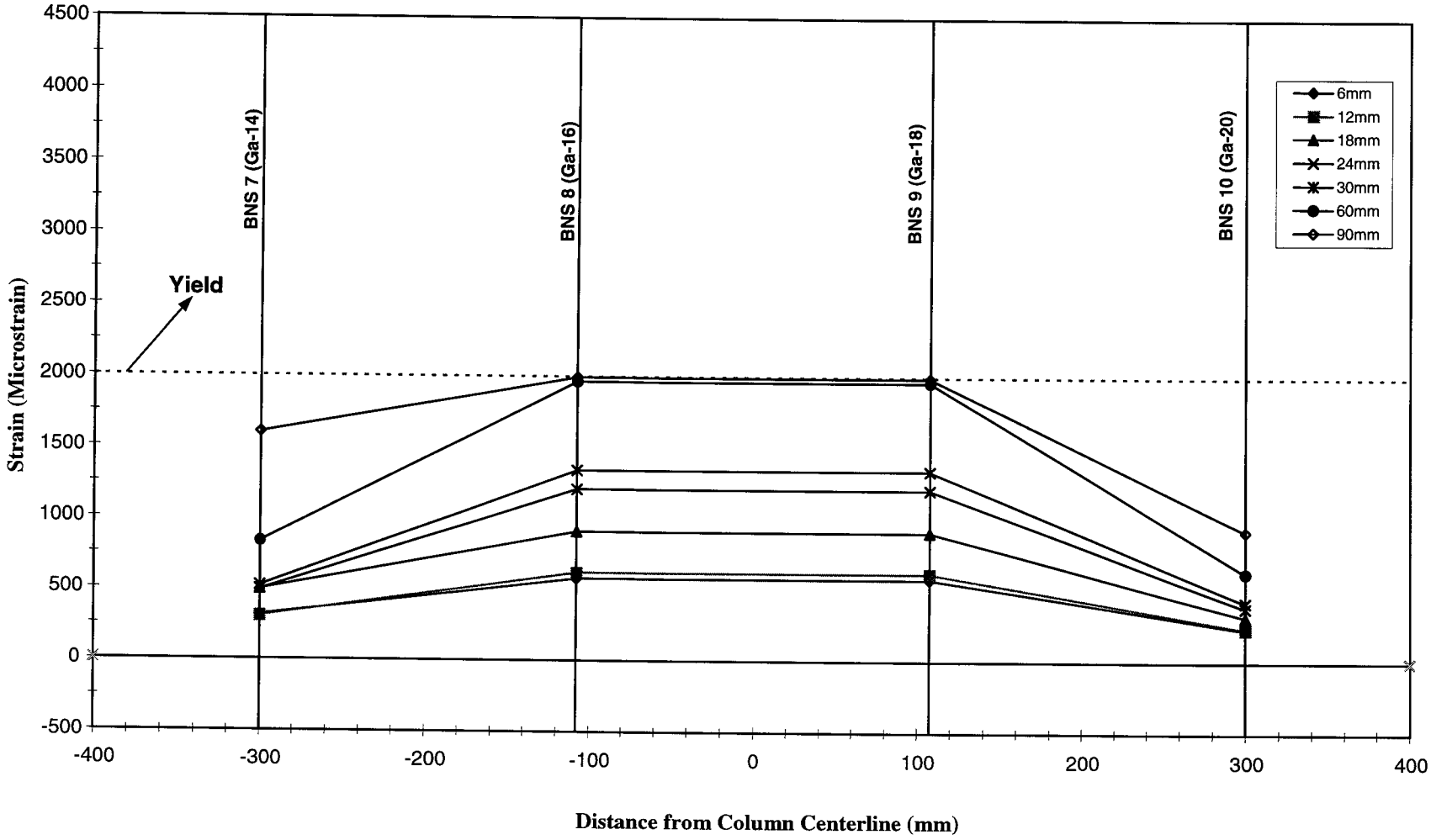

Figure 4.8 Strain profile of N-S bottom bars of SP-A at south face of column- Loading North

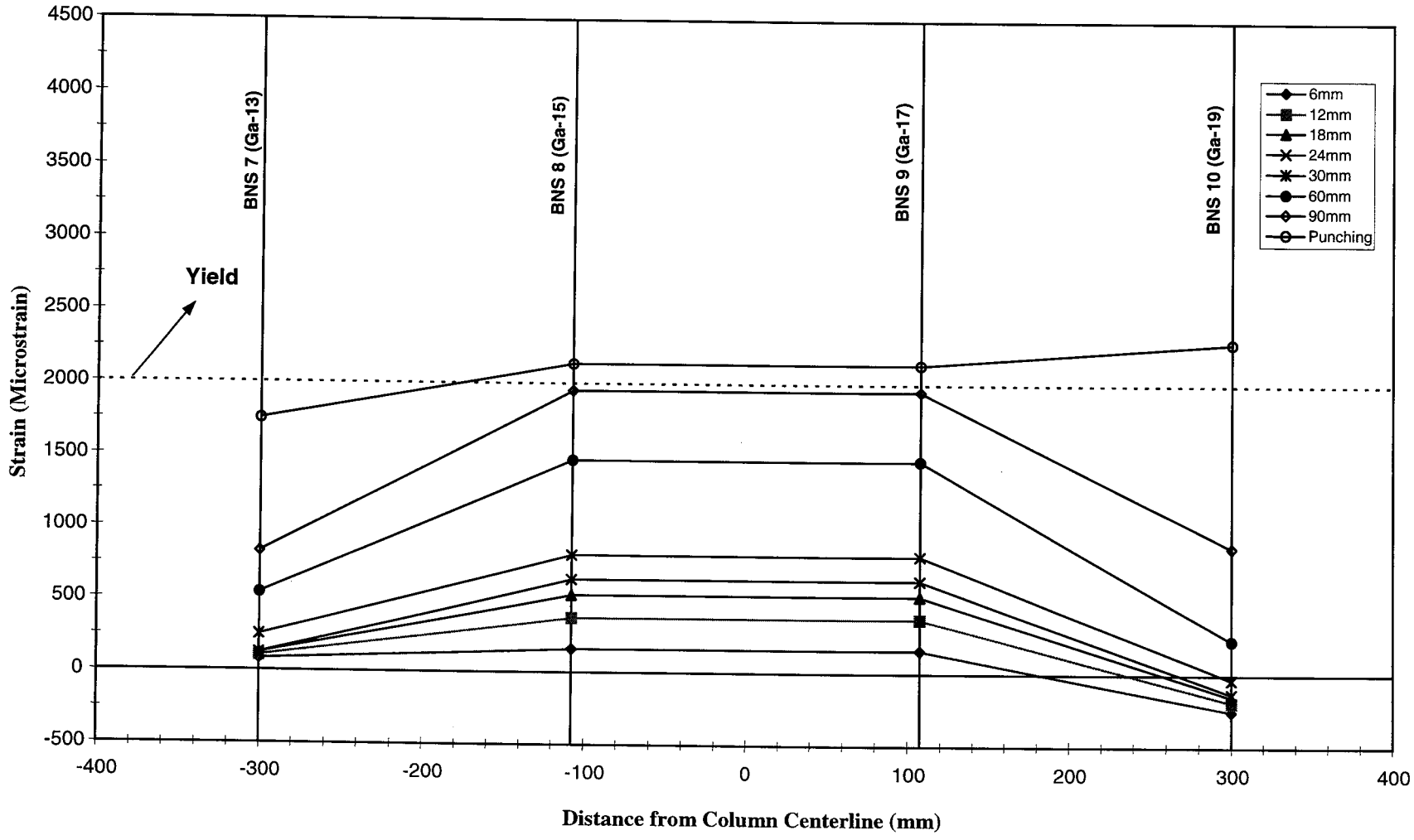

Figure 4.9 Strain profile of N-S bottom bars of SP-A at north face of column- Loading South

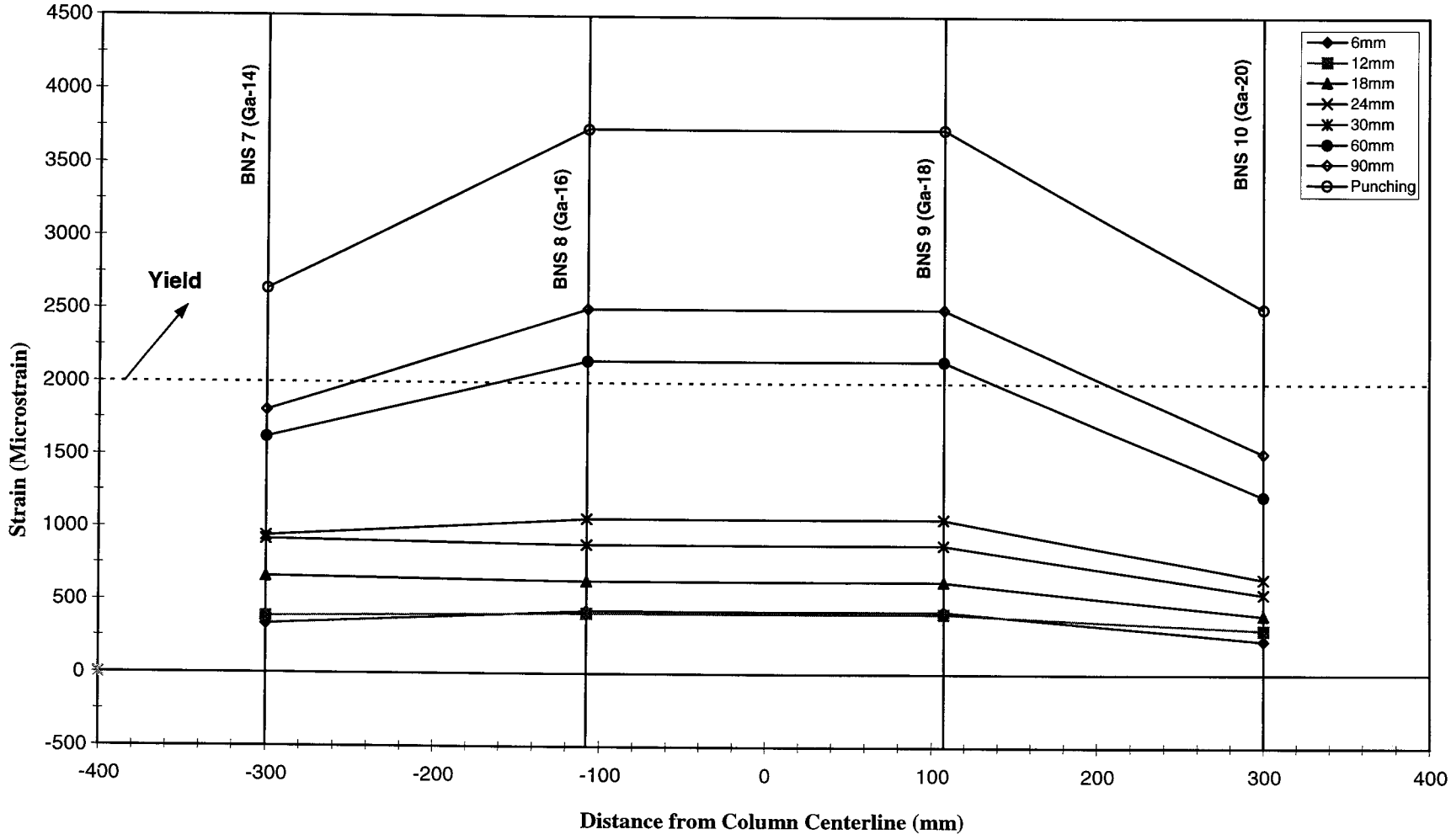

Figure 4.10 Strain profile of N-S bottom bars of SP-A at south face of column - Loading South

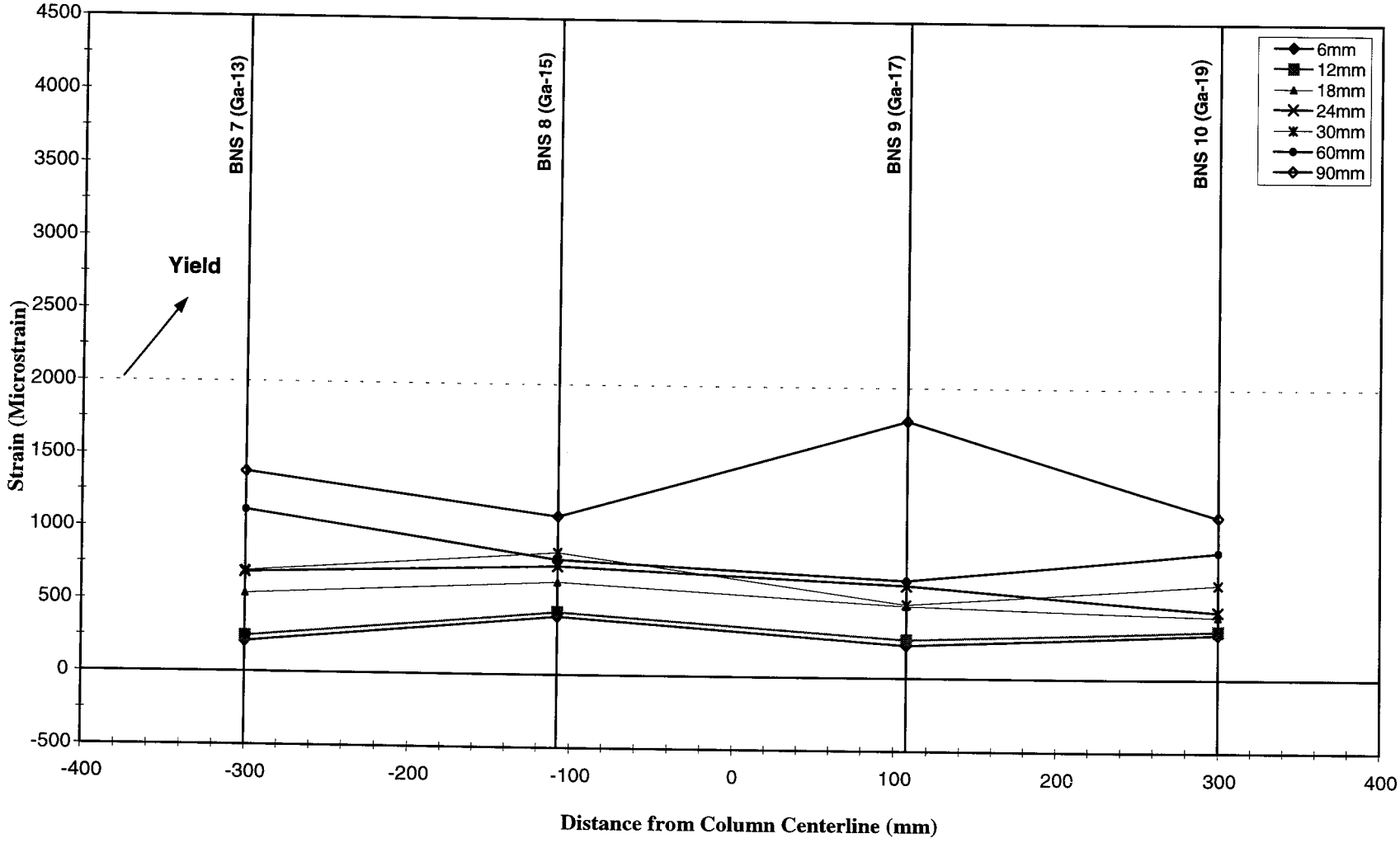

Figure 4.11 Strain profile of N-S bottom bars of SP-B at north face of column- Loading North

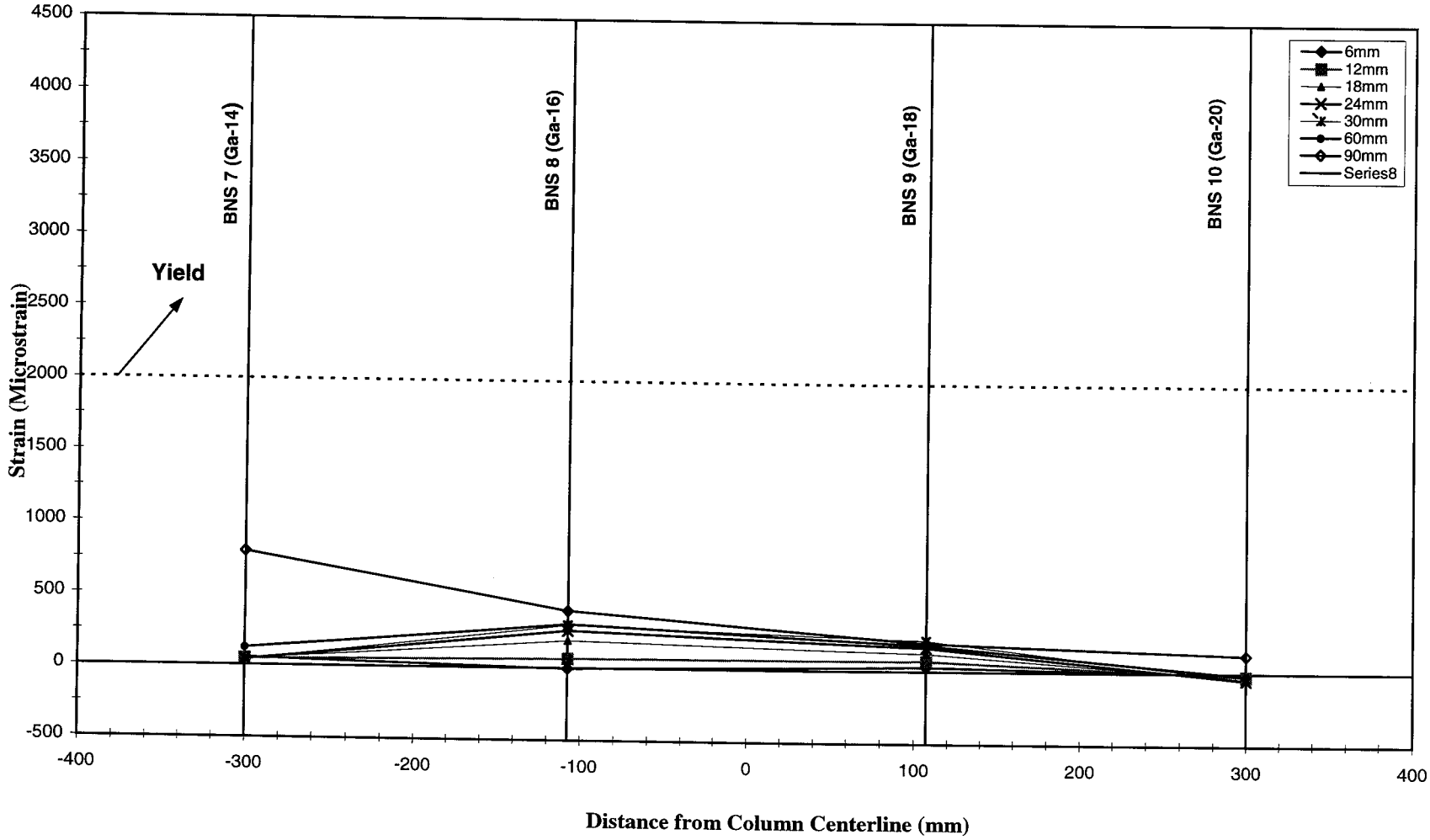

Figure 4.12 Strain profile of N-S bottom bars of SP-B at south face of column- Loading North

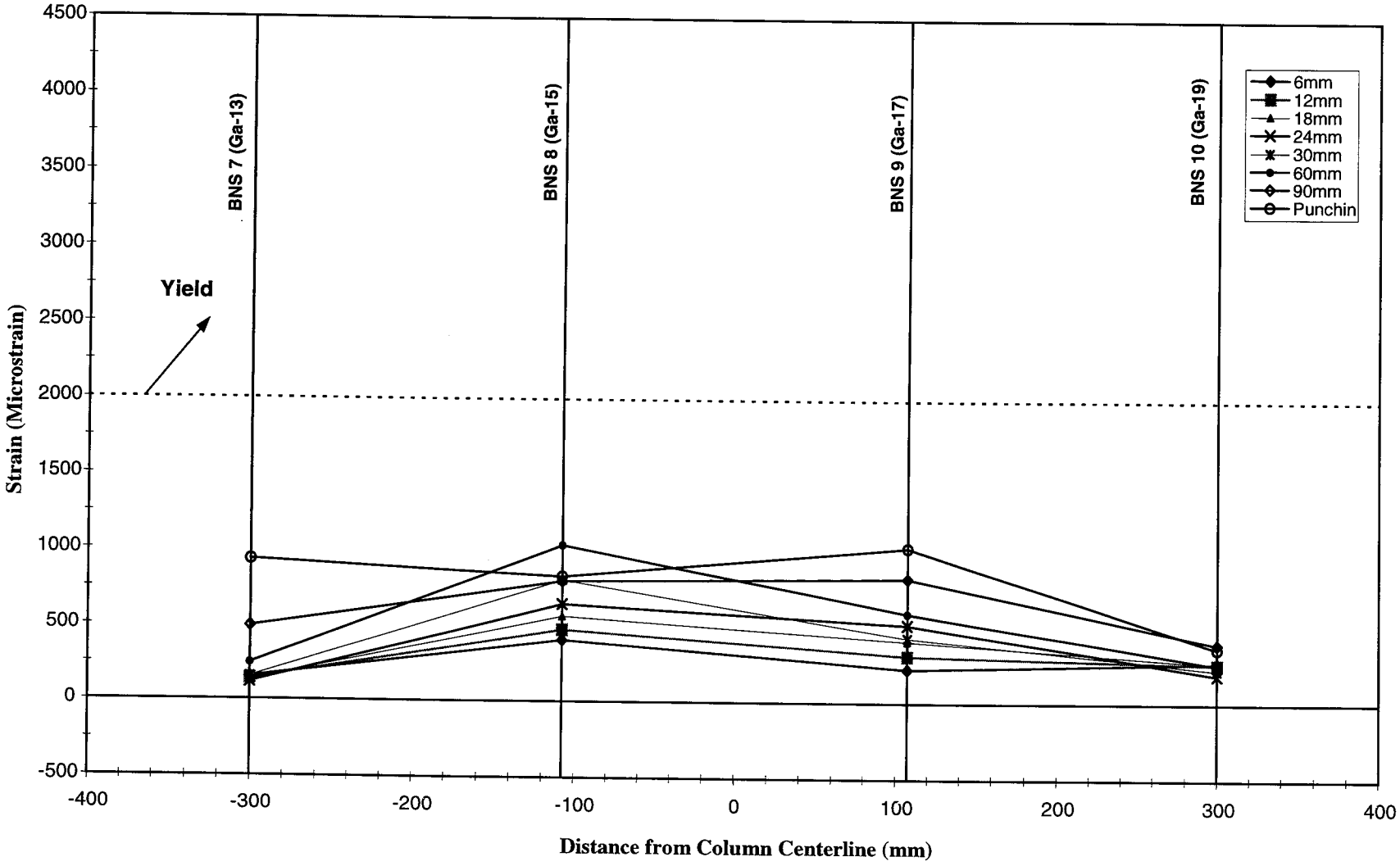

Figure 4.13 Strain profile of N-S bottom bars of SP-B at north face of column- Loading South

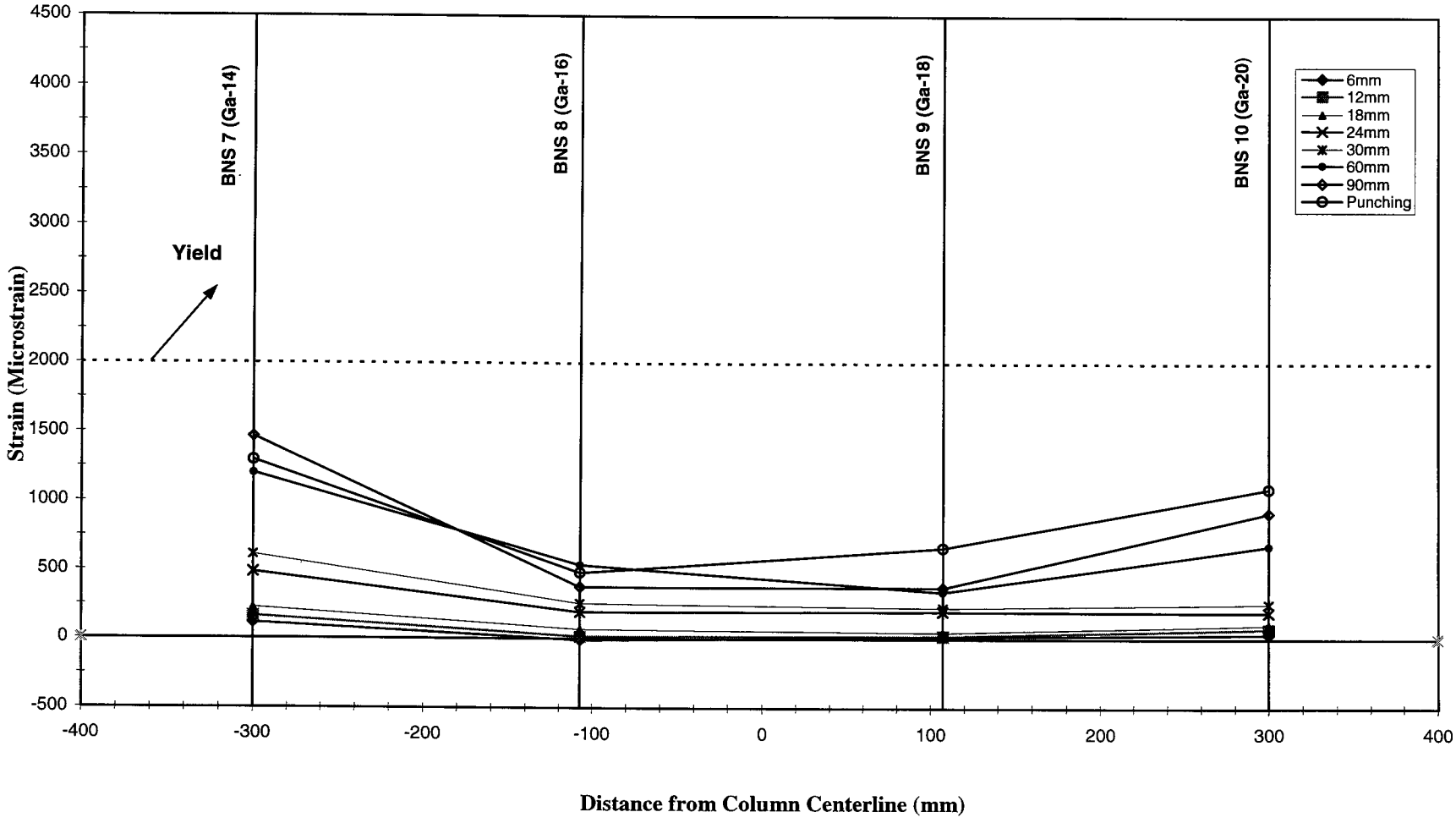

Figure 4.14 Strain profile of N-S bottom bars of SP-B at south face of column- Loading South

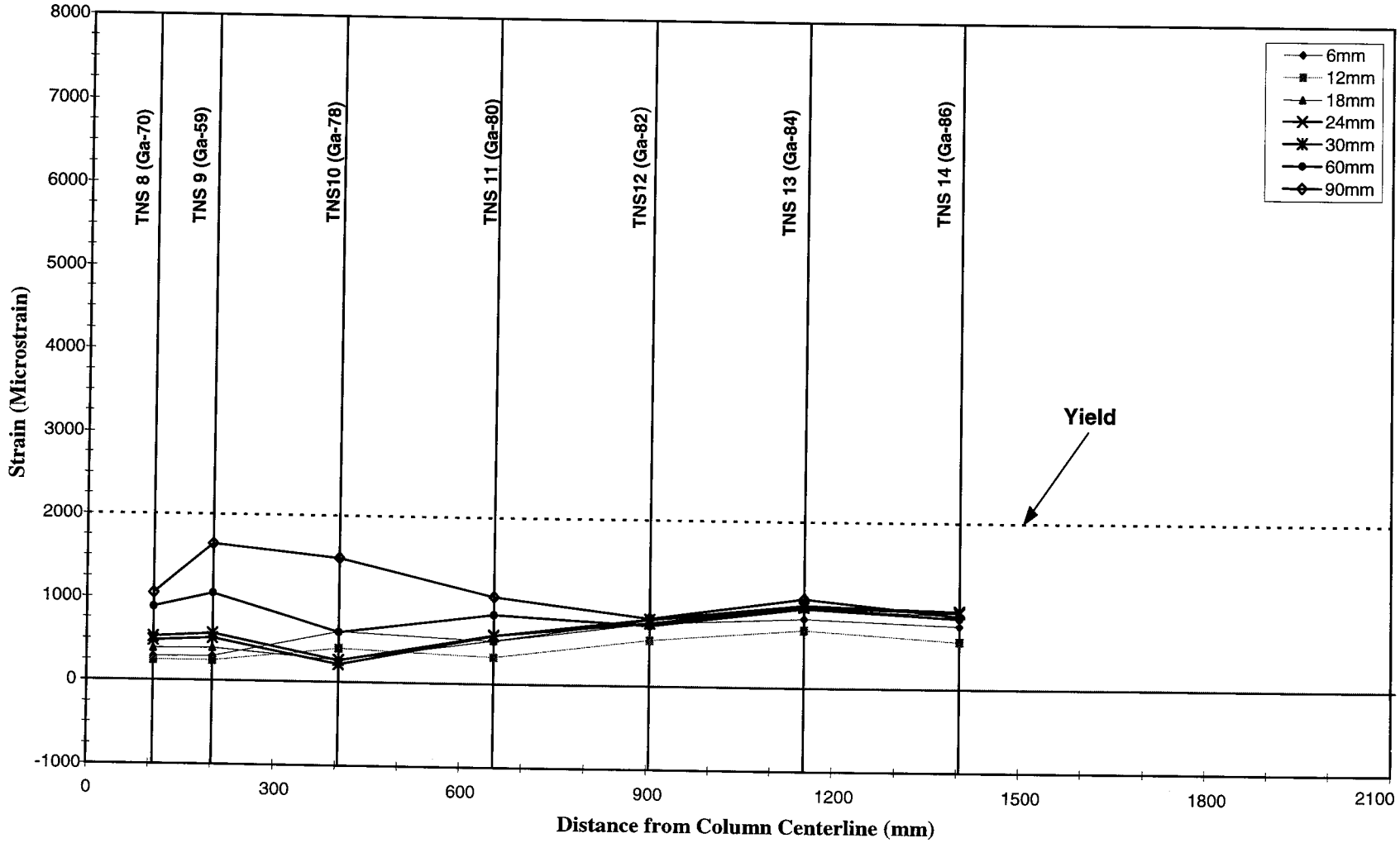

Figure 4.15 Strain profile of N-S top bars of SP-A at north face of column- Loading North

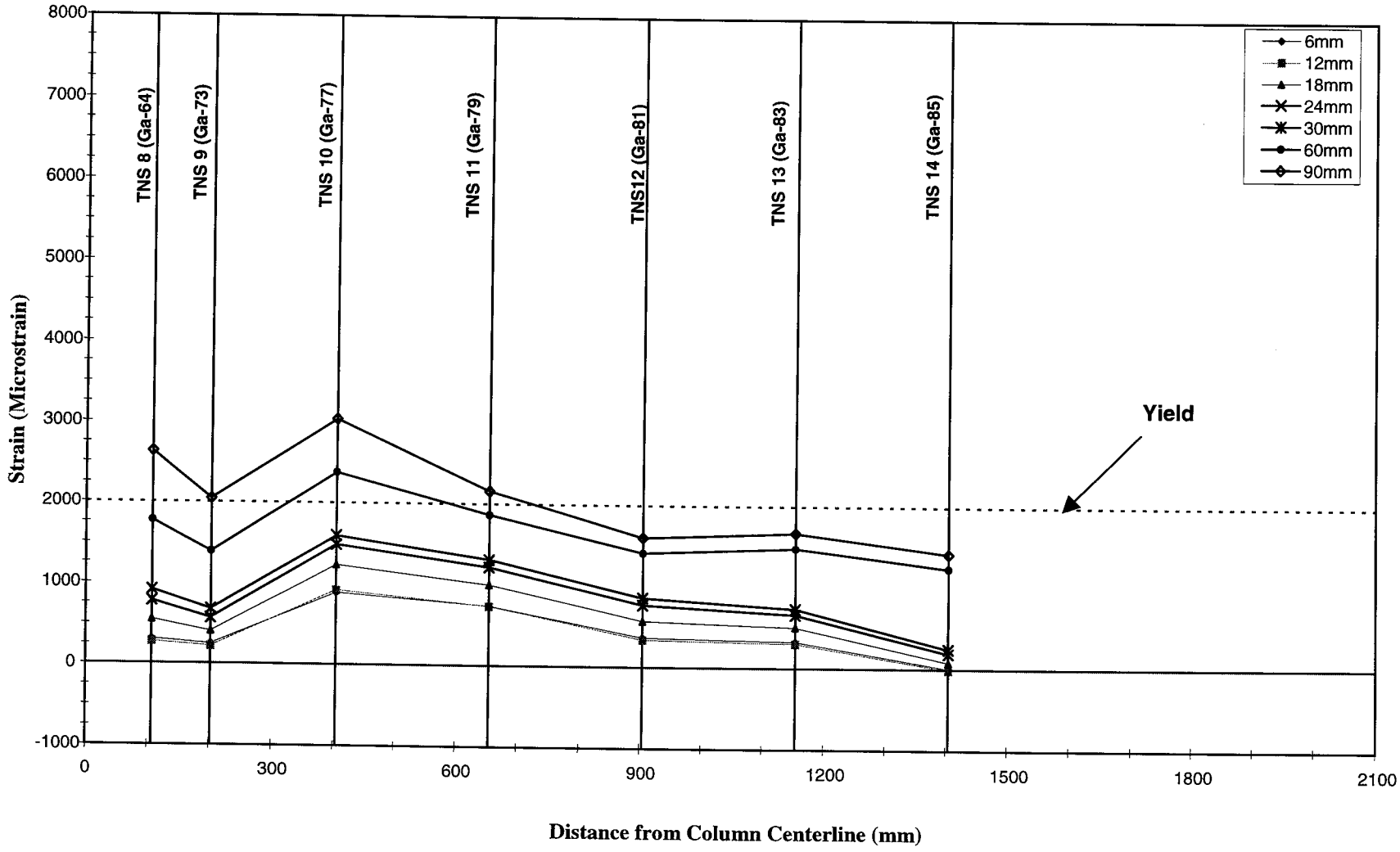

Figure 4.16 Strain profile of N-S top bars of SP-A at south face of column- Loading North

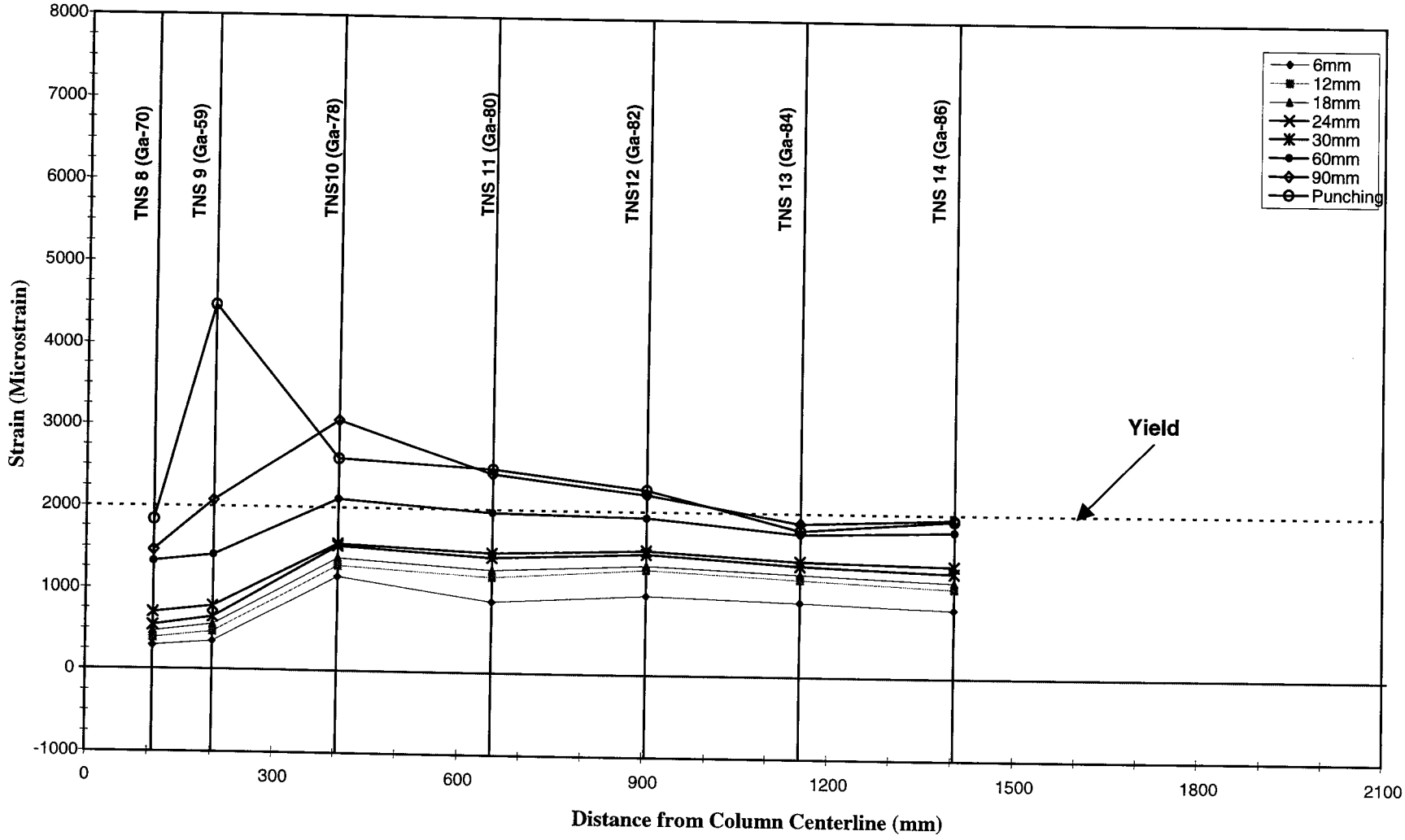

Figure 4.17 Strain profile of N-S top bars of SP-A at north face of column- Loading South

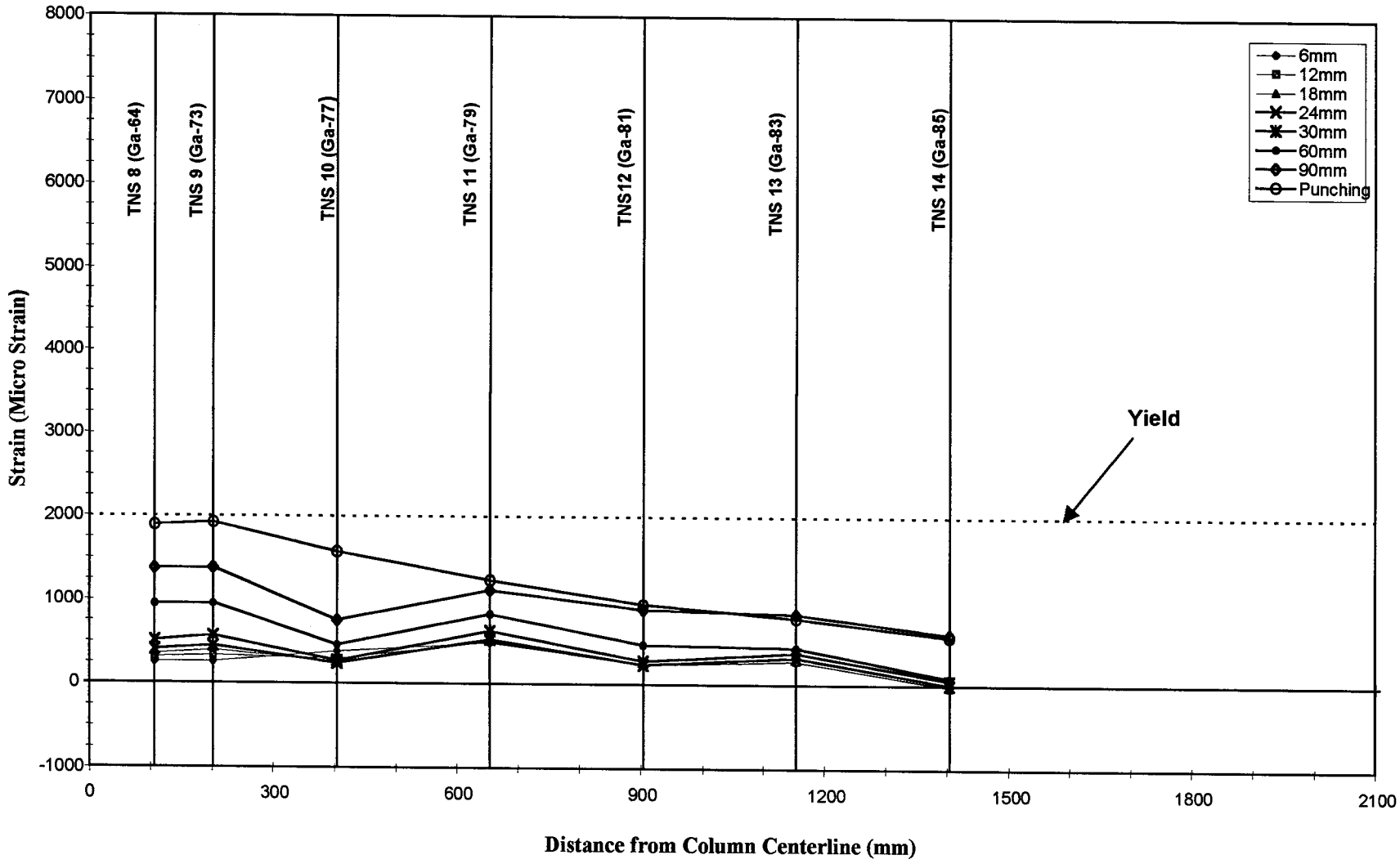

Figure 4.18 Strain profile of N-S top bars of SP-A at south face of column- Loading South

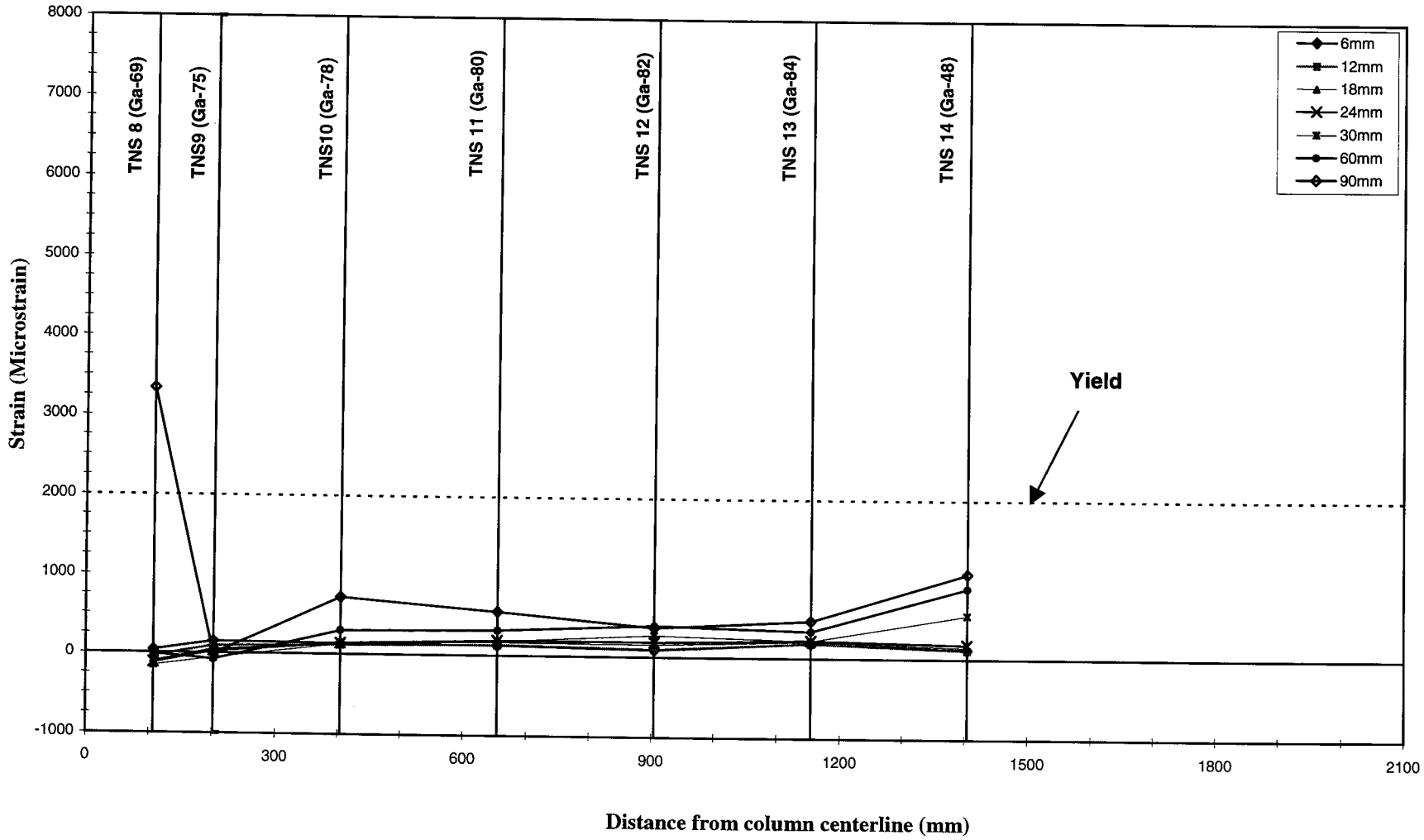

Figure 4.19 Strain profile of N-S top bars of SP-B at north face of column- Loading North

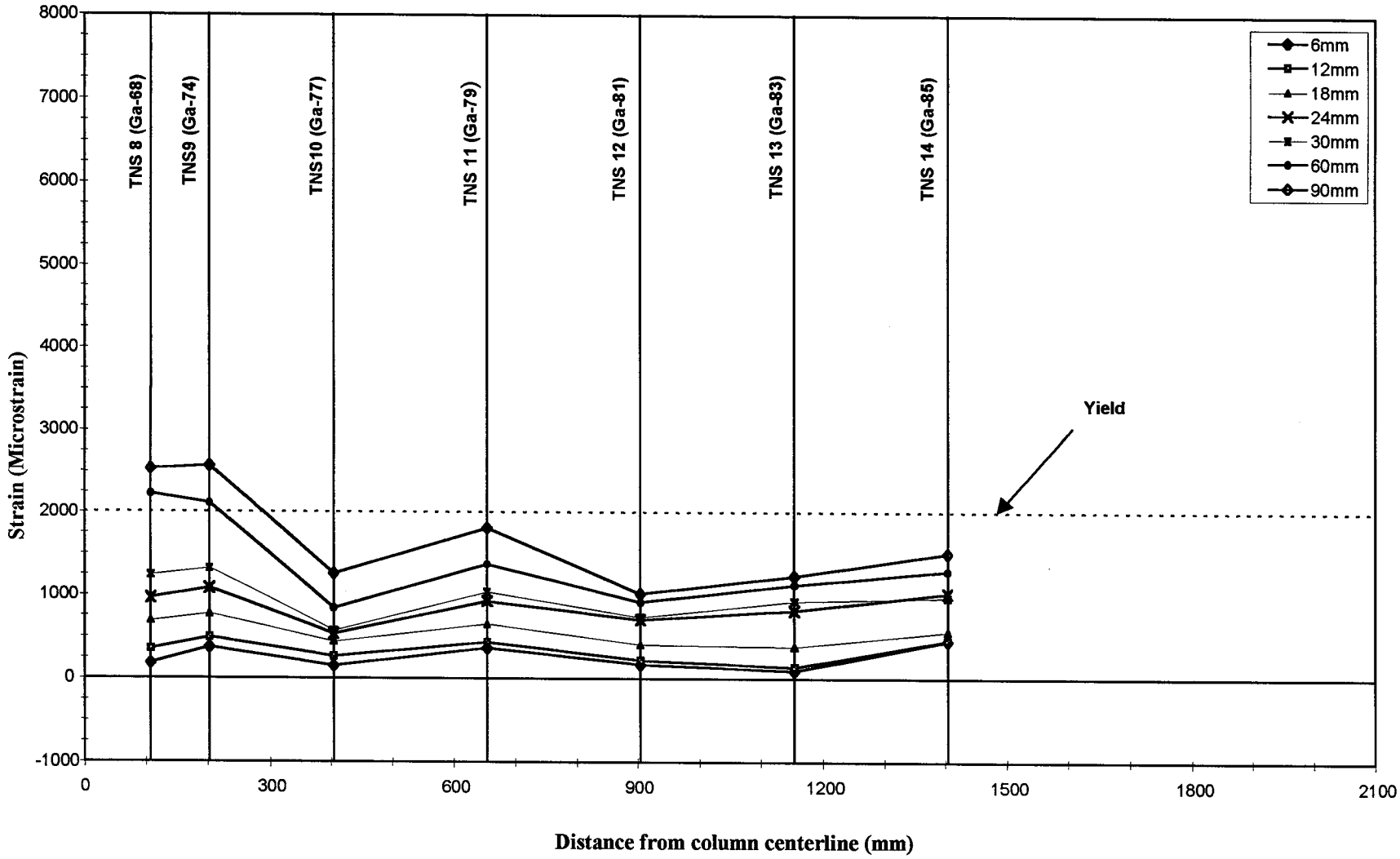

Figure 4.20 Strain profile of N-S top bars of SP-B at south face of column- Loading North

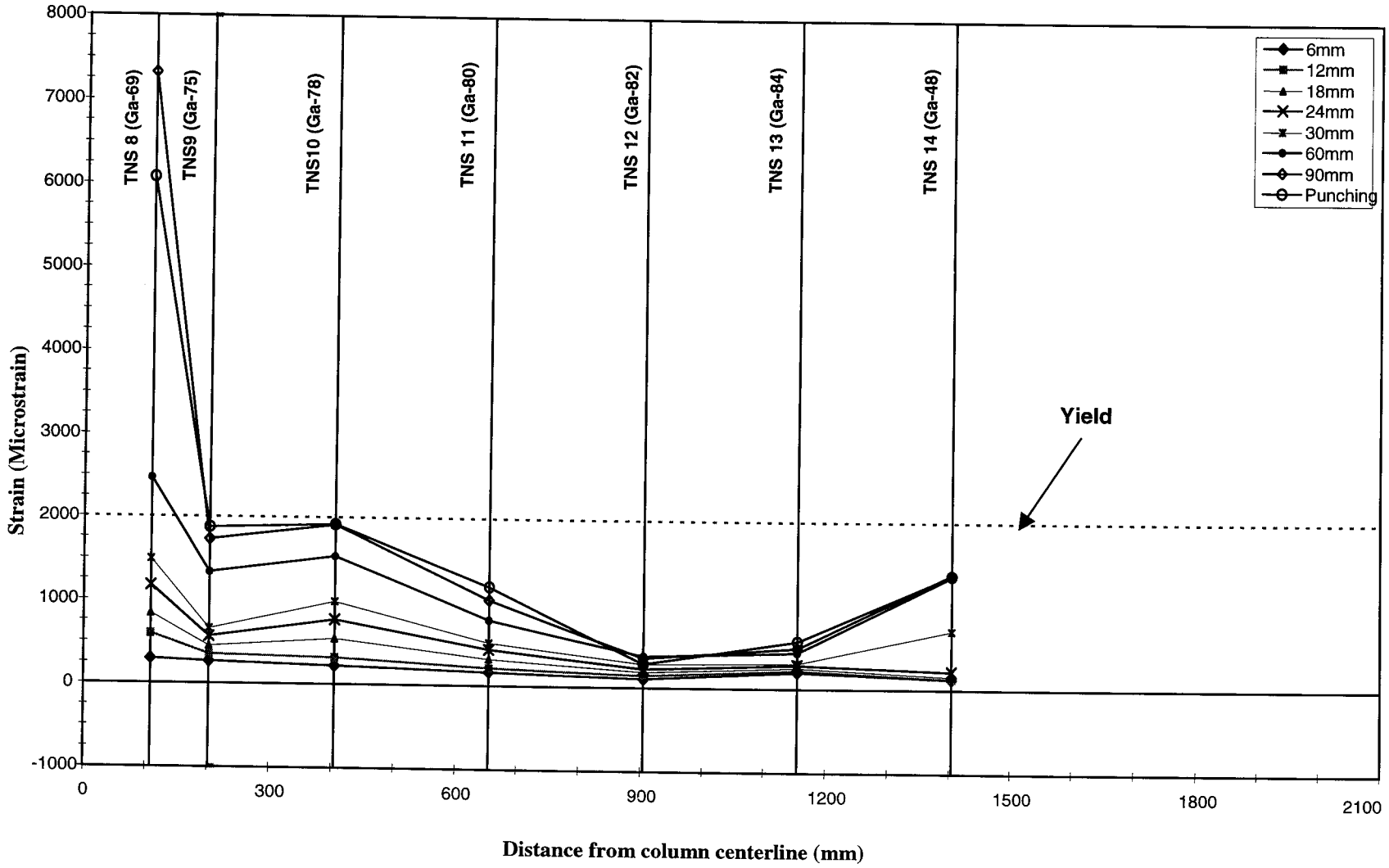

Figure 4.21 Strain profile of N-S top bars of SP-B at north face of column- Loading South

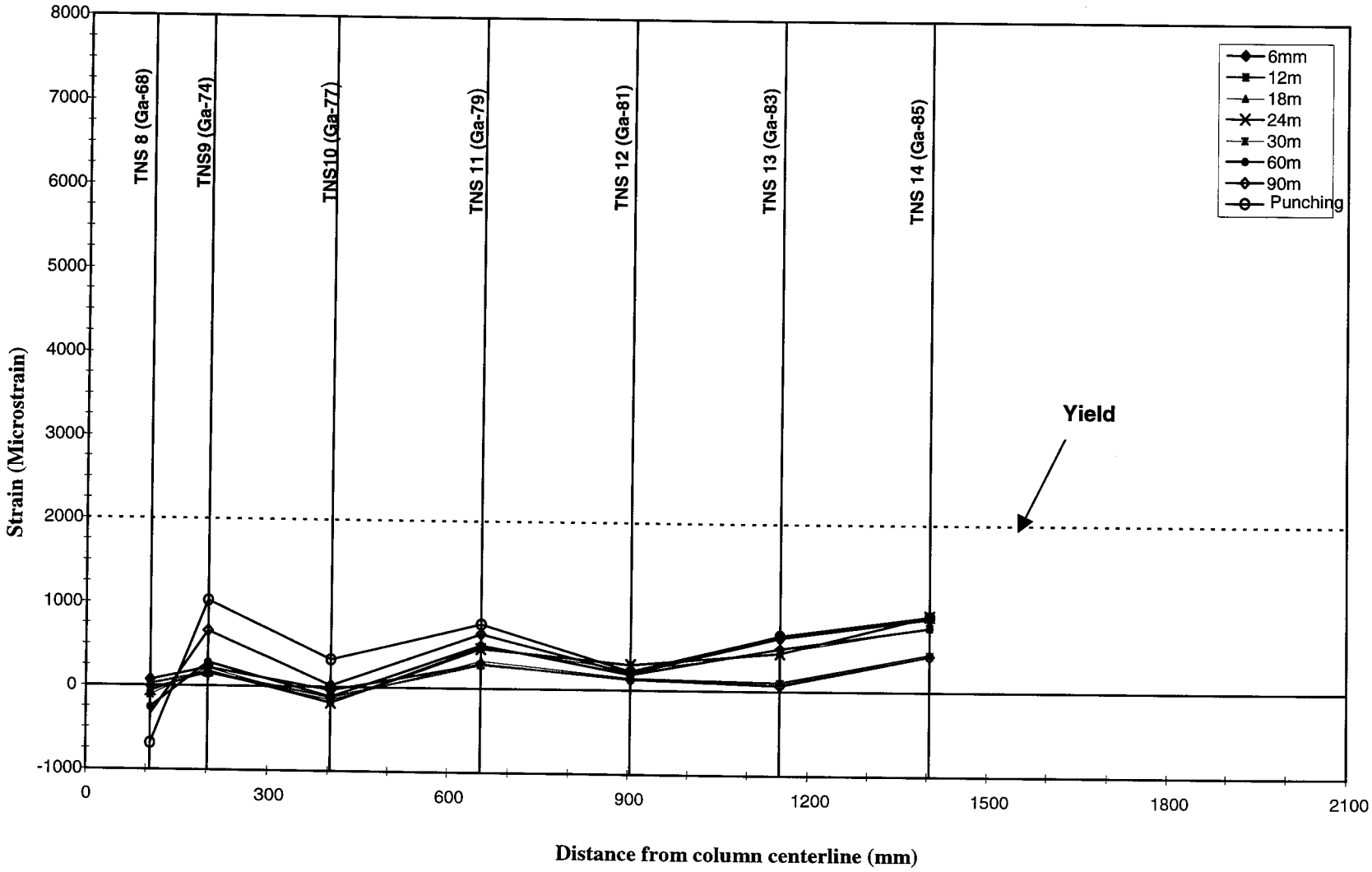

Figure 4.22 Strain profile of N-S top bars of SP-B at south face of column- Loading South

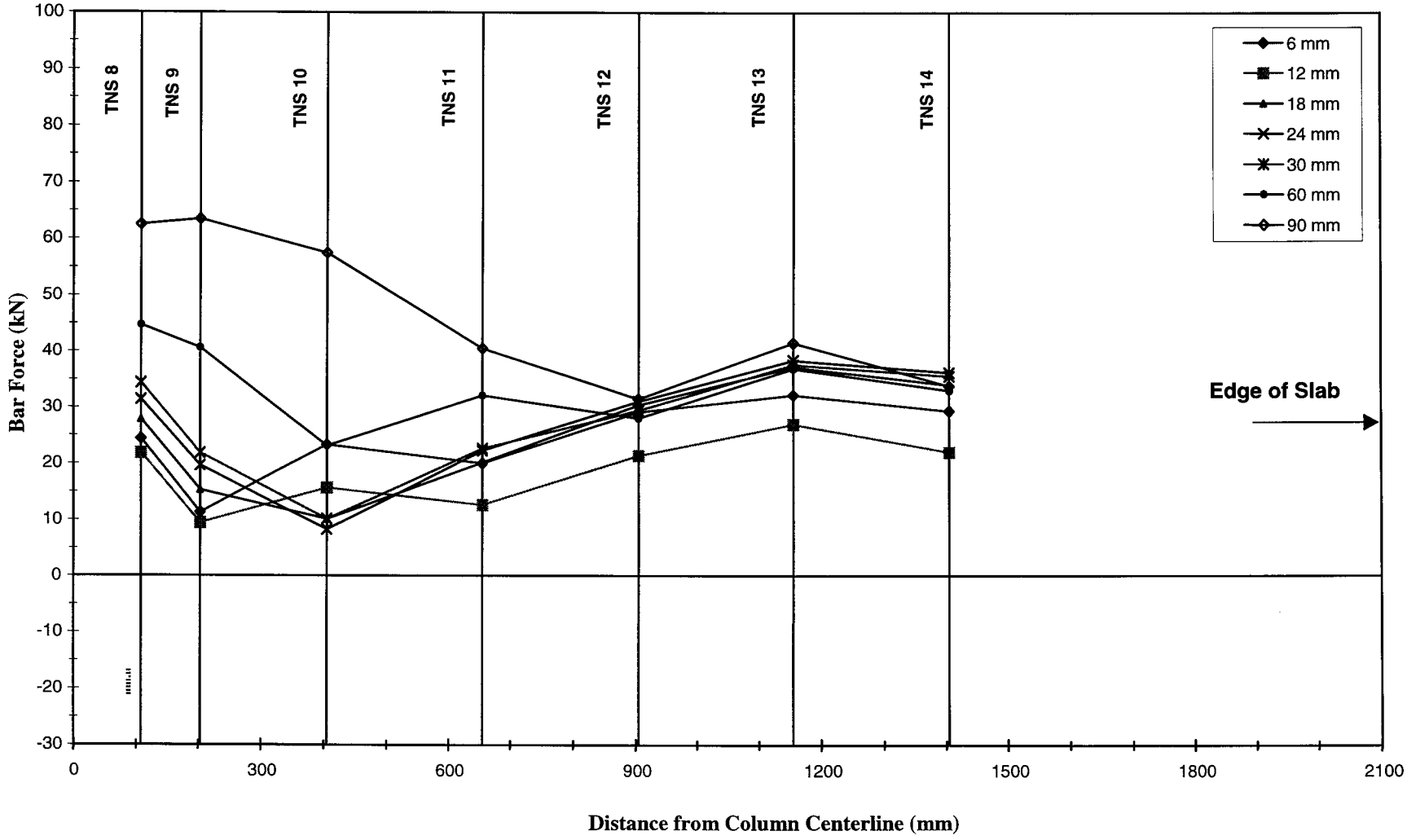

Figure 4.23 Top N-S bar force profile of SP-A at north face of column - (Loading North)

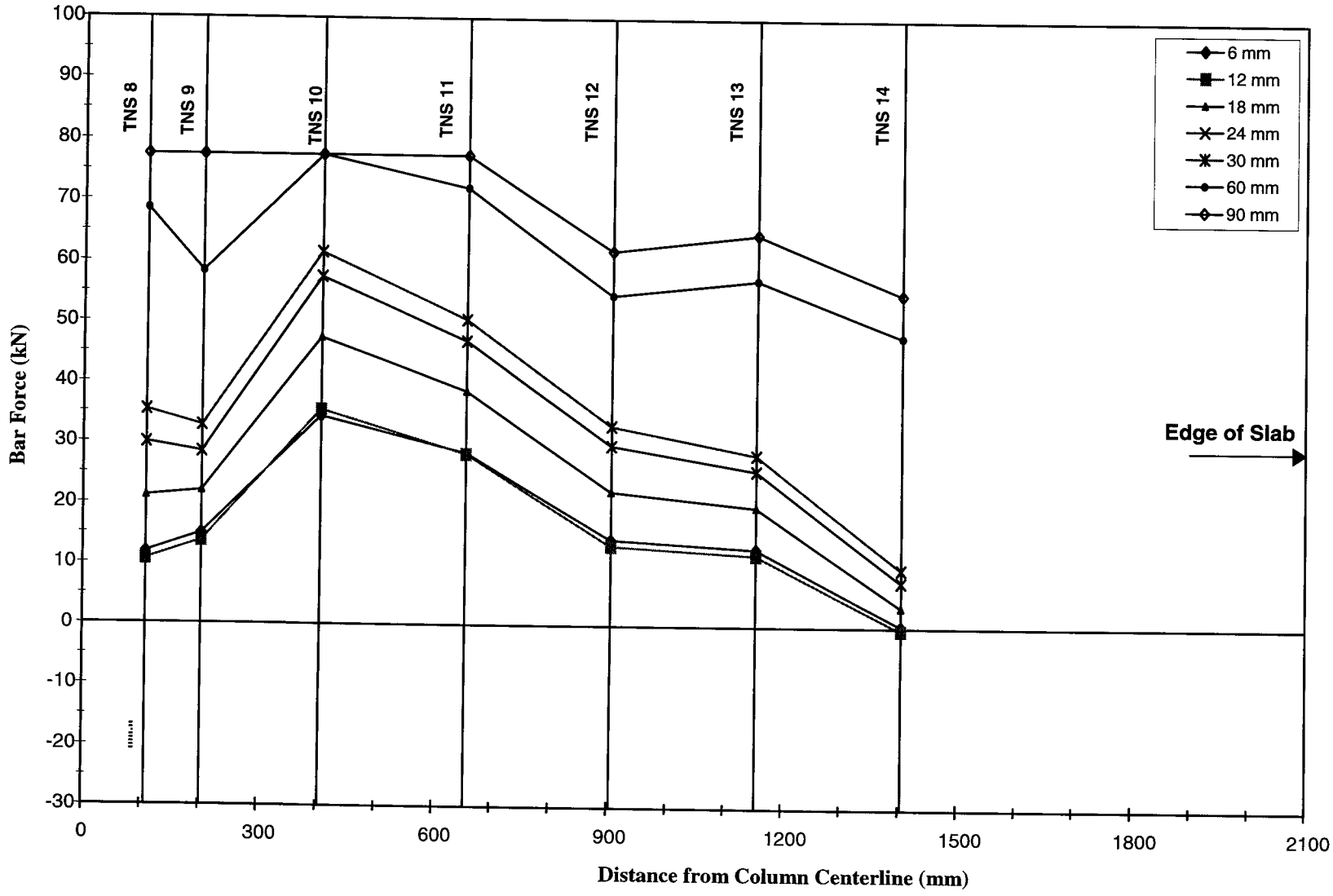

Figure 4.24 Top N-S bar force profile of SP-A at south face of column - (Loading North)

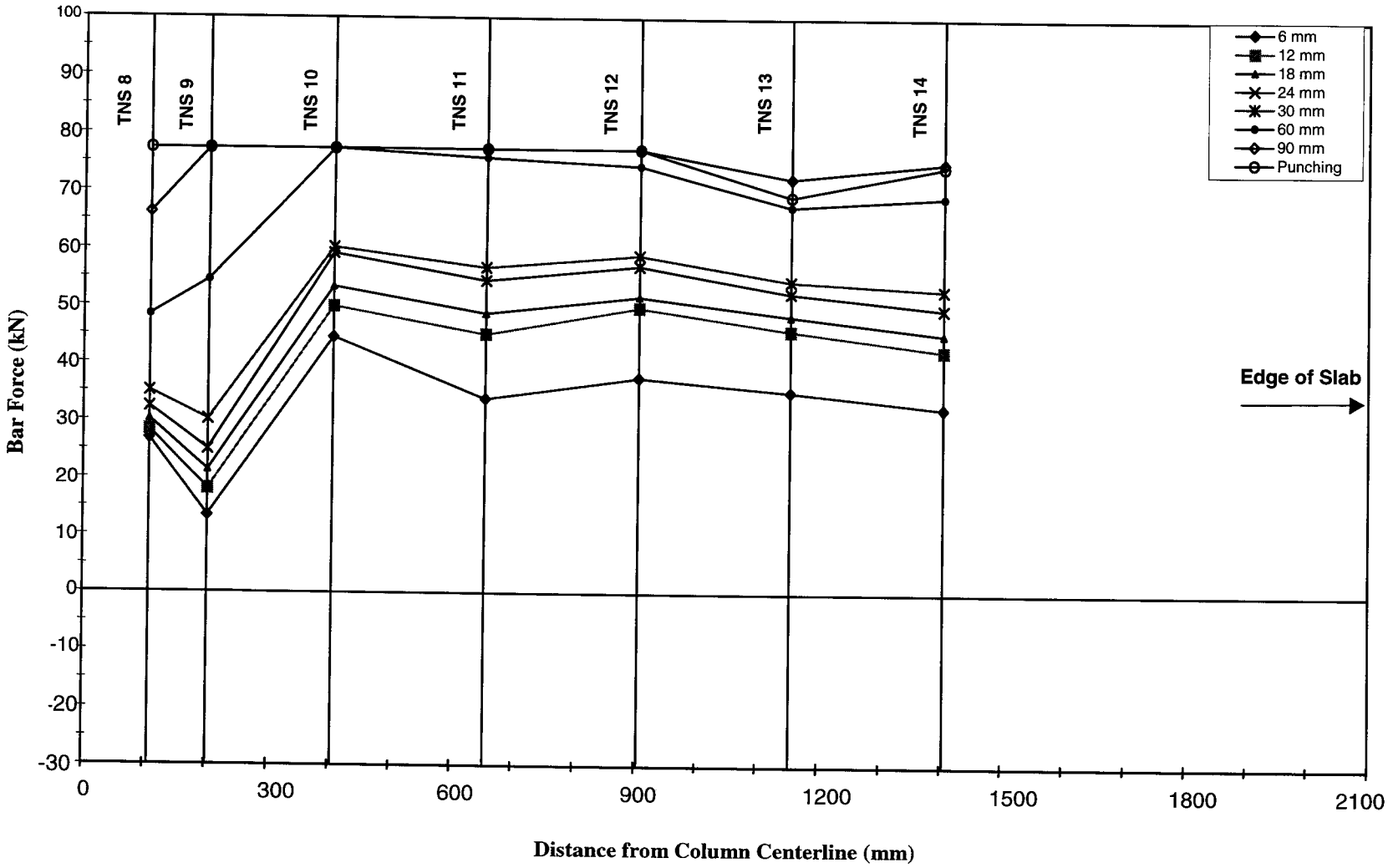

Figure 4.25 Top N-S bar force profile of SP-A at north face of column - (Loading South)

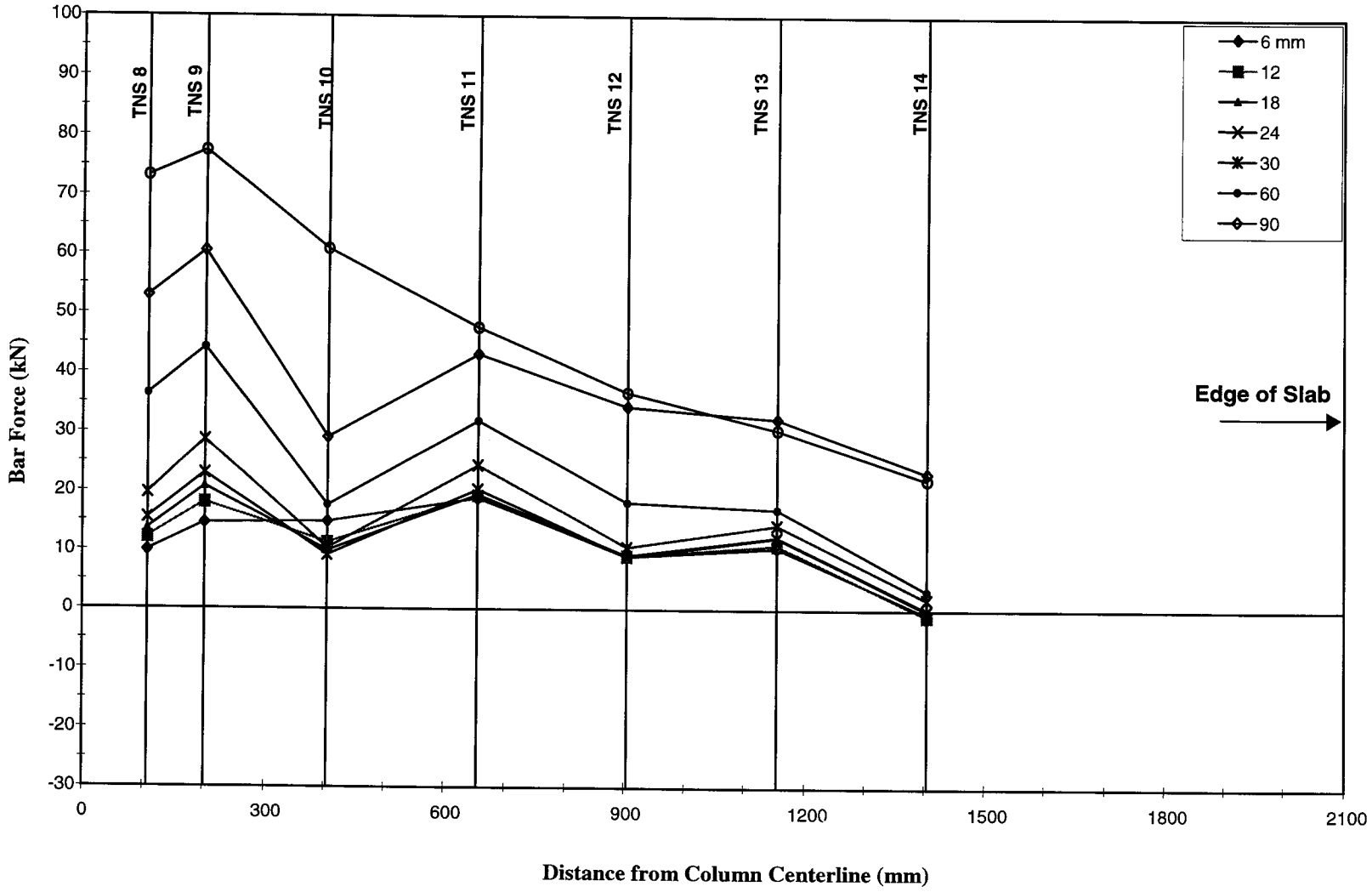

Figure 4.26 Top N-S bar force profile of SP-A at south face of column- Loading South

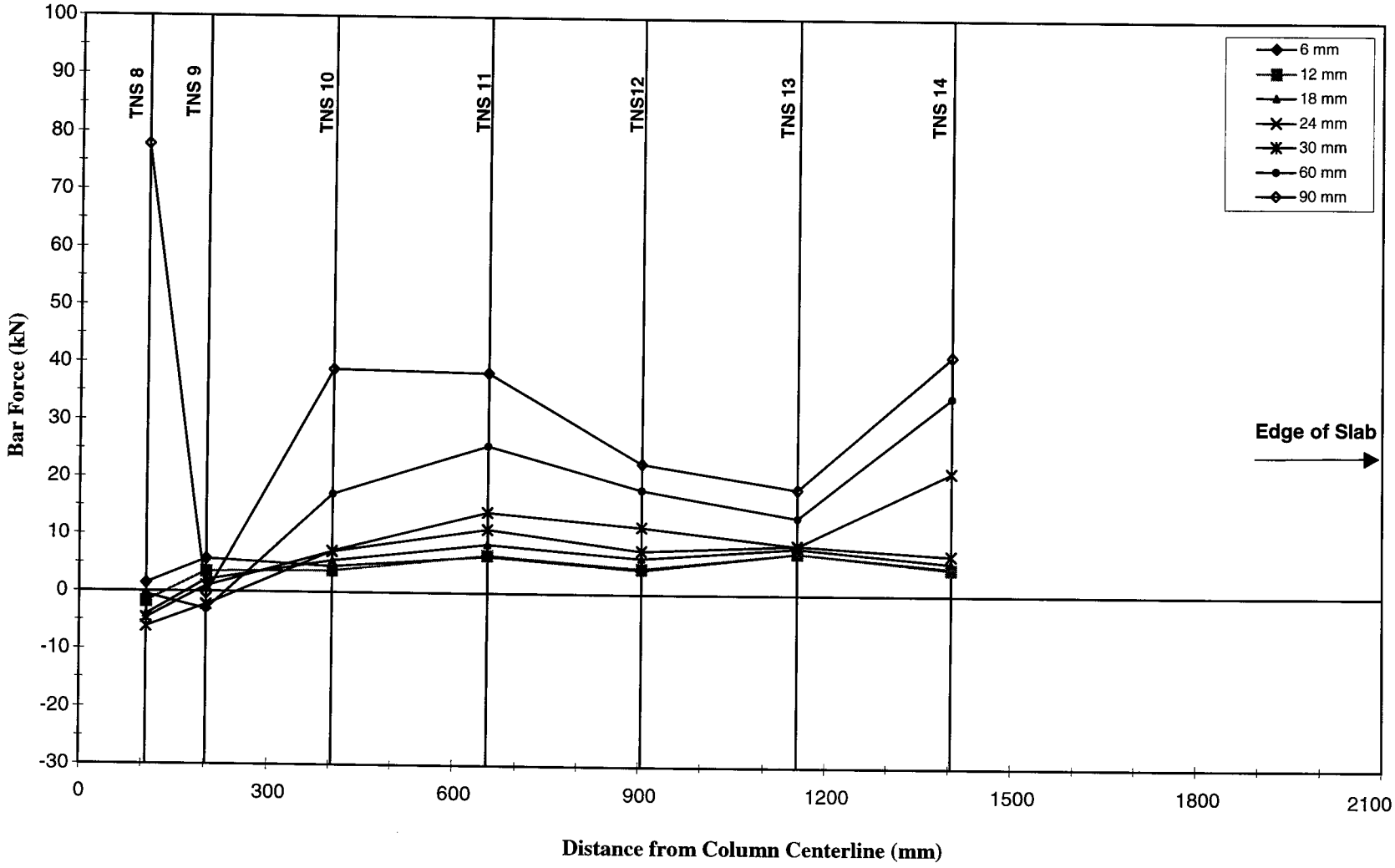

Figure 4.27 Top N-S bar force profile of SP-B at north face of column- Loading North

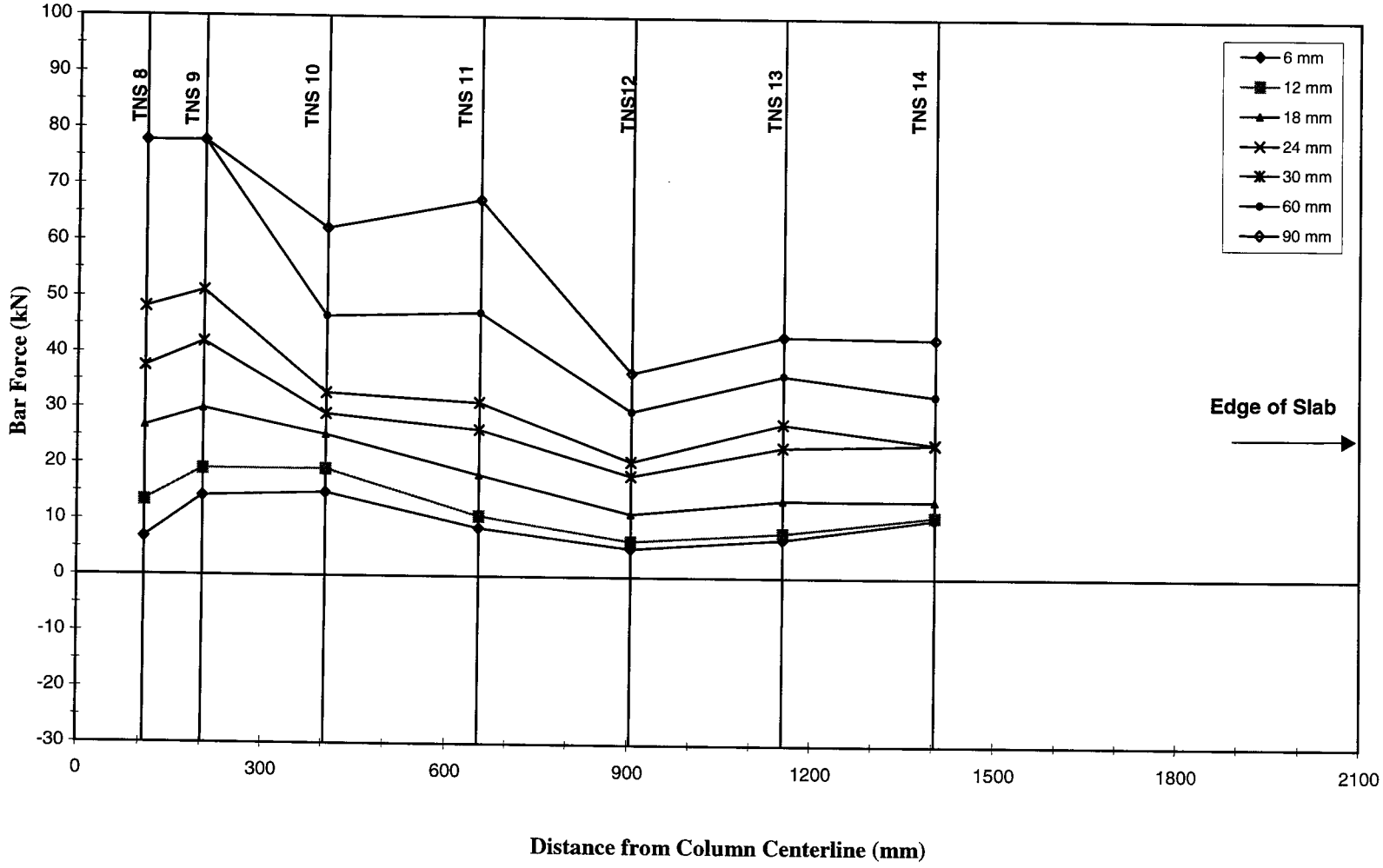

Figure 4.28 Top N-S bar force profile of SP-B at south face of column - Loading North

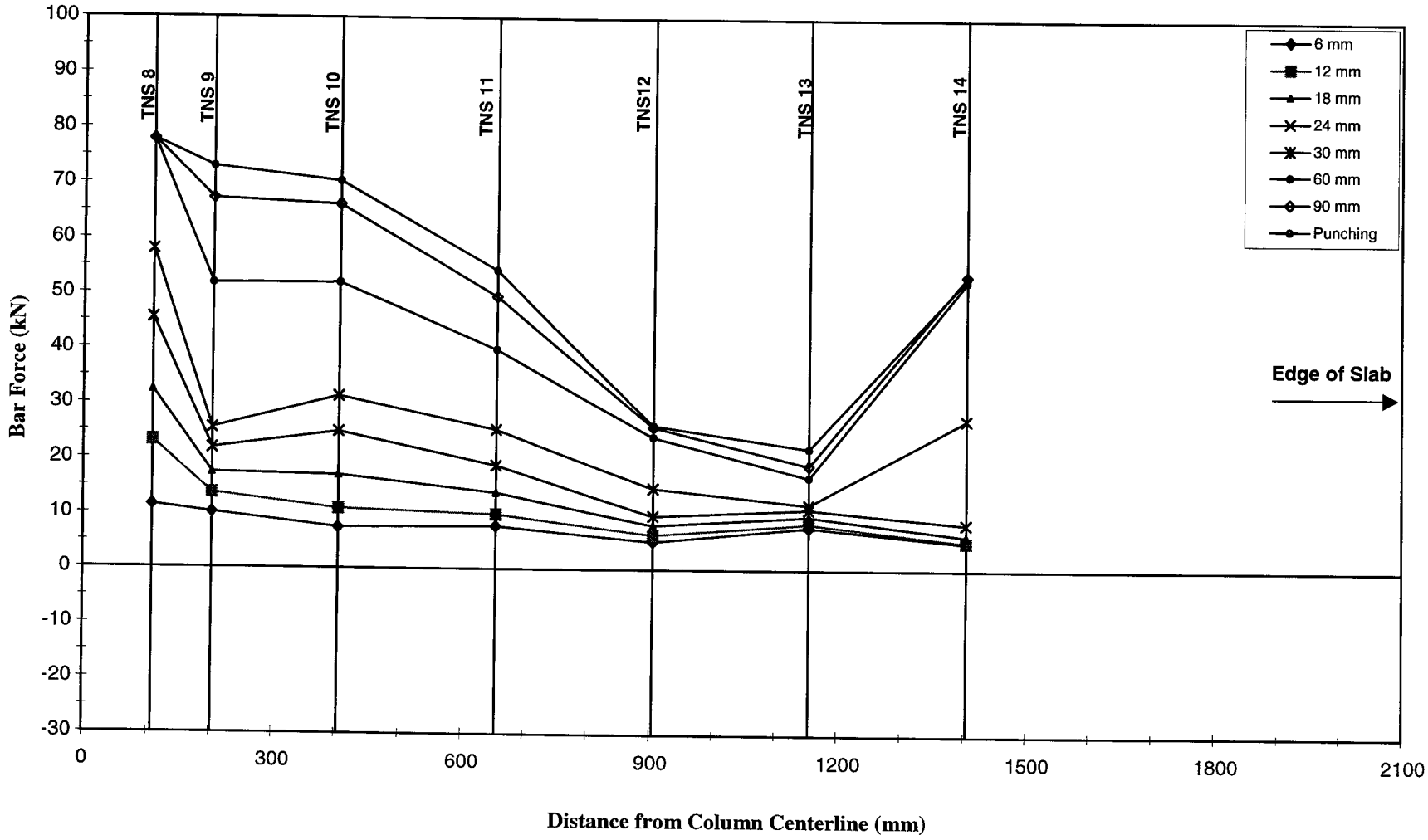

Figure 4.29 Top N-S bar force profile of SP-B at north face of column- Loading South

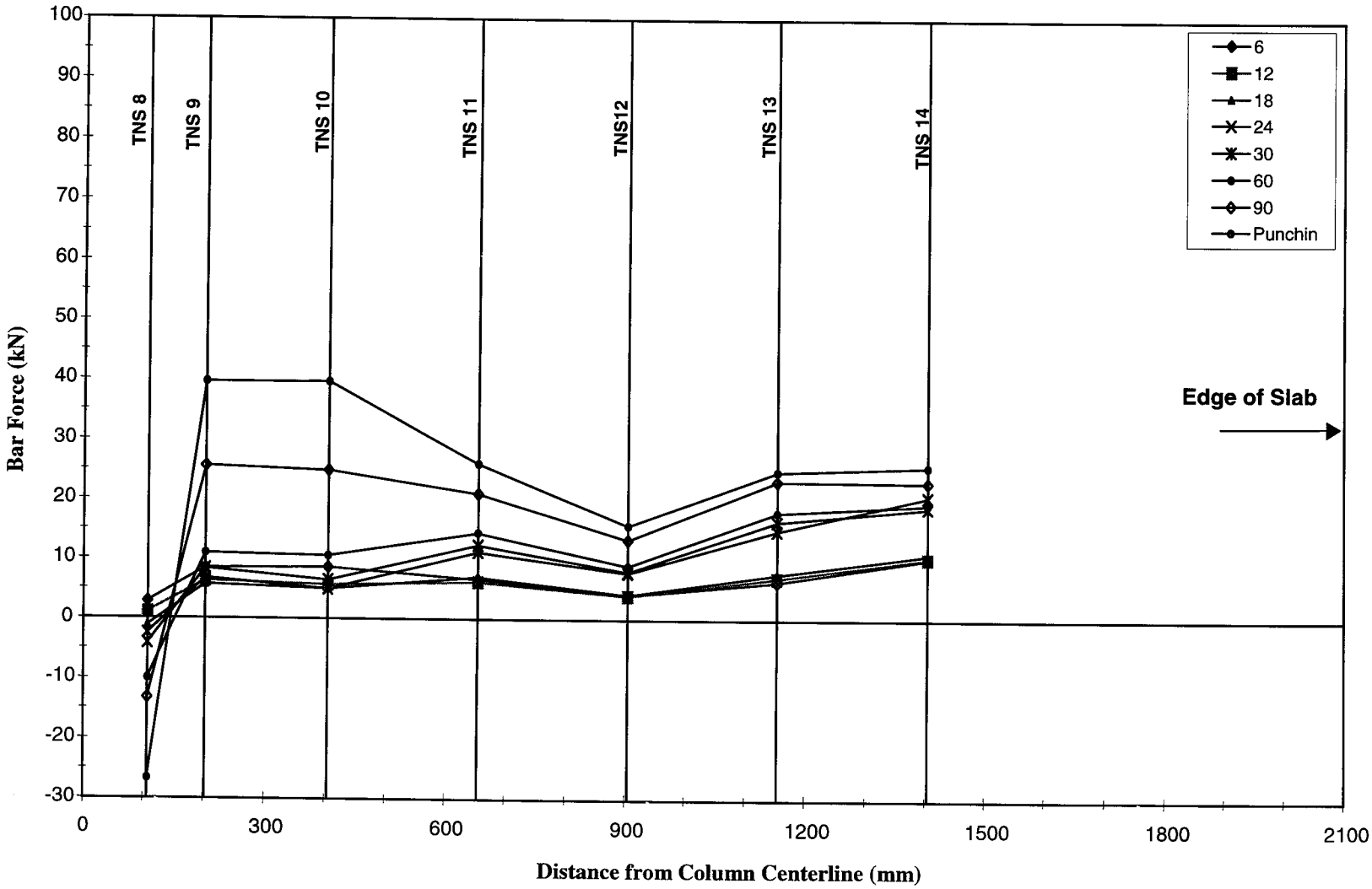

Figure 4.30 Top N-S bar force profile of SP-B at south face of column- Loading South

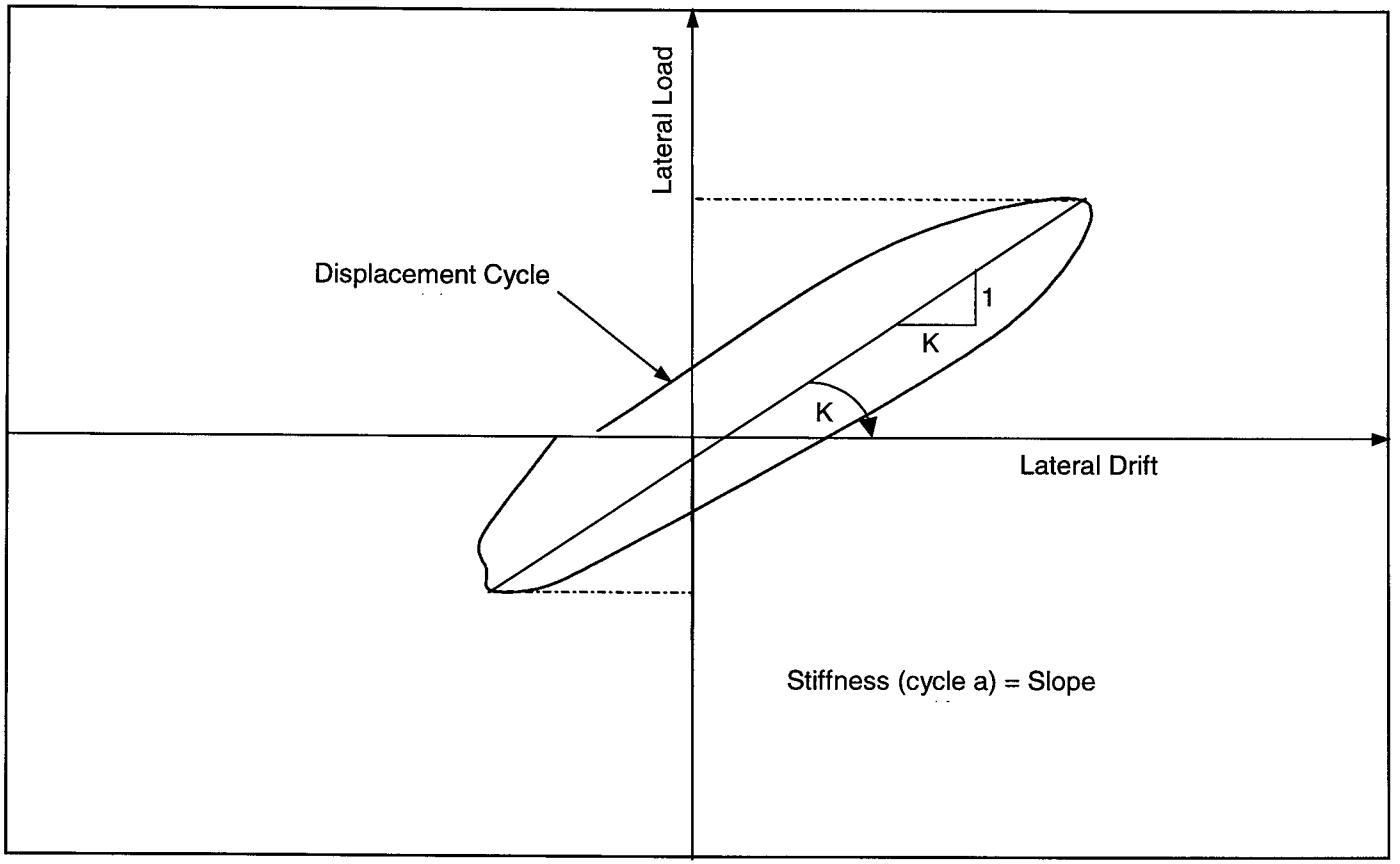

Figure 4.31 Stiffness Parameter (K)

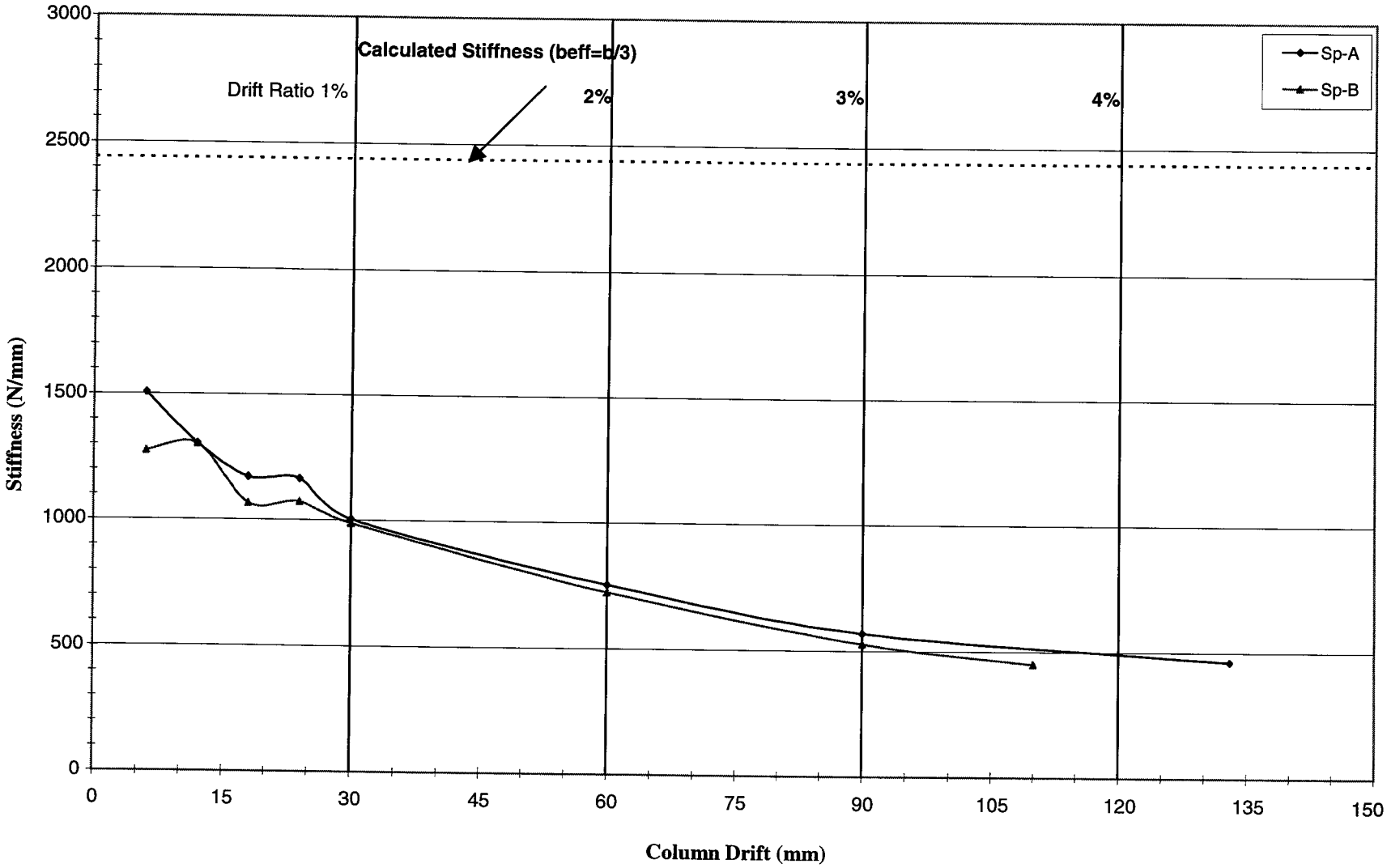

Figure 4.32 Lateral Drift Vs Stiffness

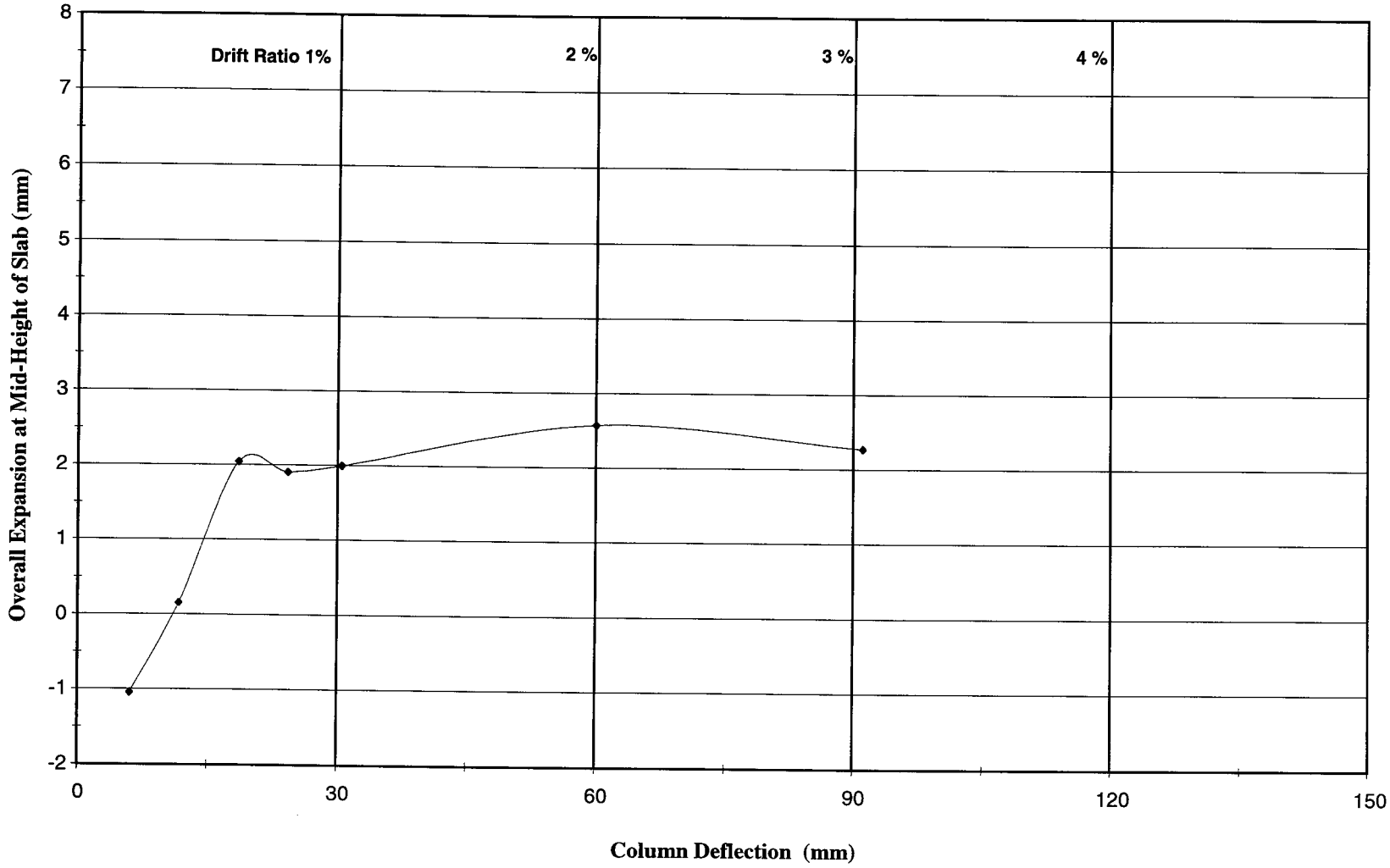

Figure 4.33 Column Deflection vs Overall Expansion at Mid-Height of Slab of SP-A - Loading North

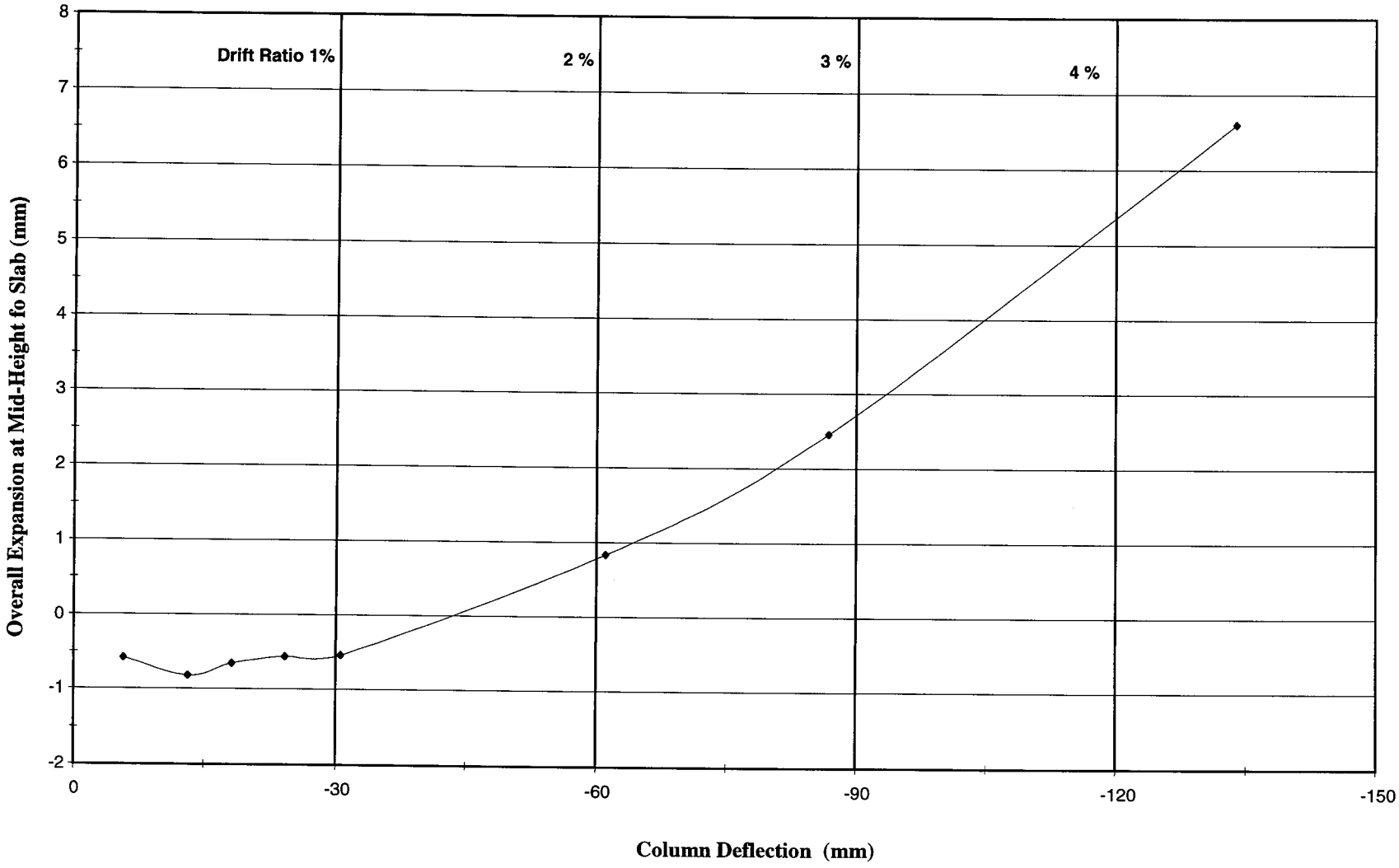

Figure 4.34 Column Deflection vs Overall Expansion at Mid-Height of Slab of SP-A - Loading South

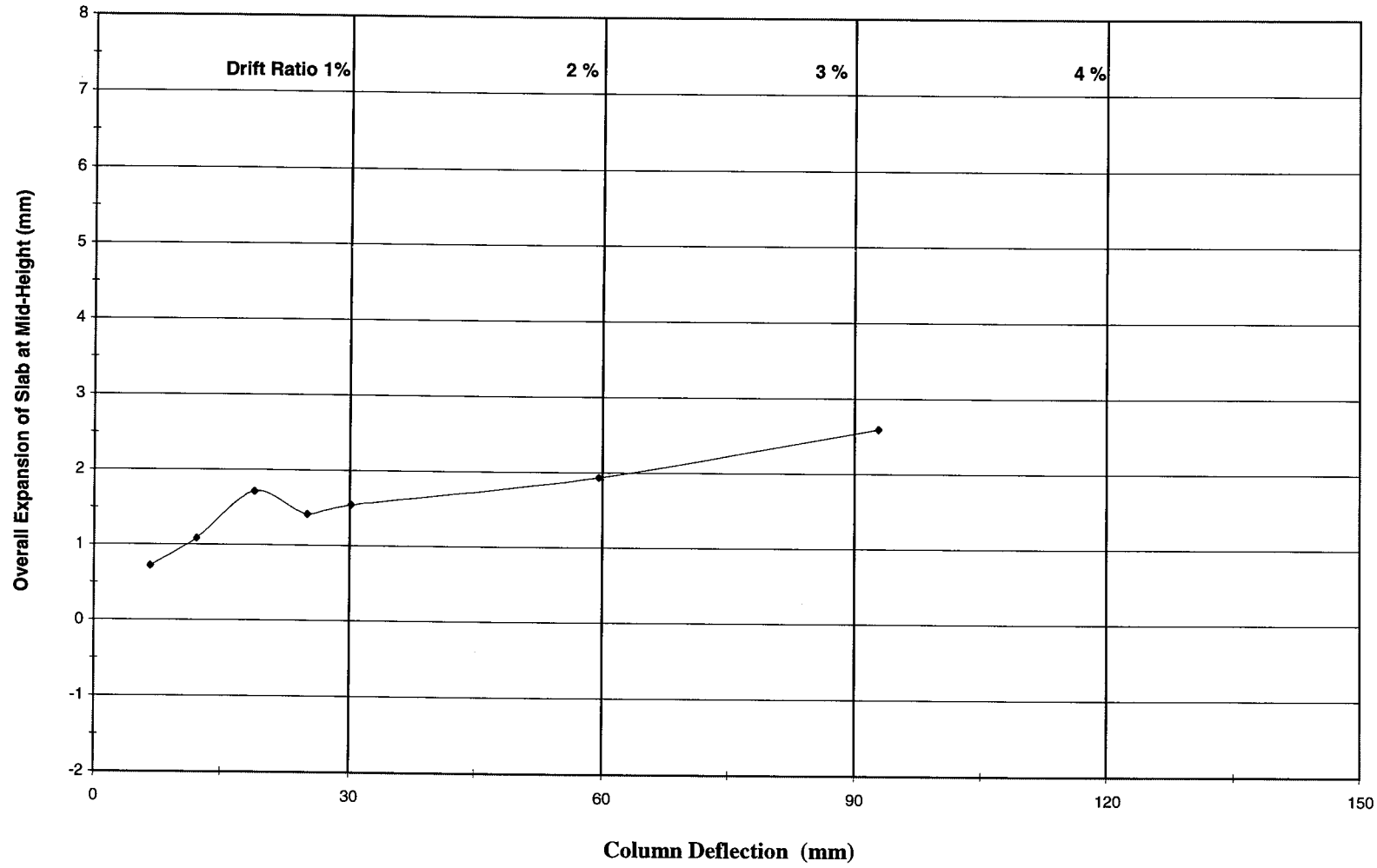

Figure 4.35 Column Deflection vs Overall Expansion at Mid-Height of Slab of SP-B - Loading North

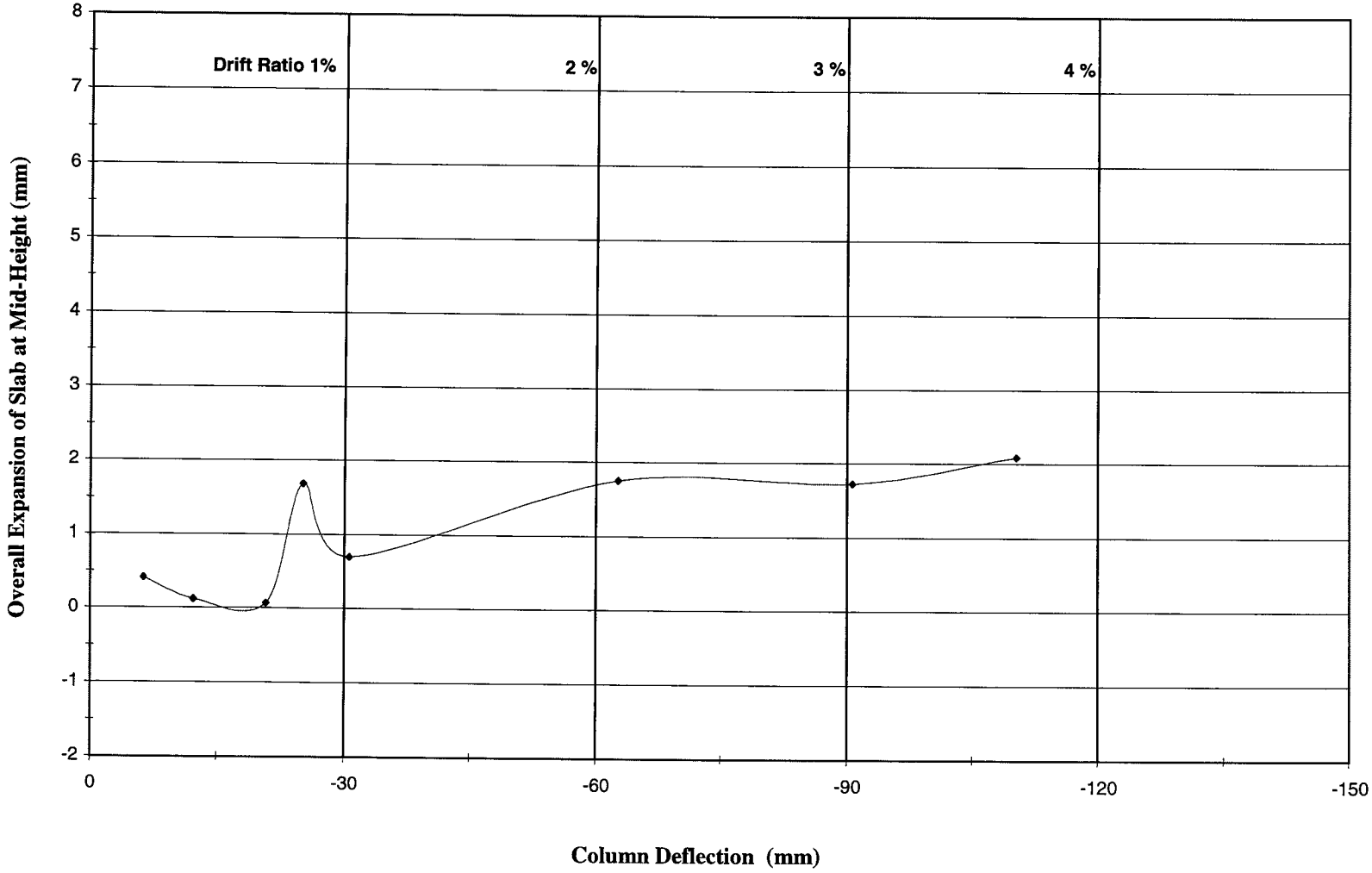

Figure 4.36 Column Deflection vs Overall Expansion at Mid-Height of Slab of SP-B - Loading South

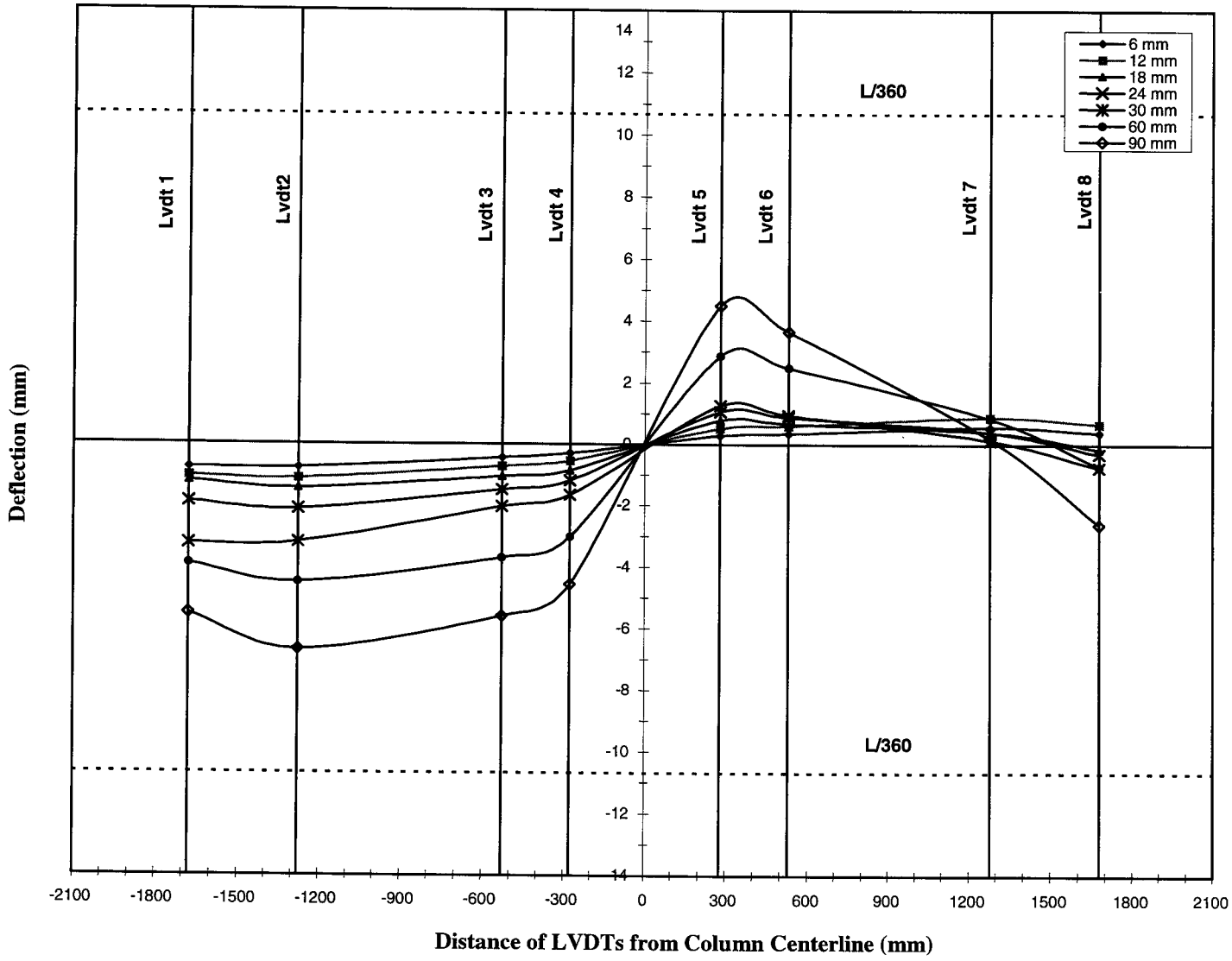

Figure 4.37 Slab Deflection Profile of SP-B at Peak Drift Values - Loading North

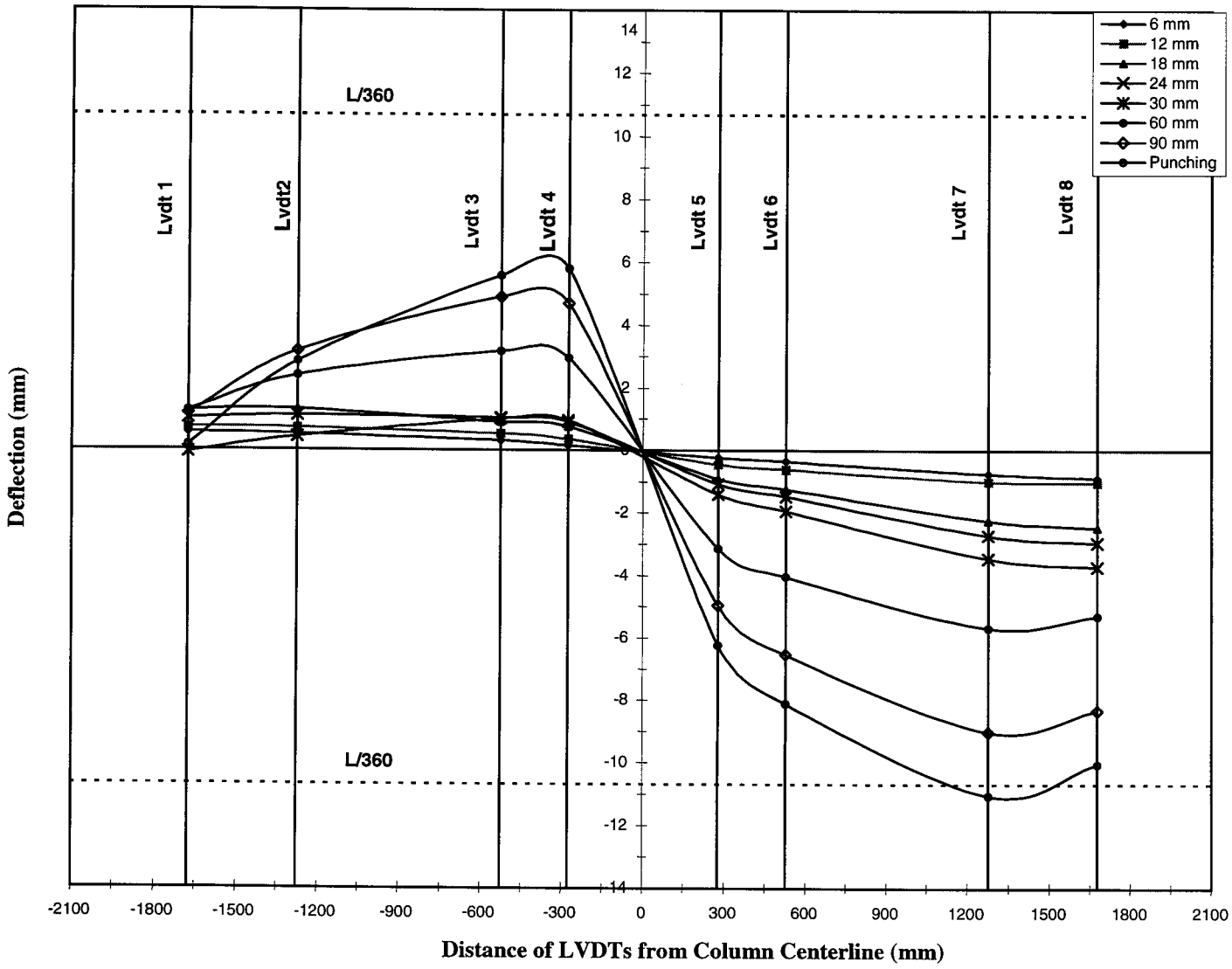

Figure 4.38 Slab Deflection Profile of SP-B at Peak Drift Values - Loading South

Figure 4.39 (a) Crack Pattern of Sp-A after Failure

Figure 4.39 (b) Failure Surface of Sp-A

Figure 4.39 Photographs of Sp-A after Failure

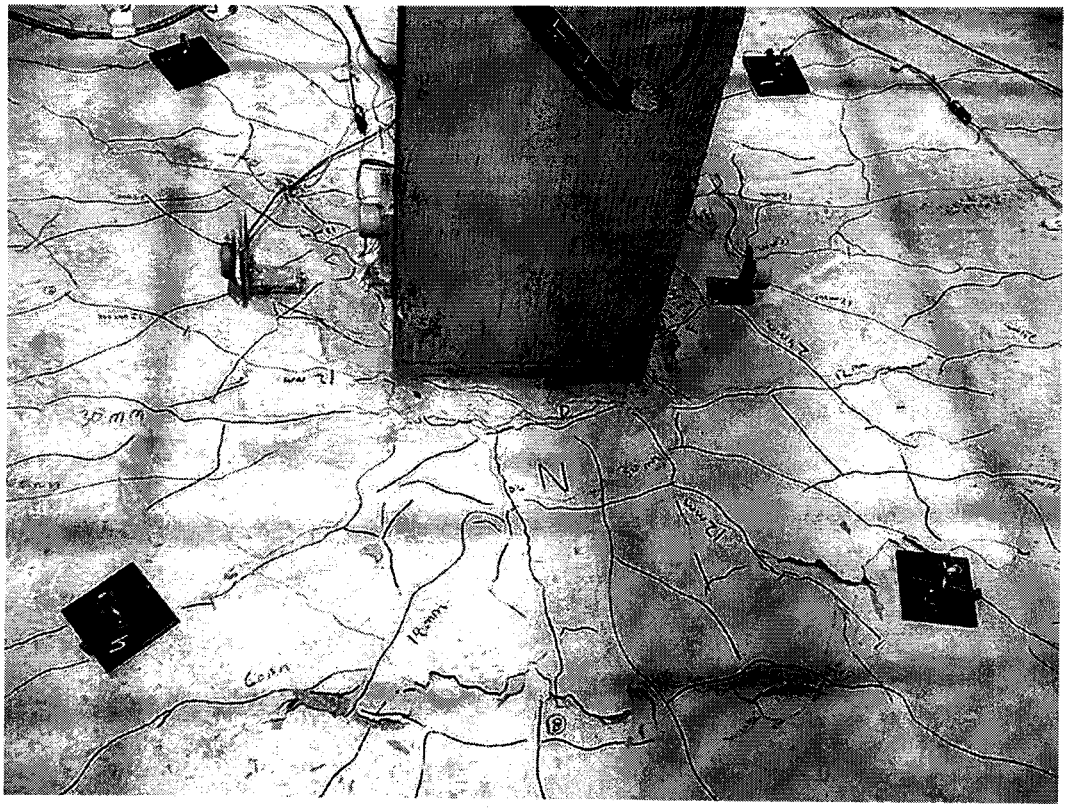

Figure 4.40 (a) Crack Pattern of Sp-B after Failure

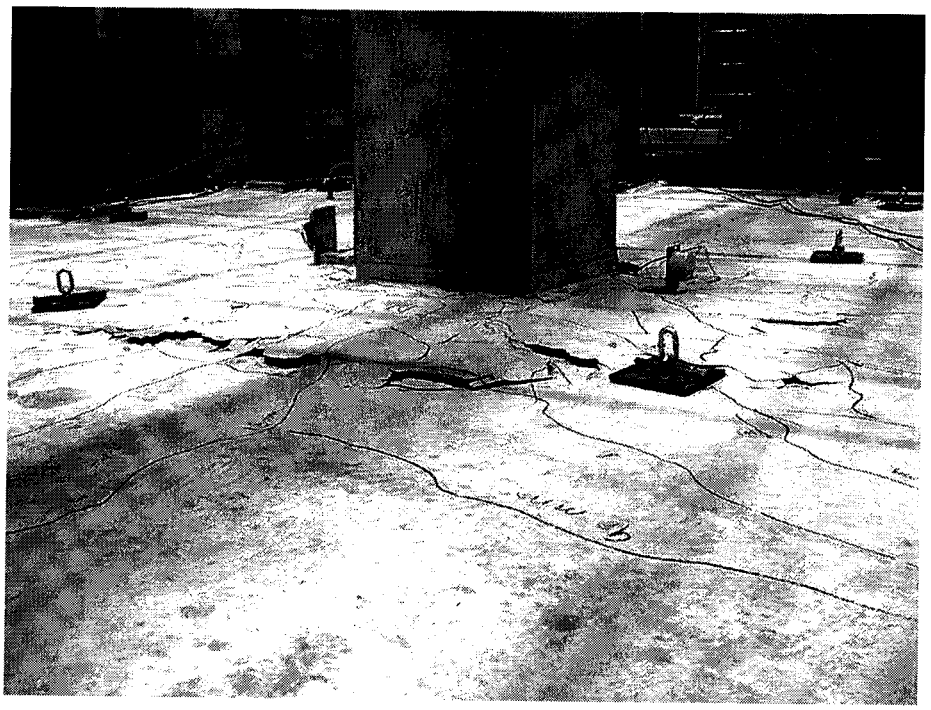

Figure 4.40 (b) Failure Surface of Sp-B

Figure 4.40 Photographs of Sp-B after Failure

5. Conclusion and Recommendations

5.1 Conclusions

Examination and analysis of the test data lead to the following conclusions. It should be remembered that a test program with only two specimens provides very limited data on the behavior of the connection and more testing would be required to support the results obtained here.

1) The concept of partially debonding the reinforcement around the column region to a distance of 2d from the column face on either side resulted in a more ductile connection.

   SP-A with partially debonded reinforcement demonstrated significantly increased ductility with a gradual failure as compared to the SP-B which experienced precipitous failure.

2) After reaching the ultimate load the lateral load response of SP-A softened gradually with increasing drift whereas the lateral load resistance of SP-B dropped sharply after reaching ultimate load.

3) For SP-A the reinforcement outside the debonded region yielded before the reinforcement inside the debonded region. All top reinforcement yielded prior to failure.

4) Debonding the reinforcement significantly reduced the cracking of slab around the critical region.

5) For these tests at drift ratios less than 0.5 % at service load, the effective moment of inertia for the slab section was approximately 1/6 of the gross moment of inertia. At drift ratio of 2 %, the effective moment of inertia was approximately 1/9 of the gross moment of inertia. Reducing the stiffness of the slab subjected to lateral load by a factor of 1/3 as recommended by Vanderbilt and Colrey, to account for cracking overestimated the stiffness.

6) In repair situations, the reinforcement may be debonded for a distance 2d from the face of column. This appears to be much easier than other methods of increasing the ductility of the connection.

5.2 Recommendations

Based on experimental and analytical test results reported here, following recommendations are made:

1) The test results reported here is the only source of data from test on partially debonded slab-column connection subjected to cyclic loading. More tests are required to confirm the test data reported here. Selection of different values of debonding length greater or smaller than 2d is recommended for future research, in order to examine if increase or decrease in debonding length result in more ductility of the connection.

2) The tests reported here focused on slab-column connections subjected to cyclic loading with constant, light, gravity loads. It would be important to produce the results from slab-column connections with partially debonded reinforcement subjected to variations of both gravity and lateral loads.

3) Further testing should also consider high gravity load. An important objective would be to achieve drift ratios of 1.5 % to 2 % with V/Vo equal to 0.4 to 0.5.

4) In general design practice, flat plate slabs are designed with the negative and positive moments at 65 % and 35 % of the panel moment, respectively, resulting in more top steel than the bottom steel. Other distributions that place for more bottom reinforcement may lead to more ductile connections. It is suggested that both top and bottom steel should be designed for 50% of the panel moment due to gravity loads only.

5) Test slabs with and without proposed rehabilitation technique.

LIST OF REFERENCES

ACI Committee 318, 1999. Building Code requirements for structural reinforced concrete. American Concrete Institute, Detroit, MI.

Canadian Standards Association, 1994, "Design of Concrete Structures for Buildings (CSA A23.3-94)," Canadian Standards Association, Rexdale, Ontario.

Ian N. Robertson and Ahmed J. Durrani, 1992, " Gravity Load Effect on Seismic Behavior of Interior Slab-Column Connections", ACI Structural Journal, Vol. 89, No.1, pp 37-45.

N. W. Hawkins and W.G. Corley., 1974, "Moment Transfer to Columns in Slabs with Shearhead Reinforcement", SP-42, American Concrete Institute, Detroit, MI, pp. 847-880.

Neil M. Hawkins, Denis Mitchell, and Samir H. Hanna., 1975, "The Effects of Shear Reinforcement on the Reversed Cyclic Loading Behavior of Flat Plate Structures", Canadian Journal of Civil Engineering, Vol 2, pp. 572-582.

Sami Megally and Amin Ghali., 2000, "Seismic Behavior of Edge Column-Slab Connections with Stud Shear Reinforcement," ACI Structural Journal, Vol 97, No.1, pp 53-60.

Shyh-Jiann Hwang and Jack P. Moehle., 2000, "Vertical and Lateral Load Tests of Nine-Panel Flat-Plate Frame," ACI Structural Journal, Vol 97, No.1, pp193-203.

Shafiqul Islam and Robert Park., 1976, " Tests on Slab-Column Connections with Shear and Unbalanced Flexure," Journal of the Structural Division, Vol.102 No.ST3., pp 549-568.

Vanderbilt, M. D., and Corley, W. G., 1983, "Frame Analysis of Concrete Building", Concrete International, V. 5, No. 12, pp 33-43.